Astronomical & Astrophysical Transactions
The Journal of the Eurasian Astronomical Society

The catalogue of structural and dynamical characteristics of 103 open star clusters and the firstresults of its investigation

V. M. Danilov [a]; A. F. Seleznev [a]
[a] Astronomical Observatory of the Urals University, Russian Federation, Ekaterinburgh

PLEASE SCROLL DOWN FOR ARTICLE

THE CATALOGUE OF STRUCTURAL AND DYNAMICAL CHARACTERISTICS OF 103 OPEN STAR CLUSTERS AND THE FIRST RESULTS OF ITS INVESTIGATION

V. M. DANILOV and A. F. SELEZNEV

Astronomical Observatory of the Urals University, Russian Federation, 620083 Ekaterinburgh, Lenin Avenue 51

The catalogue of structural and dynamical characteristics of 103 open clusters (OCl's) is presented. These characteristics were obtained by improved star counts method with the use of available photometrical data. The catalogue contains numbers of stars in the clusters up to $B \simeq 16^m$, the angular and linear radii of the OCl's, the King model parameters for the surface star density distribution and dimensionless parameters of the halo-core structure of the clusters, the lower estimates of the mass, tidal radius in the gravitational field of the Galaxy and the relaxation time of the clusters. The individual disruption times and nonstationary degrees for OCl's were calculated for the first time. The comparison is made with the results of theoretical studies and numerical experiments. A sequence is found in the space of the parameters of the halo-core structure of the clusters: the relative population and relative size of the cluster core. This sequence or correlation corresponds to the balance of the rates of stellar transitions that take place between the core and the halo during the cluster relaxation. The age dependence of the concentration of stars to the cluster centre is confirmed. Some evidence of gravitational tidal actions of gas-star complexes (GSC's) on the clusters is found. First, the young cluster stars are located deeper than the intermediate-age and old cluster ones, under the tidal surface that is determined by the Galaxy field. Second, the dependence of young cluster sizes on the distance to the centre of the GSC that contained the clusters is found. It is confirmed that the giant molecular clouds gave the main contribution to the cluster disruption. The tidal gravitational field of the GSC reduces the cluster disruption time.

1 INTRODUCTION

Star clusters (SCl's) are traditionally used to test theories, hypothesis and suppositions arising about the physical and dynamical evolution of stars and star clusters.

The main reasons for such high interest in the SCl study were formulated by Lynga (1987) and Wielen (1987):

1) Every SCl is an object whose characteristics, such as distance, age and evolutionary state, can be studied better than for single stars.

2) The systems of SCl's and associations in our Galaxy and other galaxies provide information about the structure and recent evolution of galaxies.

3) The clusters and associations are very sensitive to the conditions in the interstellar medium that surrounds them. The age distribution of clusters and the mean cluster lifetime that is derived from this distribution are a source of information about the physical conditions in the Galaxy disk and in other galaxies, first of all about the presence of massive clouds of gas and dust.

An investigation of the structure and dynamics of open star clusters (OCls) along with the data of photometry and the evaluations of astrophysical characteristics for the clusters are the main methods to obtain information about these systems that is needed for different physical and dynamical estimates of the modern state of the OCls. The estimates of relaxation times and ages of clusters and their mutual comparison, the comparison of observational data with the results of numerical experiments and with different dynamical models for the clusters give us the possibility to judge about the dynamical state, direction and the character of the cluster evolution.

The study of the star cluster spatial structure allows now to judge about the mechanisms and conditions of cluster formation at different stages of Galaxy evolution (Wielen, 1987). The study of the SCl dimensions, the evaluation of the mean density, relaxation time and other cluster characteristics allow to make conclusions not only about the dynamical state of the clusters, but also about the properties of larger-scale gravitational systems that surround the cluster at the present time (the characteristics of gas-star complexes, parameters of the giant molecular clouds subsystem, parameters of the galactic force field).

The influence of external regular and irregular force fields on the OCl plays an important role in cluster dynamics. It is known that the external Galactic field increases the rate of the dynamical evolution of the OCl. However, the cause of that is usually analyzed without taking into account the possibility of a considerable OCl departure from the regular field stationarity. The development of nonstationarity and a fast OCl disruption at the dynamical time scale may be caused by irregular forces in low-density clusters.

A considerable part of the OCl stars are situated at the cluster periphery. The stellar density, the masses of the stars and their dispersion at the cluster periphery are lower than the mean cluster values, but the velocity dispersion there is not small due to a "heating" of the OCl by external regular and irregular fields. Thus, the local two-body relaxation time at the cluster periphery may be comparable with the typical lifetime of the OCl, $(2-5) \times 10^8$ years. The regular field nonstationarity caused by both external forces and the deviation of the initial conditions from equilibrium, may be considerable in such clusters.

Up to the early 80's, the OCls were considered in general as objects whose state is close to the virial equilibrium. Quasistationary and even stationary models were used for the theoretical description of the OCl structure, that did not take into account the possibility of a considerable departure of the cluster from the

regular field stationarity. However, structural properties of young and old OCls were found even in the 50's and 60's, such as distortions of the cluster core shape, the splitting of cluster cores, the lack of coincidence between the centres of the density distributions of the cluster stars having different masses, step-like structures in cluster density profiles, etc. (Barkhatova, 1956; Artyukhina and Kholopov, 1961; Sharov, 1964; Kholopov, 1968, 1979, 1981; Chumak, 1969; Seleznev, 1992). These properties cannot be explained without the hypothesis of the cluster regular field nonstationarity.

Numerical N-body experiments for nonisolated systems that were conducted by Danilov (1985, 1987c) showed that the encounters of the cluster member stars might lead to a considerable regular field nonstationarity and even to the cluster disruption at some crossing times in the clusters with a low mean density (that was close to the critical value in the external force field) and a weak concentration of the stars to the cluster centre. The catalogues of OCl characteristics, of giant molecular clouds (GMCs) and gas-star complexes (GSCs) were published in the 80's (Danilov et al., 1987; Dame et al., 1987; Solomon et al., 1987; Efremov and Sitnik, 1988), that allowed to evaluate the influence of the GSC and GMC force fields on the OCls. The nonstationarity degree of an OCl increases in the presence of GMCs and GSC and the cluster disruption time decreases several times.

Thus, the problems of dynamics investigation of regular field nonstationary clusters, that were formed in massive and extended GSCs in the presence of the force fields of the GMC and the Galaxy, become timely now.

Let us note that the mean values of matter density in OCls are determined inaccurately, as a rule, and depend, to a great extent, on the observational evaluation of the cluster radius. Dimensions of OCls, mean OCls densities and the critical ones in the external force field should be estimated more accurately for the analysis of the nonstationary phenomena observed in the OCls. Because of that, statistical criteria should be used now to reveal the OCls on the stochastic stellar background fluctuations and to determine the OCl sizes and the numbers of stars. The development of the statistical criteria for exposing statistically significant steplike structures in the OCl stellar density distributions is also needed. Extensive determinations of the structural and dynamical characteristics for many OCls with the use of such criteria is also required. The use of the methods of evaluation of the nonstationarity degree for clusters is needed, with allowance for most important mechanisms (encounters of the cluster member stars and external force fields) for the subsequent analysis of nonstationarity phenomena observed in OCls.

The amount of observational data available about the OCl structure that can be used for the study of the OCl dynamics and for the analysis of the regular field nonstationarity phenomena in clusters is obviously insufficient for these purposes.

It is the main problem of this paper to obtain such observational data and to investigate them. The development of a new method for the evaluation of the clusters sizes and the numbers of stars in the OCls was one of the first steps in this problem solution (Danilov, Matkin and Pylskaya, 1985, hereafter DMP). The possibility of such estimates is usually restricted by the presence of background star number density fluctuations at different scales in the cluster vicinities. The

DMP method uses a statistical comparison of the cluster field and the neighbouring background fields in contrast to the methods that are usually used for the analysis of the star cluster structure. The study of the OCl structure in the last years (Danilov and Seleznev, 1988a; Danilov, Seleznev and Beshenov, 1989) has shown that in the average the stars of young clusters were situated deeper, under the tidal surface determined by the Galaxy field, than the stars of old clusters. One should take into account the joint action, on the young OCls, of the force fields of the Galaxy and the GSC where these clusters were formed, in order to analyze this phenomenon. An important role in such an analysis belongs to the investigations of the OCl stability in the external force fields. These investigations give us information about the tidal size of the clusters and about some characteristics of the GSC where the clusters were formed.

Some theoretical estimates and the first numerical experiments on the study of the GMC action on the OCl were carried out earlier by Wielen (1985), Terlevich (1987), Wielen and Fuchs (1988) and Theuns (1992a, b). It was shown in these papers that close encounters of OCls and GMCs control the OCl lifetimes in the solar vicinity in the Galaxy disk. However, these authors did not take into account the joint action of the GSC and the Galaxy on the cluster and the effects of nonstationarity development in the OCls were not considered. The theoretical estimates did not consider distortion of the cluster shape during the encounter with a GMC, the possibility of the accompanying motion of the OCl and GMC was not taken into account, obsolete data on the GMC characteristics were used, etc.

Since the effect of the interaction with GMCs is very important for the OCl dynamics, a further investigation of this mechanism is needed with application to the new physical conditions.

In connection with external factors affecting the dynamical evolution of OCl, it is interesting to study the question if the OCl structure (density profiles, etc.) is determined by internal relaxation processes or by external causes due to the action of the force fields of GMCs, GSCs and the Galaxy and what is the measure of these effects. Observational data on the characteristics of the cores and haloes of OCls play an important role in such an investigation. One of the problems of the OCl study now is to obtain and analyze the data on the cluster halo-core structure.

The aims of this paper are:

1. A wide use of the method of the cluster star numbers and the OCl size statistical evaluation on the background of star number density fluctuations.

2. Estimates of the OCl nonstationarity degree with account for the most important mechanisms (star encounters and external force fields).

3. The determination of the characteristics of the cores and haloes of the OCls in the solar vicinity. An analysis of the halo-core structures of the OCls in the solar vicinity (using observational data). Comparison with the results of numerical experiments on the open cluster dynamical evolution.

4. An analysis of the influence of the GSC force field on the sizes of the clusters that were formed in complexes (using observational data). The comparison of the observational data with theoretical and numerical estimates of the OCl tidal radii in the joint gravitational field of the Galaxy and GSC.

2   OBSERVATIONS AND STAR COUNTS

In order to ensure the homogeneity of the observational material, all the observations were carried out on the SBG camera of Carl Zeiss Jena designed for photographic observations of satellites and mounted at the Astronomical Observatory of Urals State University. This instrument is a wide-angle, candle-power Schmidt camera with the focal length of 777 mm, the aperture of 425 mm and the mirror diameter of 500 mm. The field of vision is about $6° \times 8°$. The plate scale is equal to 44.2 arcminutes per 1 cm and the plate size is 9×12 cm.

The observations were carried out in the B colour. The limiting magnitude $B_{\lim} \simeq 16^m$ was reached after the exposure time of 5 minutes. The limiting magnitudes of the stars on the plates were determined by the method of van der Bergh and Sher (1960) using cluster stars with the available photometry. The photometry of clusters does not always reach the stars with the brightness less than $B = 16^m$. Therefore the determination of the limiting magnitudes of stars on the plates was possible not for all the clusters. The plate limiting magnitudes varied approximately from 16^m to 16^m5 due to the atmosphere transparency variation. Nevertheless, the overwhelming majority of the plates used had the limiting magnitude $B_{\lim} = 16^m$.

This work uses the DMP method of the open star cluster sizes, numbers of stars and reality estimation by star counts data (see also Danilov and Seleznev, 1991). This method uses not the cluster surface star number density function $F(r)$ but the function $N(r)$, the number of the stars in the circle of radius r in the projection on the sky plane. The use of the $N(r)$ function gives the possibility to avoid the "interval error" (see Kholopov, 1981). It is also more useful for the cluster spatial star number density $f(r)$ determination (see Rastorguev, 1983). Danilov, Matkin and Pylskaya (1985) have shown that $N(r)$ was obtained from observations with a smaller relative error than $F(r)$. The DMP method allows to evaluate the cluster radius and star number errors, which are usually no more than 10%.

The star counts were carried on the PS–18 spectrum projector with the $20\times$ magnification. The round grids that consist of 20 concentric circles with the ring width of $0'.55$, $0'.77$, $1'.11$, $1'.55$, $2'.08$, $2'.43$ and $3'.36$ were used for the counts. The grid size was selected so that the 20-th circle radius would be 1.5–2 times greater than the cluster radius.

The cluster centre position was determined by a cross-like grid. The star counts were made in strips in two directions perpendicular to each other.

The grids for the cluster centre determination and the round grids with the ring widths of $0'.55$, $0'.77$, $1'.11$ and $1'.55$ were drawn on paper and disposed in the projection plane. The round grids of the greater size were made by photography on 9×12 cm plates with the reproduction from the original drawn on paper. The background fields of the big grids have the form of ring sectors for a more complete use of the astronegative under investigation and for a greater convenience of the telescope field photometric error calculation. These big grids were superimposed on the investigated astronegative with emulsion to emulsion and centered on the cluster when the stars were counted.

1-3-400

The results of star counts in 102 OCl and one globular cluster (GCl) NGC 6838 were used in this work. The cluster angular radii and numbers of stars up to $B_{lim} \simeq 16^m$ obtained from the star counts are listed in the catalogue (see Section 7 and Appendix).

When using the DMP method one needs to count stars in the fields that are situated at a large distance from the plate optical centre. Then it is needed to take into account the influence of the camera field photometric error on the star count results. This problem has been solved by Seleznev (1988). Calculations show that the geometric vignetting gives a visible effect on the star count results only when the 3'.36-ring-width grid is used. These results were corrected.

3 DETERMINATION OF THE CLUSTER STRUCTURAL PARAMETERS

A statistical analysis of the star number distributions $N(r)$ in the cluster fields that were obtained from star counts was carried out in order to determine the cluster structural parameters. The star number values were presented as

$$N(r) = 2\pi \int_0^r F(r')r' \, dr', \tag{1}$$

where $F(r)$ follows from the King model for the surface star number density in the cluster (see King, 1962) taking into account background stars:

$$F(r) = k \left\{ \left[1 + \left(\frac{r}{r_c} \right)^2 \right]^{-\frac{1}{2}} - \left[1 + \left(\frac{r_t}{r_c} \right)^2 \right]^{-\frac{1}{2}} \right\}^2 + F_b. \tag{2}$$

Here the F_b is the surface background star number density. If F_b =const then integration in (1) can be easily performed:

$$N(r) = \pi k r_c^2 \ln \left[1 + \frac{r^2}{r_c^2} \right] - \frac{4\pi k r_c^2}{\sqrt{r_c^2 + r_t^2}} \left[\sqrt{r^2 + r_c^2} - r_c \right] + \frac{\pi k r_c^2 r^2}{r_c^2 + r_t^2} + \pi r^2 F_b. \tag{3}$$

The King function is used for the following reasons: first, it fits satisfactorily the density distribution in star clusters (King, 1962; Kholopov, 1981); second, there is an analytic solution of the Abell equation for the spatial star number density $f(r)$ in this model (King, 1962); third, the King model parameters are available for the Galactic GCls and many well-studied rich clusters in the Magellanic Clouds.

The approximation of the observed $N(r)$ distribution with the functions (3) for the sample clusters was carried out using the Marquardt algorithm of nonlinear least squares method (see Bard, 1979). The use of this algorithm allows, in particular, to estimate the mean square deviations for the model parameters.

The catalogue of the structural and dynamical OCl characteristics (see Section 7 and Appendix) includes the sample cluster King model parameters k and r_c obtained

using the following approach. The parameters k, r_c and F_b were determined for the clusters. It was assumed that $r_t = R$, with R, the cluster radius, determined from star counts. The values of $N(r)$ with $r \in [0, r_t = R]$ were used for approximation. The parameters k and r_c were obtained for 99 clusters. The mean square deviations of these parameters are also listed in the catalogue.

The inclusion of r_t in the parameter set affects noticeably the method convergence. We recall that r_t is the cluster limiting radius. This quantity describes the star distribution in the cluster halo region. Thus we may conclude that the King model describes inadequately the star distribution in the OCl halo on the average. The parameters k and r_c that are listed in the catalogue characterize in general the cluster core. According to Kholopov (1981), r_c is close to the core central region radius and k is connected with the central surface star number density.

Due to the uncertainty of r_t for open clusters, R/r_c is used in this work as an OCl concentration parameter. Then one should keep in mind that these parameters and the GCl concentration parameters are obtained with different methods when these values are compared.

$\langle R^{-1} \rangle$, $\langle R \rangle$ and $\langle R^2 \rangle$ were computed during the statistical processing for the King models of the sample clusters, they are necessary for the calculation of some cluster dynamical parameters (see Sections 5, 6):

$$\langle R^{-1} \rangle = \int_0^R f(r) r \, dr \left[\int_0^R f(r) r^2 \, dr \right]^{-1}, \tag{4}$$

$$\langle R \rangle = \int_0^R f(r) r^3 \, dr \left[\int_0^R f(r) r^2 \, dr \right]^{-1}, \tag{5}$$

$$\langle R^2 \rangle = \int_0^R f(r) r^4 \, dr \left[\int_0^R f(r) r^2 \, dr \right]^{-1} \tag{6}$$

Here $f(r)$ is the spatial star number density of the cluster King model (King, 1962).

In spite of the difficulties, for some clusters, with the density profile approximation by the King formula (large mean square deviations of the parameters), the parameters of these models were used in this work because this allowed to employ a uniform system of structural parameters and to compare these parameters with those for Galactic GCls and Magellanic Clouds clusters.

Besides the King model parameters, the dimensionless OCl halo-core structure parameters were used in this work. The estimates of these parameters were obtained from the histograms of the cluster surface number density distributions (Danilov and Seleznev, 1989).

The value of the cluster radius R obtained from star counts was used as the halo radius. The internal radius of the grid ring that divided the densest central part of the system (core) and a wide region of low density (halo) was used as the core radius R_1. When a transition region of higher density between the core and

1-4-400

the halo is distinctly visible, the outer radius R_1' of this transition (intermediate) region was determined in our work.

It is supposed here that a cluster consists of two components, the core and the halo, that penetrate each other. The surface density of the halo stars in the core region was accepted to be a constant equal to the $F(r)$ value at the cluster core boundary $(r = R_1)$. With this supposition, the star numbers in the core and the halo, N_1 and N_2, and the ratios $\xi = R_1/R$ and $\mu = N_1/N_2$ are determined in our work.

The ξ and μ values are listed in the catalogue of the OCl structural and dynamical characteristics (see Section 7 and Appendix). The values of $\xi' = R_1'/R$ and $\mu' = N_1'/N_2'$ are listed also for the clusters with a transition region. Here the R_1' is the outer radius of the transition region, N_1' is the number of stars in the core and transition region, N_2' is the number of stars in the "outer" halo.

Note that these parameters of the halo-core structure correspond better to Kholopov's (1981) scheme of the cluster halo-and-core division than the King model parameters do.

The $N(r)$ profiles for the clusters NGC 1502, HGC 2420 and IC 1848 were fitted with eq. (3) using the above method for different limiting magnitudes (see Seleznev, 1992). It was demonstrated there that the concentration parameter R/r_c on the average decreased with the increase of the counted stars limiting magnitude. This indicates that brighter stars are more concentrated to the cluster center than lower-brightness stars, and it takes place for both young clusters (NGC 1502, IC 1848) and the old cluster NGC 2420.

4   PHOTOMETRY DATA FOR THE SAMPLE CLUSTERS

The data of photometry (colour-magnitude diagrams) for the sample clusters were used for the determination of the OCl dynamic parameters. The references are listed in Table 1. There are two distance scales that were used in our work: the scale of the mean photometrical distance (hereafter MPD, see Barkhatova and Pylskaya, 1980) and the distance scale based on the zero-age main sequence (ZAMS) by Kholopov (1981).

The MPDs for the sample clusters were taken from the catalogue of Barkhatova and Pylskaya (1980). The values of the MPD for 420 clusters have been obtained there as the mean of the distances determined by different authors with the use of Johnson or Blaauw ZAMS's which were close to each other. The distance according to Arp and Hartwick (1971) was taken for NGC 6838, the only globular cluster in our work. The distance for the cluster King 4 was taken according to Moffat and Vogt (1973) and for Stock 8, according to Malysheva (1990).

The cluster distances corresponding to Kholopov's ZAMS were taken mainly from the catalogue of Barkhatova and Pylskaya (1980), and determined in this work by the method of superposition of the colour-magnitude diagrams with the ZAMS for the rest of the clusters.

Table 1 Photometry data for sample clusters

Name	References	Name	References	Name	References
NGC 103	1	NGC 2254	9	NGC 7086	2
NGC 129	2	NGC 2269	8	NGC 7128	2
NGC 188	3	NGC 2309	–	NGC 7142	–
NGC 381	–	NGC 2323	2	NGC 7226	19
NGC 436	4,5	NGC 2324	2	NGC 7235	2
NGC 457	2	NGC 2335	1	NGC 7245	19
NGC 559	3	NGC 2343	10	NGC 7261	2
NGC 581	2	NGC 2353	2	NGC 7380	2
NGC 637	5	NGC 2355	–	NGC 7419	–
NGC 654	2	NGC 2395	3	NGC 7510	2
NGC 659	3	NGC 2420	11	NGC 7654	2
NGC 663	2	NGC 2423	3	NGC 7788	3
NGC 744	2	NGC 2437	3	NGC 7789	3
NGC 957	2	NGC 2506	12	NGC 7790	3
NGC 1027	2	NGC 6604	13	IC 1369	20
NGC 1245	2,6	NGC 6649	3	IC 1442	19
NGC 1444	2	NGC 6664	3	IC 1805	2
NGC 1502	2	NGC 6694	2	IC 1848	2
NGC 1528	2	NGC 6704	13	IC 2157	4,21
NGC 1582	4	NGC 6705	3	IC 4996	2
NGC 1664	2	NGC 6755	2	Berk 3	22
NGC 1778	2	NGC 6756	14	Berk 8	–
NGC 1857	1	NGC 6802	2	Berk 94	19
NGC 1893	2	NGC 6811	15	Harv 21	23
NGC 1907	2	NGC 6819	16	King 4	24
NGC 1912	2	NGC 6823	2	King 16	–
NGC 1960	2,7	NGC 6830	2	King 19	3
NGC 2126	4	NGC 6834	2	Stock 7	24
NGC 2129	2	NGC 6838	17	Stock 8	25
NGC 2169	2	NGC 6866	2	Tomb 5	26
NGC 2186	8	NGC 6910	2	Tr 1	3
NGC 2194	4	NGC 6913	2	Tr 2	2
NGC 2236	9	NGC 6939	6,18	Tr 35	2
NGC 2244	3	NGC 7031	2		
NGC 2251	2	NGC 7062	2		

References to Table 1: (1) Mermilliod, 1976. (2) Hoag et al., 1961. (3) Hagen, 1970. (4) Barkhatova, 1958. (5) Barkhatova, 1961. (6) Piskunov, 1977a. (7) Barkhatova et al., 1985. (8) Moffat and Vogt, 1985. (9) Ananyeva, student graduation work. (10) Claria, 1972. (11) Sarma and Walker, 1962. (12) McClure, Twarog and Forrester, 1981. (13) Forbes and Du Puy, 1978. (14) Svolopoulos, 1965. (15) Barkhatova, Zakharova and Shashkina, 1978. (16) Auner, 1974. (17) Arp and Hartwick, 1971. (18) Cannon and Lloyd, 1969. (19) Yilmaz, 1970. (20) Hassan, 1973. (21) Grubissich, 1973. (22) Balasz, 1961. (23) Barkhatova and Zhelvanova, 1963. (24) Moffat and Vogt, 1973. (25) Malysheva, 1990. (26) Reddish, 1954.

Colour-magnitude diagrams for the clusters NGC 436, 637, 2126 and 2194 were taken from the diagram atlas of Barkhatova (1958, 1961) and converted from the international stellar magnitude system m_{pg}, m_{pv} into the UBV system using formulae from Martynov (1977). The RGU magnitudes were converted into UBV using formulae of Steinlin (1968) for clusters having the photometry data available in RGU only. The data on interstellar extinction were used in accordance with Janes and Adler (1982).

The cluster ages t, that were listed in the catalogue of Barkhatova and Pylskaya (1980, see references therein), were also used in this work. The age data for the cluster NGC 559 were taken from Lindoff (1969), for NGC 1778, from Barbon and Hassan (1973), for NGC 2335 and 6866, from Wallenquist (1975), for NGC 6838, from Arp and Hartwick (1971), for NGC 7031, from Hassan and Barbon (1973), for Stock 8, from Malysheva (1990), and for IC 1369, from Hassan (1973). For the clusters NGC 637, 1502, 2186, 2254, 2269, 6604, 7142, 7226, 7245, IC 1442, 1848, 2157, King 4 and Stock 7 the ages were determined by the calibration $(B-V)_t - \lg t$ from Janes and Adler (1982). Here $(B - V)_t$ is the colour of the main sequence turn-off point on the cluster colour-magnitude diagram. The $(B - V)_t$ values for these clusters were also taken from Janes and Adler (1982). The $(B-V)_t$ values for the clusters NGC 1582, 1857 and 2126 were determined in this work by the colour-magnitude diagrams (see references in Table 1) and their ages were determined by calibration from Janes and Adler (1982).

5   ESTIMATES OF THE OPEN CLUSTER MASS, TIDAL RADIUS AND RELAXATION TIME

In order to determine the OCl dynamical parameters, estimates of the mean stellar masses $\langle m \rangle$ in clusters up to the limiting magnitude $B_{\lim} = 16^m$ were obtained in this work.

The data of Piskunov's catalogue (1977a) were used for the determination of $\langle m \rangle$ in the clusters NGC 188, NGC 6866 (for both distance scales), NGC 1245, NGC 6819, NGC 6939 (for the MPD scale) and IC 1369 (the distance scale was based on Kholopov's ZAMS). This catalogue was used in the cases when the cluster distance and extinction values accepted there coincided with the values accepted in this work.

The $\langle m \rangle$ estimates for the rest of the clusters were obtained from $(V, B - V)$ diagrams (see references in Table 1) with the use of the Salpeter mass function or with the use of the evolution track system of Paszynski (1970).

The method of the $\langle m \rangle$ determination from the $(V, B - V)$ diagram and the evolution track system was used for clusters with $\lg t \gtrsim 8.6$: NGC 559, 1245, 2194, 2236, 2324, 2420, 2506, 6802, 6819, 6939, 7031, 7789 and IC 1369. This method is analogous to that used by Piskunov (1977a) to obtain the "Catalogue of the Masses and Ages of Stars in 68 Open Clusters".

The errors for the method of individual star mass determination in clusters from photometry data was discussed by Piskunov (1977b). In accordance with the results

of this investigation, the value of 0.25 was accepted in our work for the $\langle m \rangle$ relative error.

For the rest of the clusters ($\lg t < 8.6$), $\langle m \rangle$ was determined under the assumption that the star mass spectrum in the cluster is the Salpeter function $n(m) \propto m^{-2.35}$:

$$\langle m \rangle = \int_{m_{min}}^{m_{max}} m \cdot n(m) \cdot dm \left[\int_{m_{min}}^{m_{max}} n(m) \cdot dm \right]^{-1} \tag{7}$$

Here m_{min} is the mass of the cluster stars having the magnitude of $B_{lim} \simeq 16^m$; m_{max} is the stellar mass corresponding to the top of the cluster colour-magnitude diagram.

The values of $M_c = N_c \cdot \langle m \rangle$ (N_c is the cluster number of stars from counts) were accepted as the lower cluster mass estimates. It is interesting to compare these estimates with other ones. Thus, the mass estimate $M_c = (2330 \pm 680)M_\odot$ (in the MPD scale) was obtained in our work for NGC 6705 (M 11). It is nearly one half of the virial mass estimate 5094 $M_\odot$ for this cluster (Jun-Liang Zhao and Yan-Ping He, 1988) and of the mass estimate of 4671 $M_\odot$ obtained for this cluster from the luminosity function by Mathiew (1984).

The extrapolation of the lower cluster mass estimates obtained in this work to the total cluster mass cannot give a reliable result. The unknown mass function of the OCl low-mass stars is the main cause of that. The use of a different initial mass function and the different suppositions about the lower mass limit for individual cluster stars give a significantly different value of the total cluster mass and the total cluster star number. Furthermore, we do not know the spatial distribution of low-mass stars in the clusters investigated. Then it would not be possible to use the information of the total cluster mass for the purposes of this work. That is why the lower cluster mass estimates are used here. The influence of the lack of information about the low-mass stars from the OCl observations on the results of our investigation is discussed below in more detail.

The lower estimates of the cluster tidal radius R_t and cluster relaxation time τ were obtained in this work with the use of the lower cluster mass estimates M_c and the mean star masses $\langle m \rangle$.

The lower estimates of the cluster tidal radius in the galactic gravitational field were determined using the formula of King (1962):

$$R_t = \sqrt[3]{\frac{GM}{4A(A-B)}}. \tag{8}$$

Oort's constants A and B were determined according to the Galaxy gravitational potential model of Kutuzov and Osipkov (1981):

$$\Phi(R, z) = \Phi_0 \varphi(\xi), \quad \varphi(\xi) = \frac{\alpha}{\beta + \sqrt{1 + \kappa\xi^2}}, \quad \beta = \alpha - 1,$$

$$\xi^2 = (p - \varepsilon^2) + (1 - \gamma)\rho^2 - 1, \quad p^2 = \gamma(1 - \varepsilon^2)\rho^2 + (1 + g)^2, \quad g^2 = \gamma\varepsilon^2\rho^2 + \zeta^2 + \varepsilon^2, \tag{9}$$

$$\rho = R/R_0, \quad \zeta = z/R_0,$$

with $\Phi_0 = 1.76 \times 10^5$ km^2/s^2, $R_0 = 2$ kpc, $\alpha = 2$, $\kappa = 1$, $\varepsilon = 0.1$ and $\gamma = 0$. Here R and z are the galactocentric cylindrical coordinates, R_0 and Φ_0 are the units of length and potential, respectively; ρ, ζ and φ are the dimensionless coordinates and potential; and α, κ, γ and ε are the dimensionless structural parameters of the model. The mass of this Galaxy model is $1.63 \times 10^{11} M_\odot$. The solar galactocentric distance was accepted to be 8.2 kpc, and $z_\odot = 8$ pc (Kutuzov and Osipkov, 1981).

Note that $R_t \propto M_c^{1/3}$, so that a variation of the OCl mass estimate by a factor of two results in R_t variation only by 1.26 times.

The lower estimate of the cluster relaxation time was determined using the formula of Chandrasekhar (1948):

$$\tau_E = \frac{1}{16}\sqrt{\frac{3\pi}{2}}\sqrt{\frac{N\langle 1/R\rangle^{-3}}{G\langle m\rangle}}\frac{1}{\ln\left(N/2^{3/2}\right)}, \tag{10}$$

where $N = N_c$ is the cluster star number, $\langle m\rangle$ is the mean mass of the cluster star and $\langle 1/R\rangle^{-1}$ is the harmonic mean cluster radius.

The errors of these estimates listed in the catalogue (see Appendix) were calculated without taking into account the error of $\langle 1/R\rangle$ (see Section 3). It was noted above that the mean square deviations of the cluster King model parameters were significant for some clusters. The error of τ is strongly underestimated for these clusters. However, the relative error of $\langle 1/R\rangle$ does not exceed 0.2 in the case of the most probable value of the r_c relative error that is about 0.2. This in turn leads to the τ relative error increase by about 0.2.

6 ESTIMATES OF THE NONSTATIONARITY PARAMETERS AND DISRUPTION TIME FOR THE CLUSTERS. THE INFLUENCE OF GAS-DUST CLOUDS WITH DIFFERENT MASSES ON THE OCL DISRUPTION

The presence of gas-dust clouds in the open cluster vicinities puts limitations on the evolution time scale, structure and dynamics of OCls. Starting from the work of Spitzer (1958), the influence of the gas-dust clouds (including giant molecular clouds) on OCls was considered repeatedly by different authors in theoretical estimates (Bouvier, 1971; Wielen, 1985; Danilov and Beshenov, 1987; Danilov, 1987; Danilov and Seleznev, 1988; Wielen 1988) and numerical experiments (Bouvier and Janin, 1970; Terlevich, 1987; Devadas, Ramamani and Alladin, 1987; Danilov and Beshenov, 1988; Danilov, Seleznev and Beshenov, 1989; Theuns, 1992 a, b). Physically similar questions of the stellar system dynamical evolution for other time scales and encounter parameters were considered in numerical simulations of the gravitational perturbations of galactic nuclei during close encounters (or mergers) of galaxies in galaxy clusters (e.g. see Fujishima, Fujimoto and Tosa, 1985 and references therein).

According to Wielen (1987), the dynamic disruption of star clusters can control, to a considerable extent, the observed distribution of the SCl characteristics at the present time. The age distribution of the OCls in the solar vicinities in the Galaxy and the SCl distribution along the radius in the elliptical galaxy M87 contain information about the cluster disruption (Wielen, 1987). The anticorrelation of the distribution of the globular cluster orbits parameters and the distribution of the molecular hydrogen surface density with the distance from the Galaxy centre may imply the efficiency of GMCs and GCls interactions according to Surdin (1986). In the work of Chernoff, Kochanek and Shapiro (1986) the comparison of the GCl "heating" mechanisms by encounters with GMCs and by crossings of the Galaxy disc along the z-coordinate is carried out. It is shown there that the "heating" by the disc field is dominant.

Wielen (1987) considered approximately the disruption mechanisms of the OCls in the solar vicinity by passing-by massive objects such as GMCs and massive black holes (MBHs), the latter ones being assumed to be located in the dark galactic corona. The OCl disruption time estimates obtained by Wielen (1985) agree with the cluster lifetimes based on the OCl age distribution. In a more recent work Wielen (1988) presented a simple procedure of the calculation of the OCl disruption time t_d as a function of the cluster total mass and radius. Star dissipation due to cluster two-body relaxation, external tidal field of the Galaxy and the action of passing-by massive objects were taken into account approximately. This method was applied by Wielen (1987, 1988) for the analysis of the rich SCl disruption in the Large Magellanic Cloud (LMC) and the elliptical galaxy M87. Taking into account the coronal MBHs in M87 allows to account for the SCl observed deficiency in the M87 central regions. With the method suggested, Wielen and Fuchs (1988) discussed the OCl disruption time t_d increase in our Galaxy with the increase of the distance from the galactic centre.

Note that the available estimates of the SCl disruption time t_d can be improved. So, for example, very frequent remote encounters with massive objects almost are not taken into account by Wielen (1985, 1988) and Wielen and Fuchs (1988). It is not correct to introduce factor 1/2 into equation (8) of Wielen (1985) and to use the "impulsive" approximation (Spitzer, 1958) for large impact parameter in eq. (9) of Wielen (1985) because a numerical computation of the corresponding integrals of the "slow" approximation (Spitzer, 1958) is needed. The description of the star escape from a cluster due to the cluster internal relaxation in the work of Wielen (1988) is based on models for dense, highly centrally concentrated, long-lived SCls which evolve during many relaxation times τ. In our opinion, then eqs. (1)–(9) of Wielen (1988) describe inadequately the situation in a real OCl, among which many diffused objects with a small mean density are present that dissipate during the period of order τ. Eqs. (1)–(9) of Wielen (1988) provide a phenomenological description of the dynamics of only one type of the SCl N-body models. All possible ways of the cluster core and halo time evolution are not considered there; the effects of the star escape from the core due to close stellar encounters and from the halo (through the tidal surface) due to the OCl regular field nonstationarity are not isolated, etc. In our opinion, since an acceptable gross-dynamical description of the joint action of

these effects for star clusters is not available now, it is expedient to refuse including these effects when estimating t_d. Then lesser uncertainty is introduced in the t_d value (as compared with using eqs. (1)–(9) of Wielen (1988)), because in that case we can say only about the t_d overestimation. This overestimation is not strong because the resulting t_d estimates are close to the mean lifetime of the clusters in the solar vicinity (Wielen, 1971b).

The interactions of OCls and GMCs were discussed also by Danilov (1987b), Danilov and Beshenov (1987, 1988), Danilov *et al.* (1989) and Theuns (1992a, b). Close and remote encounters of OCls and GMCs were taken into account by Danilov (1987b), corrections to Spitzer's "impulsive" approximation due to the "stretching" of the OCl in the direction of the GMC during the encounter were considered by Danilov and Beshenov (1987, 1988). These works confirm the conclusion that the OCl lifetime in the external galactic field is determined by the encounters with GMCs. However, the external tidal action onto young OCls is not restricted only to the Galaxy field. The tidal field of a giant gas-star complex with mass $2 \times 10^7 M_\odot$. and size up to ~ 1 kpc that accompanies the OCl may give a considerable contribution to the cluster disruption (Danilov and Beshenov, 1988b; Efremov, 1989; Danilov, 1990).

The knowledge of the true GMC characteristics in the solar vicinity such as the cloud spatial concentration, their sizes, masses, velocity dispersion of their motions in the Galaxy, structure, etc. is an important component of the above studies.

Recent Galaxy surveys of $^{13}CO(J = 1 \rightarrow 0)$, a tracer of molecular hydrogen, have resulted in the compilation of GMC catalogues. A catalogue of 273 GMCs in the first Galactic quadrant with the distances up to 16 kpc was presented by Solomon *et al.* (1987). Data on GMCs in the closest solar vicinity up to distances of 1 kpc were published by Dame *et al.* (1987). These data lead to smaller values of the GMC mean mass and number density in the solar vicinity than those accepted earlier for the estimates of the GMC disruptive influences on the OCls (Wielen, 1985; Danilov and Beshenov, 1988). Thus, the mean number density is $\bar{n} \simeq 1.1 \times 10^{-8}$ pc^{-3} with the mean cloud mass of $\bar{M}_{gmc} \simeq 2.2 \times 10^5 M_\odot$ for the GMCs within 3 kpc from the Sun and the mass exceeding $7 \times 10^4 M_\odot$ (Solomon *et al.*, 1987). According to Dame *et al.* (1987), $\bar{n} \simeq 2 \times 10^{-8}$ pc^{-3} and $\bar{M}_{gmc} \simeq 3.4 \times 10^5 M_\odot$ for the GMCs with $M \geq 10^5 M_\odot$. The preference was given here to the data of Dame *et al.* (1987) because the cloud distances were determined there using the whole complex of distance indicators but not using the cloud kinematics only as Solomon *et al.* (1987) did. We consider three GMC mass intervals in the data of Dame *et al.* (1987). The cloud mean number density was determined in our work for each of the following mass intervals:

$$M_{gmc} \in \left[1 \times 10^4; \ 1 \times 10^5\right] M_\odot, \quad \bar{M}_1 \simeq 0.4 \times 10^5 M_\odot, \quad n_1 \simeq 1.6 \times 10^{-8} \text{ pc}^{-3},$$

$$M_{gmc} \in \left[1 \times 10^5; \ 2 \times 10^5\right] M_\odot, \quad \bar{M}_2 \simeq 1.6 \times 10^5 M_\odot, \quad n_2 \simeq 1.4 \times 10^{-8} \text{ pc}^{-3},$$

$$M_{gmc} \in \left[2 \times 10^5; \ 9 \times 10^5\right] M_\odot, \quad \bar{M}_3 \simeq 8.3 \times 10^5 M_\odot, \quad n_3 \simeq 5.4 \times 10^{-9} \text{ pc}^{-3}. \quad (11)$$

In this work we used these GMC number density values for the redetermination of the typical OCl disruption time in the presence of the GMCs and for the evaluation of the nonstationarity degrees of the clusters.

In this work, estimates of the OCl disruption time t_d are presented for the disruption caused by encounters of the OCl with gas-dust clouds of different masses, taking into account the above remarks. Action on the OCl of the tidal field of the Galaxy and the tidal field of gas-star complex that accompanies the OCl is also considered.

A discrete matter distribution in a star cluster and irregular forces are the causes of random "thermal" oscillations of the kinetic and potential energies, T and Ω, respectively, near the virial values T_0 and Ω_0 (Danilov 1987c, Danilov and Beshenov, 1988). In turn, this leads to oscillations of the virial coefficient $\alpha = 2E/\Omega$ ($E = T+\Omega$ being the total cluster energy). The amplitude of the virial coefficient α oscillations is used to characterize the star cluster nonstationarity degree (Danilov, 1985).

The time average of thermal fluctuations $\langle \delta\alpha \rangle_{th}$ is estimated by Danilov (1987c) via the ratio of the volume Q_1, where the irregular forces predominate over the regular force, to the system total volume Q_0. Danilov (1987c) have obtained an estimate of $\langle \delta\alpha \rangle_{th}$ for a nonisolated uniform cluster moving in the Galaxy tidal field:

$$\langle \delta\alpha \rangle_{th} \simeq 0.08 \sqrt{\frac{50}{N}} \kappa \frac{1}{\left[1 - R_0^2 R_t^{-2}\right]^{3/2}}, \tag{12}$$

where N is the number of the cluster stars, $\kappa = \langle m^{3/2} \rangle \cdot \langle m \rangle^{-3/2}$ characterizes the stellar mass spectrum, R_0 is the virial value of the cluster radius, and R_t is the cluster tidal radius in the Galactic force field. The scale factor was determined by the comparison of the Q_1/Q_0 values with the $\delta\alpha$ values, the latter obtained by Danilov (1985) from numerical simulations of a cluster moving along a circular orbit in the Galactic plane with the star number $N = 50$. The dependence $\langle \delta\alpha \rangle_{th} \propto \kappa N^{-1/2}$ was confirmed by numerical N-body experiments with $N = 50 \div 500$ and $\kappa = 1 \div 2.6$ (see, e.g., Danilov and Beshenov, 1988).

In accordance with (12), $\langle \delta\alpha \rangle_{th}$ increases with R_0 tending to R_t. The regular forces of the cluster and the Galaxy, that are mutually opposed in the action on the test star, are nearly balanced in the clusters with a weak concentration of stars to the cluster centre and with the matter density close to the critical value. In this case the total action of the regular forces of the cluster and the Galaxy on the star is close to zero in the mean along the star orbit. Then small changes in the star motions due to stellar encounters lead to sharp and strong changes of the stellar orbits, to nonstationarity and even to the cluster disruption.

Following the method of Danilov (1987c) let us write out an expression for the time average of the virial coefficient thermal oscillations amplitude for the King star number density distribution in the cluster:

$$\langle \delta\alpha \rangle_{th} = 0.08 \sqrt{\frac{50}{N_c}} \kappa \int_0^{r_t} \frac{r^5 \, dr}{\left[x\left(1 - \frac{r^2}{R_t^2 x^{2/3}}\right)\right]^{3/2}} \left[\int_0^{r_t} \frac{r^5 \, dr}{x^{3/2}}\right]^{-1}, \tag{13}$$

$$\kappa = \langle m^{3/2}\rangle \langle m\rangle^{-3/2}, \quad x = \int_{b^{-1}}^{z} \psi(z')\,dz' \cdot \left[\int_{b^{-1}}^{1} \psi(z')\,dz'\right]^{-1}, \quad R_t \propto M_c^{1/3},$$

$$\psi(z) = \frac{\sqrt{b^2 z^2 - 1}}{z}\left[\frac{\arccos z}{z} - \sqrt{1-z^2}\right], \quad b = \sqrt{1 + \frac{r_t^2}{r_c^2}}, \quad z = b^{-1}\sqrt{1 + \frac{r^2}{r_c^2}},$$

where m and $\langle m\rangle$ are the star mass and the mean star mass in the cluster, resp
tively. When $R > R_t$ (R_t is the cluster tidal radius in the external forces field),
integration over r in (13) was taken in the limits $r \in [0, 0.99R_t]$. That is, ext
nal OCl regions were not taken into account for the cluster nonstationarity deg
computation. The mean values $\langle m\rangle$ and $\langle m^{3/2}\rangle$ were obtained with the use of 1
cluster star mass distribution n(m) (see Section 5).

The action on the OCl of encounters with GMCs having different impact 1
rameters p leads to the enhancement of the virial coefficient oscillations amplitu
The cluster "collision" relaxation due to stellar encounters in the cluster leads t
reduction of $\delta\alpha$.

The change of $\delta\alpha$ by the OCl and GMC encounters was investigated in numeri
N-body experiments ($N = 50, 100$) by Danilov and Beshenov (1988) and Danilov
al. (1989). Danilov and Beshenov (1988) have shown that $\delta\alpha$ linearly depends
the cluster kinetic energy increment δT_s, produced during the encounter (δT_s w
calculated using Spitzer's (1958) formula for the impulsive approximation):

$$\delta\alpha = \gamma\delta T_s = (\delta\alpha_{max}\delta T_{max}^{-1})\delta T_s, \tag{1}$$

where $\delta\alpha_{max}$ and δT_{max} are, respectively, the virial coefficient and the kinetic ener
increment that lead to the cluster disruption (see Danilov and Beshenov (1988):

$$\delta T_{max} = (0.7 \div 0.8)|E_0|\left[1 - \frac{12}{5}\cdot\frac{\langle R^{-1}\rangle^{-1}}{R_t}\right], \tag{}$$

where E_0 is the cluster initial total energy,

$$E_0 = -GM_c^2\langle R^{-1}\rangle/4, \tag{1}$$

$\langle R^{-1}\rangle^{-1}$ is the harmonic mean cluster radius and M_c is the cluster mass,

$$\delta\alpha_{max} = (0.85 \div 0.90)\left[1 - \frac{12}{5}\cdot\frac{\langle R^{-1}\rangle^{-1}}{R_t}\right]. \tag{1}$$

It was shown by Danilov et al. (1989) that $\delta\alpha$ depends nearly linearly on κ
$\kappa = 1 \div 1.6$.

The balance of two processes, namely the $\delta\alpha$ increase due to the GMC encount
and the $\delta\alpha$ decrease during the collision relaxation, leads to equilibrium oscillatic
of α with the amplitude of $\langle\delta\alpha\rangle_{eq}$ by the time of collision (two-body) relaxatior
(see Danilov and Beshenov, 1988):

$$\langle\delta\alpha\rangle_{eq} = \xi\tau, \tag{1}$$

where ξ is the rate of $\delta\alpha$ increase due to the OCl and GMC encounters. The ξ value may be evaluated if the linear dependence of $\delta\alpha$ on δT_s is used and the number of the encounters that the OCl experiences in unit time interval is estimated (Danilov and Beshenov, 1988):

$$\xi = \frac{4\pi G}{3V}\langle R^2\rangle M_c\gamma\left\{\sum_{i=1}^{3}\left[n_{\text{gmc}_i}M_{\text{gmc}_i}^{-2}q_{\text{gmc}_i}\int_{p_{\min_i}}^{p_{\max}}L(\beta)p^{-3}\,dp\right]\right\}. \qquad (19)$$

Spitzer's L-function (Spitzer, 1958) appears in the integral over the impact parameters. Its argument is given by

$$\beta = \frac{2\omega p}{V} = \frac{2p}{V}\sqrt{\frac{GM_c}{R^3}}. \qquad (20)$$

The mean distance between GMCs $\bar{r} = \bar{n}_{\text{gmc}}^{-1/3} \simeq 300$ pc was used as $p_{\max}$ (for all the GMCs with $M_{\text{gmc}} > 10^4 M_\odot$, see (11)). The GMC radius from Solomon $et\ al.$ (1987) was used as $p_{\min_i}$:

$$R_{\text{gmc}_i}\left[\bar{M}_{\text{gmc}_i}\right] = \sqrt{\bar{M}_{\text{gmc}_i}\cdot 540^{-1}}. \qquad (21)$$

The summation in (19) was made with respect to GMCs from different mass intervals. Here $\langle R^2\rangle$ is the mean square of the cluster radius, V is the velocity of encounter of the OCl and the GMC. In accordance with eqs. (13), (14) and (19) of Danilov and Beshenov (1988), $\gamma \simeq 1.17|E_0|^{-1}$. Factors q_{gmc} take into account the truncation of the integration region because GMCs are located in a thin layer of the semithickness 87 pc (Dame $et\ al.$, 1987).

The total amplitude of the virial coefficient oscillations in the cluster can be evaluated as

$$\delta\alpha = \langle\delta\alpha\rangle_{\text{th}} + \langle\delta\alpha\rangle_{\text{eq}}. \qquad (22)$$

This value may be regarded as the degree of cluster nonstationarity in the field of regular forces. The results of the OCl nonstationarity degree computation are presented in the catalogue (see Appendix).

The time t_d of the cluster disruption under the action of encounters with gas-dust clouds of different masses were obtained in this work with allowance for the gravitational fields of Galaxy and the gas-star complex (or the HI supercloud), where the cluster is situated. The interstellar cloud parameters used in these computations are listed in Table 2.

The sizes of the clouds of the corresponding types were taken as the lower limits of the impact parameters.

Spitzer's (1958) formulas were used to evaluate the OCl total energy variation ΔE in a single cloud encounter. Only "impulsive" encounters with the OCl were taken into account for "standard" HI clouds. The OCl total energy variation in the time interval dt and for the encounters with the impact parameters from p to $p+dp$ is written as:

Table 2   Parameters of gas-dust clouds

Cloud type	Mean number density n, pc^{-3}	Mean mass M, $M_\odot$	Mean velocity of encounter with the OCl, $pc/Myrs$	Impact parameter interval, pc		References
				p_{min}	p_{max}	
"Standard" HI clouds	4×10^{-5}	200	7	5.8	∞	[1]
GMC $(M > 10^5 M_\odot)$	2×10^{-8}	3.4×10^{-5}	10	$R_{gmc} \simeq 25$	$n_{gmc}^{-1/3} \simeq 370$	[2, 3]
GSC (or HI supercloud)	2×10^{-9}	2×10^7	10	$R_{sc} \simeq 300$	3000	[4, 5]

References to Table 2:
(1) Bouvier and Janin, 1970. (2) Dame *et al.*, 1987. (3) Sanders, Scoville and Solomon, 1985. (4) Efremov, 1989. (5) Elmegreen, 1987.

$$dE = \Delta E 2\pi p \, dp \, V \, dt. \qquad (23)$$

It is necessary to integrate eq. (23) over the impact parameter and to sum up the contributions from the clouds of all types in order to obtain the total cluster energy variation. The disruption time is determined as

$$t_d = \int_{E_0}^{E_*} \left\{ \frac{\pi G^4 M_c^5}{12 q_*^2} \left[\frac{2 n_n M_n^2}{V_{n,OCl}} 2.25 \int_{p_{1,n}}^{\infty} \frac{dp}{p^3} + \right. \right.$$
$$\left. \left. + \frac{n_{gmc} M_{gmc}^2}{V_{gmc,OCl}} q_{gmc} \int_{p_{1,gmc}}^{p_{2,gmc}} \frac{L(\beta) \, dp}{p^3} + \frac{n_{sc} M_{sc}^2}{V_{sc,OCl}} q_{sc} \int_{p_{1,sc}}^{p_{2,sc}} \frac{L(\beta) \, dp}{p^3} \right] \right\}^{-1} E^2 dE. \qquad (24)$$

The terms in square brackets correspond to the contributions into the OCl energy variation due to the interaction with the gas-dust clouds of different types: the first term corresponds to the interaction with "standard" HI clouds, the second term, with the GMCs, and the third term, with HI "superclouds". Here $q_* = \langle R^{-1} \rangle^{-1} \langle R^2 \rangle^{-1/2}$ is the ratio of the harmonic mean cluster radius to its mean-square radius. The factors q_{gmc} and q_{sc} arise because GMCs and HI "superclouds" are distributed in thin layers with the semithicknesses of 100 and 250 pc, respectively. Factor 2.25 is due to frontal collisions with low-mass clouds (in accordance with Bouvier, 1971). The virial theorem condition for the OCl was used in the calculations, according to which $\Omega = 2E$, then

$$\langle R^2 \rangle^{1/2} = \frac{GM_c^2}{4 q_* E}. \qquad (25)$$

Then the encounter parameter β (Spitzer, 1958) can be written as

$$\beta = \frac{2\omega p}{V} = \frac{16(\lambda q_*)^{3/2}}{V G M_c^{5/2}} p E^{3/2}, \tag{26}$$

where $E = |E|$ and $\lambda = \langle R^2 \rangle^{1/2} R^{-1}$, with R the cluster radius. This formula is derived from β in (19) with R expressed in terms of E. In equation (24), E_0 is the cluster energy at the present time and E_s is that at the time of disruption:

$$E_s = -\frac{3}{5}\frac{G M_c^2}{R_t}, \tag{27}$$

where R_t is the OCl tidal radius in the Galaxy gravitational field.

The cluster disruption time computation was carried on in this work allowing for both the Galaxy gravitational field alone and the joint tidal action on the OCl from the Galaxy and the GSC. The tidal radius corresponding to such a joint action was used in (24) (see Danilov, 1990, 1991). The mean parameters from the first part of the catalogue of structural and dynamical OCl characteristics (which correspond to the MPD scale, see Table 4) were taken for the OCl in (24)–(27). The results for the mean OCl characteristics are listed in Table 3.

Table 3   Cluster disruption time (years)

	The Galaxy tidal field alone	Joint tidal field of the Galaxy and the GSC
Joint action of all clouds	7.0×10^8	2.3×10^8
"Standard" HI clouds alone	7.2×10^9	2.3×10^9
Only GMC	8.4×10^8	2.6×10^8
Only HI "superclouds" or GSC	6.4×10^{10}	4.9×10^{10}

It can be seen from Table 3 that the action of GMCs on OCls is the strongest. The cluster heating under the action of the encounters with HI "superclouds" is negligible. However, the force field of the "supercloud" or GSC, which accompanies OCl, reduces noticeably the cluster tidal radius R_t, which leads to a shorter OCl lifetime.

The OCl disruption time close to Wielen's (1985) value is obtained for the following parameters of the heterogeneous HI "supercloud", or the GSC (see Danilov, 1990): $M_{sc} = 2 \times 10^7 M_\odot$, and the semiaxes $\alpha = 300$ pc and $c = 35 \div 100$ pc.

Heating due to encounters with HI "superclouds" was not taken into account when the individual cluster disruption time was calculated (listed in the OCl characteristics catalogue). The disruption time is given by

$$t_{d1} = \int_{E_0}^{E_S} \left\{ \frac{\pi G^4 M_c^5}{12 q_*^2} \left[\frac{n_n M_n^2}{V_{n,\text{OCl}}} 2.25 \frac{1}{R_n^2} + \right. \right.$$

$$+ \frac{1}{V_{gmc,OCl}} \sum_{i=1}^{3} \left(n_{gmc_i} \bar{M}_{gmc_i}^2 q_{gmc_i} \int_{p_{min_i}}^{p_{max}} \frac{L(\beta)\, dp}{p^3} \right) \right]\right\}^{-1} E^2\, dE. \qquad (28)$$

The limits of integration over impact parameters, the GMC characteristics and the values of q are taken as in (19).

The cluster disruption time t_{d2} was also calculated, defined as the time interval between two successive disruptive encounters with the GMCs:

$$t_{d2} = \left\{ \pi V_{gmc,OCl} \sum_{i=1}^{3} \left[p_0^2 \left(\bar{M}_{gmc_i} \right) n_{gmc_i} \right] \right\}^{-1} \qquad (29)$$

These are the encounters with the impact parameter $p \leq p_0$, where p_0 is the critical impact parameter (Danilov and Beshenov, 1988):

$$p_0 \left(M_{gmc} \right) = \left[\frac{M_c \langle R^2 \rangle}{3 \delta T_{max}} \right]^{\frac{1}{4}} \left[\frac{2 G M_{gmc}}{V_{gmc,OCl}} \right]^{\frac{1}{2}} \qquad (30)$$

It was taken into account for clusters with $\lg t > 8.0$ that they can leave the GMC layer when moving in the Galaxy. Here the epicyclic approximation was used for the OCl orbit description. In order to take into account this effect, a factor was introduced into the cloud density; the following quantity was used as the cloud number density:

$$n' = n \frac{2 \langle z \rangle}{\pi \alpha_z}, \qquad (31)$$

where $\langle z \rangle$ is the semithickness of the cloud layer (100 pc for "standard" HI clouds and 87 pc, for the GMCs) and α_z is the semiaxis of the OCl epicyclic motion along z. The α_z value is determined as

$$\alpha_z = \max(z, a_{z,max}), \qquad (32)$$

$$\text{where} \quad \alpha_{z,max} = \frac{V_{z,max}}{\kappa_2} \quad \text{and} \quad \kappa_2^2 = -\left. \frac{d^2 \Phi}{dz^2} \right|_{z=0},$$

z is the cluster z-coordinate; $\alpha_{z,max}$ is the maximum height above the Galaxy plane that can be reached by the cluster having velocity $V_{z,max}$ in the z-direction at $z = 0$; and Φ is the Galaxy gravitational potential. The value of the field stellar velocity dispersion by Wielen (1977) was taken as the $V_{z,max}$ estimate:

$$V = (\sigma_0^2 + c_v t)^{1/2}, \qquad (33)$$

with $\sigma_0 = 10$ km/s, $c_v = 6 \times 10^{-7}$ km^2/(s^2 year) and t, the cluster age. The value of 0.070 km/(s pc) was accepted for κ_2 (see Agekyan et al., 1962, p. 544; Ogorodnikov, 1958, p. 334). The introduction of this factor into the cloud density corresponds to a cloud layer "spreading" along the cluster orbit. It was accepted that $V_{n,OCl} = V_{gmc,OCl} = V$.

The cluster motion outside the cloud layer in the Galaxy was also taken into account for clusters with $\lg t < 8.0$ and $z \gg 100$ pc (NGC 457, 2126 and 2395). Here we adopted $\alpha_z = z$, and $V_{n,\text{OCl}} = V_{\text{gmc,OCl}} = \alpha_z \kappa_2$.

The dynamical OCl parameters obtained, the nonstationarity parameter and the clusters disruption time are listed in the catalogue of the OCl structural and dynamical characteristics (see Section 7 and Appendix).

7 DESCRIPTION OF THE CATALOGUE

The catalogue of structural and dynamical characteristics of 103 OCls is presented in Appendix. It consists of three parts:

the 1st part (Tables A.1.1 and A.1.2) – OCl parameters that correspond to the MPD scale;

the 2nd part (Tables A.2.1 and A.2.2) – OCl parameters that correspond to the distance scale based on Kholopov's ZAMS;

the 3rd part (Table A.3) – the dimensionless parameters of the cluster haloes and cores.

Tables A.1.1 and A.2.1 contain the values of the OCl structural and dynamical parameters:

the 1st column – index number,

the 2nd column – the cluster name (NGC, IC or An),

the 3rd column – the cluster heliocentric distance r in parsecs,

the 4th column – colour excess $E(B - V)$,

the 5th column – the number of stars in the cluster N_c up to the limiting value $B_{\text{lim}} \simeq 16^m$, obtained from star counts,

the 6th column – the cluster angular radius in arc minutes obtained from star counts,

the 7th column – the cluster linear radius R in parsecs,

the 8th column – the cluster core linear radius r_c in parsecs, a parameter of the King model for the cluster star number surface density distribution,

the 9th column – the k parameter of the King model,

the 10th column – the concentration parameter of stars to the cluster centre, R/r_c,

the 11th column – mean cluster radius $\langle R \rangle$,

the 12th column – mean square of the cluster radius $\langle R^2 \rangle$,

the 13th column – harmonic mean cluster radius $\langle R^{-1} \rangle^{-1}$ ($\langle R \rangle$, $\langle R^2 \rangle$ and $\langle R^{-1} \rangle^{-1}$ are determined by averaging with the distribution function $f(r)$ of the cluster star number spatial density that corresponds to the King model),

the 14th column – mean cluster stellar mass $\langle m \rangle$ up to the apparent limiting magnitude $B_{\text{lim}} \simeq 16^m$, in solar masses,

the 15th column – the parameter $\kappa = \langle m^{3/2} \rangle / \langle m \rangle^{3/2}$ that characterizes the dispersion of the cluster star masses,

the 16th column – lower estimate of the cluster mass $M_c = N_c \langle m \rangle$, in solar masses, .

2-3-400

the 17th column – lower estimate of the cluster tidal radius R_t in the Galaxy gravitational field, in parsecs,

the 18th column – lower estimate of the cluster collision (two-body) relaxation time τ, in Myrs,

the 19th column – logarithm of the relaxation time $\lg \tau$ (τ in years),

the 20th column – the cluster age logarithm $\lg t$ (t in years),

the 21st and 22nd columns – the cluster galactocentric cylindrical coordinates R_G and z, respectively, in parsecs.

The sign ">" in Tables A.1.1 and A.2.1 means that large-scale background star number density fluctuations do not allow to determine the radius and star number of the cluster, or the used grid size is not sufficient to reach the cluster border. In that case, we list only the lower estimates of the cluster size and star number (see Danilov, Matkin and Pylskaya, 1985). The sign ">" for the dynamical parameters means that the lower estimates of the cluster radius and star number were used for their determination.

Tables A.1.2 and A.2.2 contain the values of the OCl disruption time and non-stationarity parameter:

the 3rd column – the cluster disruption time t_{d1}, in years, associated with the heating due to encounters with GMCs, in this case only the Galaxy tidal field was taken into account,

the 4th column – the cluster disruption time t_{d2}, in years, defined as the time interval between two encounters with GMCs at the impact parameter less than the critical one, $p \leq p_0$ (the cluster disruption occurs after such encounters),

the 5th column – the critical impact parameter p_0, in parsecs,

the 6th column – the estimate $\langle \delta \alpha \rangle_{eq}$ of the amplitude of the virial coefficient α oscillations ($\alpha = 2E/\Omega$, where E is the total cluster energy and Ω is the potential energy of the cluster) that occur due to encounters of the cluster with GMCs at different impact parameters,

the 7th column – the estimate $\langle \delta \alpha \rangle_{th}$ of the amplitude of the virial coefficient oscillations that occur due to thermal fluctuations,

the 8th column – the value of $\delta \alpha = \langle \delta \alpha \rangle_{eq} + \langle \delta \alpha \rangle_{th}$, which is the regular field nonstationarity degree for the cluster,

the 9th column – the ratio of $\delta \alpha$ to $\delta \alpha_{max}$, which is the oscillation amplitude, that corresponds to the cluster disruption by an encounter with a GMC,

the 10th column – the value of $\delta \alpha_{max}$.

Table A.3 contains dimensionless parameters of the haloes and cores of the open star clusters:

the 3rd column – the ratio of cluster core radius r_c (which is the parameter of the King model for the surface stars number density) to cluster halo radius R (that is determined from star counts),

the 4th column – the ratio of cluster core stars number n_1 to halo stars number n_2 (for the King model; the formula for the spatial stars number density was used to determine this ratio).

Table A.3 also contains the cluster parameters determined from the histogrammes of the surface density distribution (see Section 3):

the 5th column – the ratio of the cluster core radius R_1 to the cluster halo radius R,

the 6th column – the ratio of the cluster core star number N_1 to the halo star number N_2,

the 7th column – the ratio of the transition region outer radius to the cluster halo radius R_1'/R,

the 8th column – the ratio of the core and transition region star number N_1' to the "outer" halo star number N_2' (the parameters R_1'/R and N_1'/N_2' are listed for the clusters having the transition region, see Section 3).

8   THE SAMPLE DESCRIPTION. THE DEPENDENCE OF THE OCL PARAMETERS ON THE ABSOLUTE LIMITING MAGNITUDE

In order to diminish selection effects, the clusters in relatively-narrow intervals of heliocentric distance were selected for this investigation. There were two such intervals: $r \in [1, 1.5]$ kpc and $r \in [1.5, 2.25]$ kpc. In addition, some more remote and closer clusters were included into the sample. Finally 45 clusters have the distance moduli $(m - M)_0 \in [11^m, 12^m]$ and 28 clusters have $(m - M)_0 \in [10^m, 11^m]$ in the first part of the catalogue. In the second part of the catalogue, 33 clusters have $(m - M)_0 \in [11^m, 12^m]$ and 41 clusters have $(m - M)_0 \in [10^m, 11^m]$. The distribution of the distance modulus for the sample clusters is shown in Figure 1.
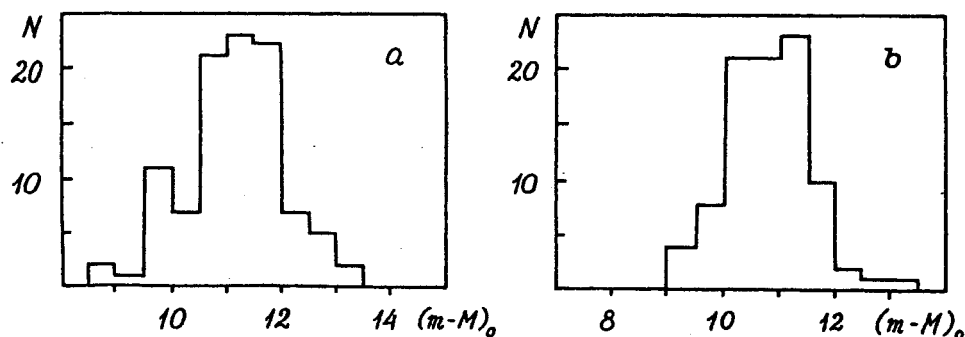
Figure 1   The distribution of the distance modulus for the sample clusters: a) the MPD scale; b) the distance scale according to Kholopov's ZAMS.

If the interstellar absorption of light were absent, this distribution would be also the cluster distribution of the absolute limiting magnitude. However, the absorption washes away this distribution. The distribution of the absolute limiting magnitude of the counted stars $M_{B,\text{lim}}$ is shown in Figure 2 for the sample clusters.

The dependence of the cluster parameters on the absolute limiting magnitude $M_{B,\text{lim}}$ was studied in this work, as well as the influence on the results of the $M_{B,\text{lim}}$ differences between the sample clusters.
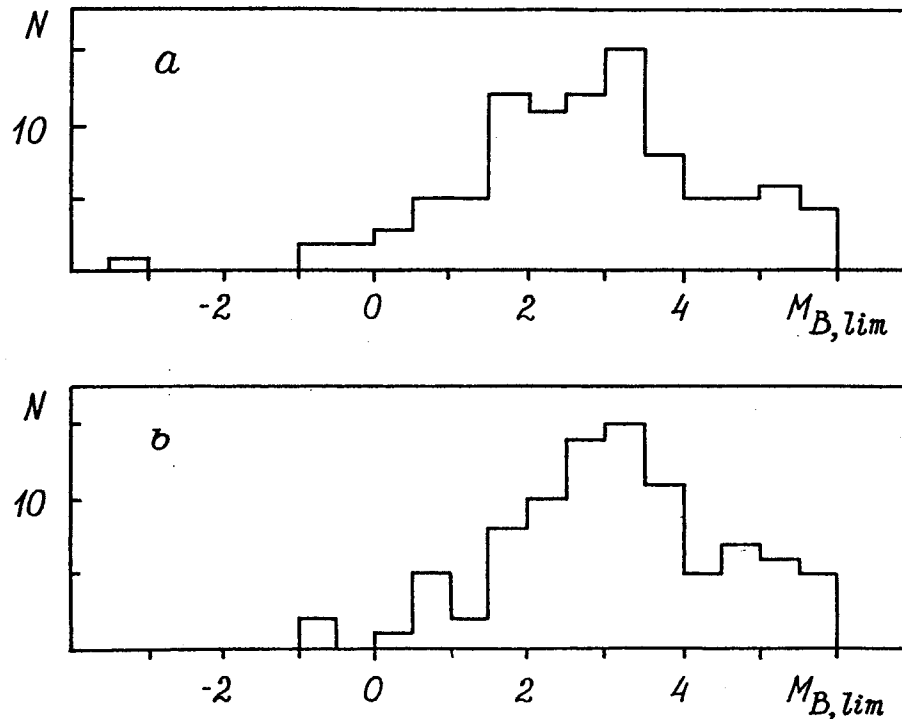
Figure 2   The distribution of the absolute limiting magnitude $M_{B,\mathrm{lim}}$ for the sample clusters: a) the MPD scale; b) the distance scale according to Kholopov's ZAMS.

For this purpose the star counts up to different limiting magnitudes were carried out for the clusters NGC 1502, NGC 2420 and IC 1848 using plates taken with different exposures (see Seleznev, 1992). In addition, the following three statistical approaches were used:

1) the dependences of the cluster individual parameters on the absolute limiting magnitude were obtained;

2) the distributions of the cluster individual parameters for the sample clusters were plotted in different intervals of the absolute limiting magnitude (the interval width was selected to be $1.^{m}5$ as a rule);

3) diagrams of the kind "parameter 1–parameter 2" investigated in this work were also plotted in the selected absolute limiting magnitude intervals.

Note that the cluster star number changes $1.5 \div 1.8$ times if $M_{B,\mathrm{lim}}$ changes by $1.^{m}5$ in the range $M_B \in [1.^{m}1, 8.^{m}7]$ (with the Salpeter mass spectrum and with the use of the mass-luminosity relation from Allen (1977)). However it seems impossible to use narrower intervals of $M_{B,\mathrm{lim}}$ since the sample is small.

The dependence of the cluster star number logarithm (obtained from star counts) on the absolute limiting magnitude is shown in Figure 3 (the distance scale with Kholopov's ZAMS). Solid lines show the results of star counts in three clusters up
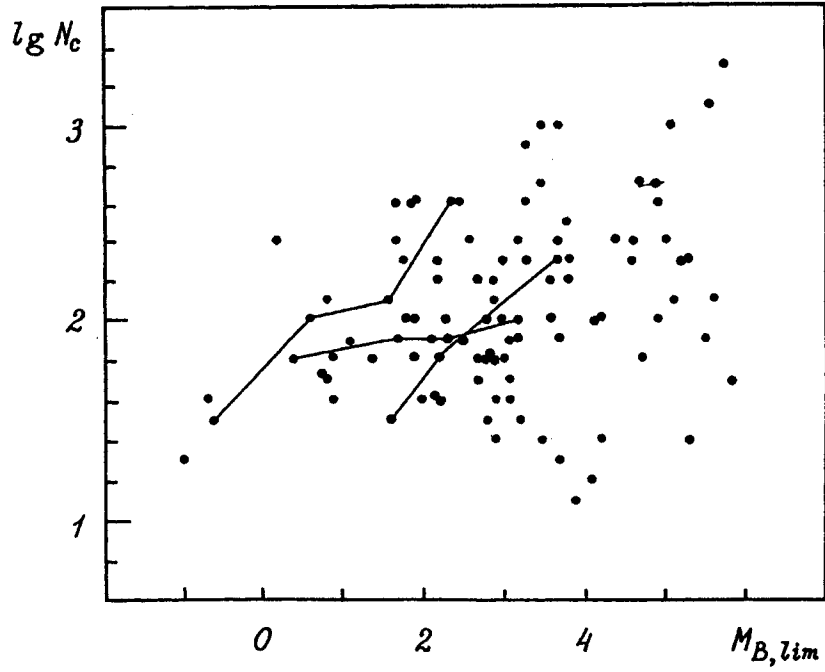
Figure 3 The cluster stars number (from the counts data) is plotted against the absolute limiting magnitude.
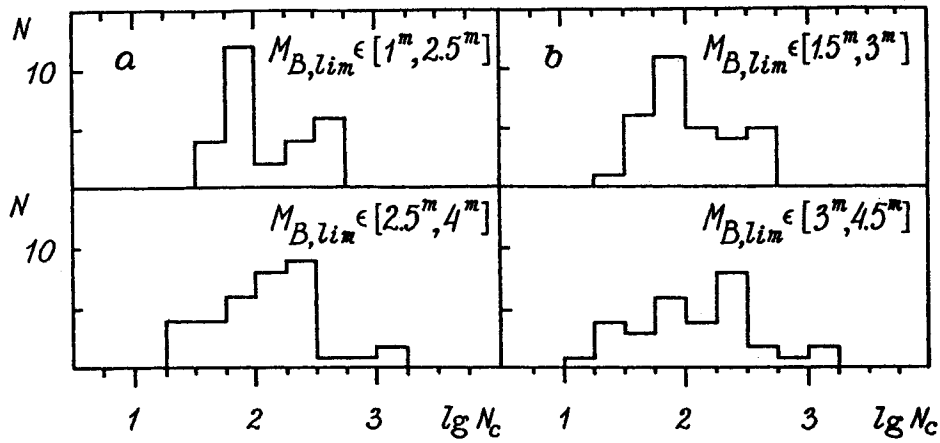
Figure 4 The distributions of the lg N_c values for the sample clusters for different $M_{B,lim}$ intervals: a) the MPD scale; b) the distance scale according to Kholopov's ZAMS.
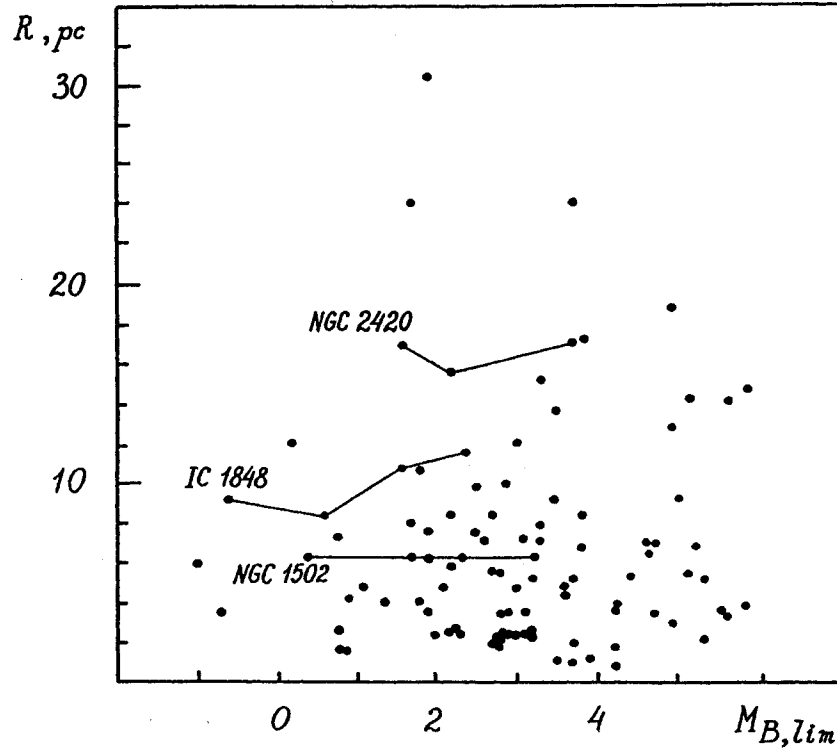
Figure 5   The cluster radius (from the counts data) is plotted against the absolute limiting magnitude.
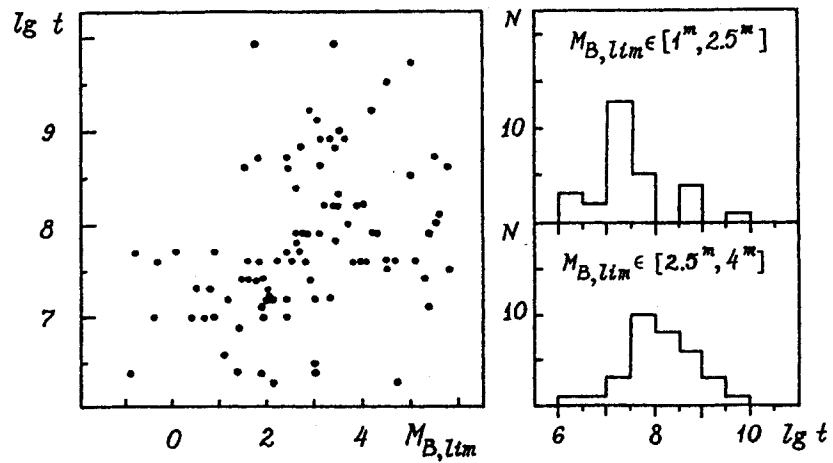
Figure 6   The cluster age selection (the MPD scale).
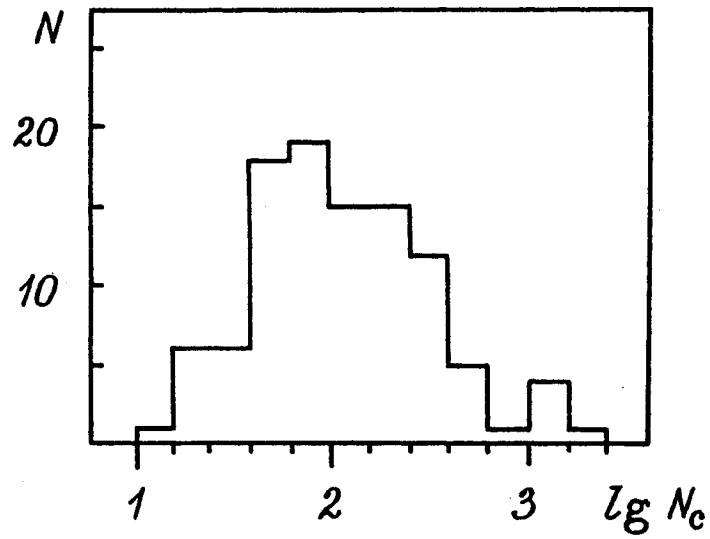
Figure 7 The distribution of lg N_c for the sample clusters.
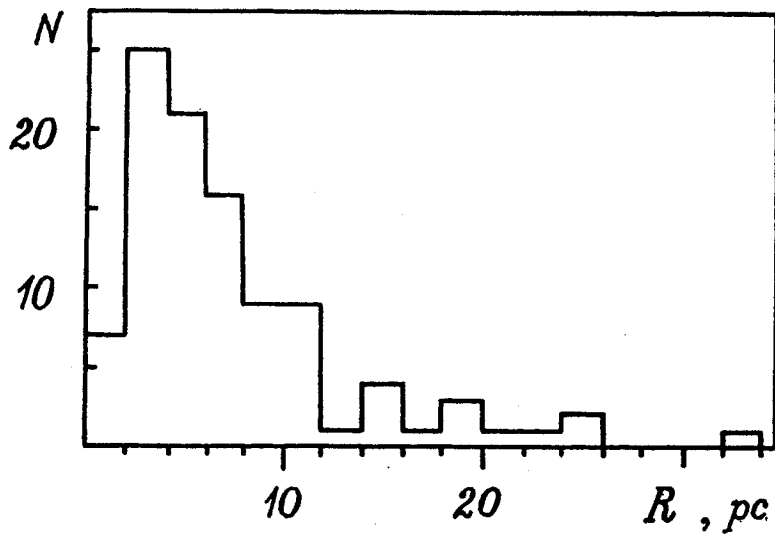
Figure 8 The distribution of the linear radius R for the sample clusters.
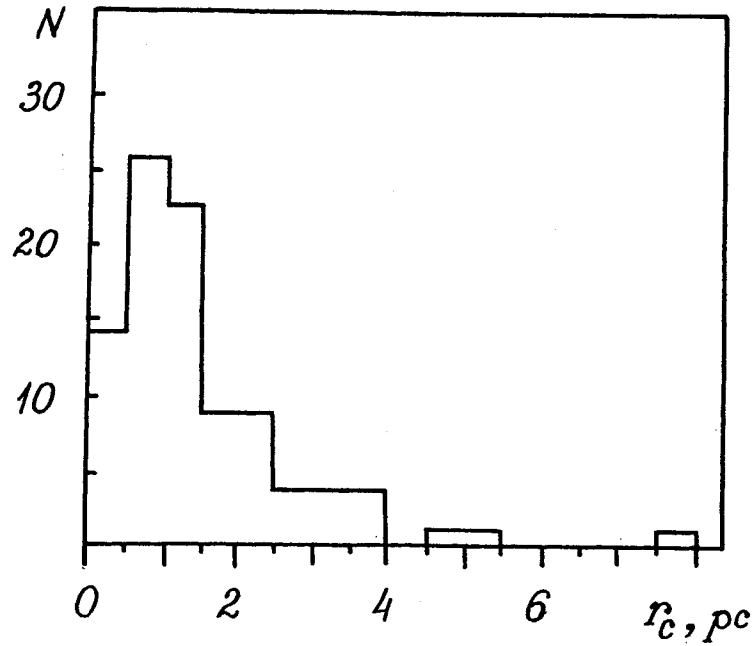
Figure 9   The distribution of the core radius for the sample clusters.
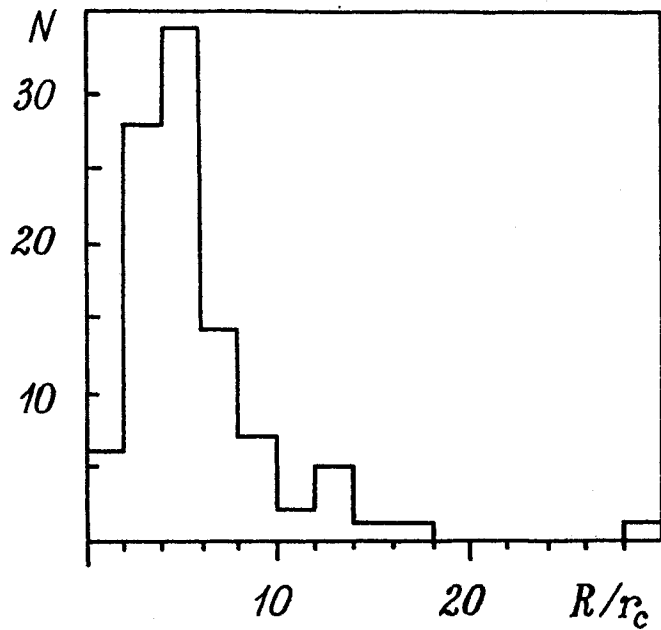
Figure 10   The distribution of the concentration parameter for the sample clusters.
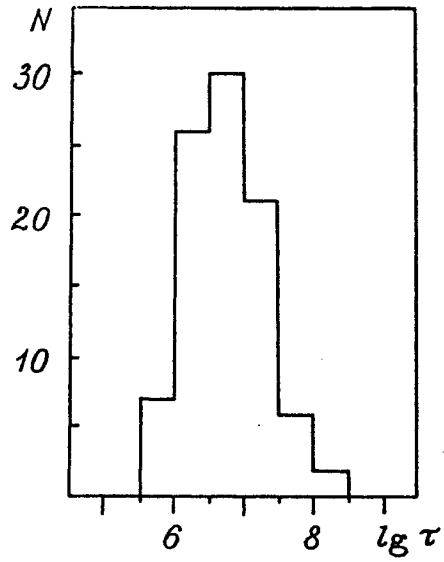
Figure 11 The distribution of the relaxation time for the sample OCls.
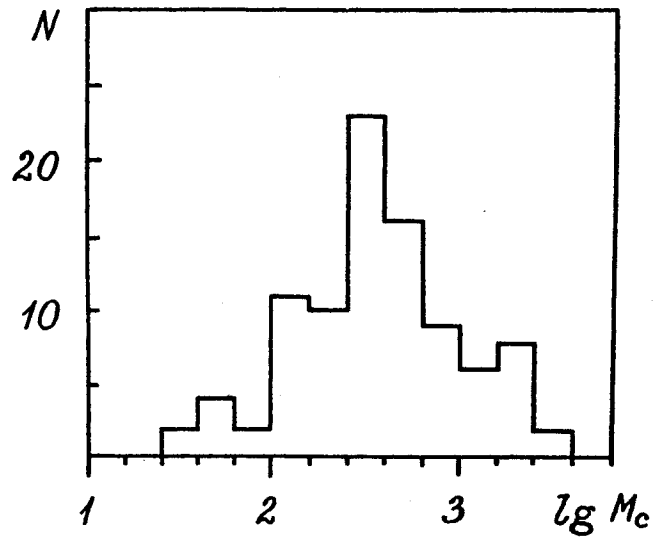
Figure 12 The distribution of $\lg M_c$ for the sample clusters.
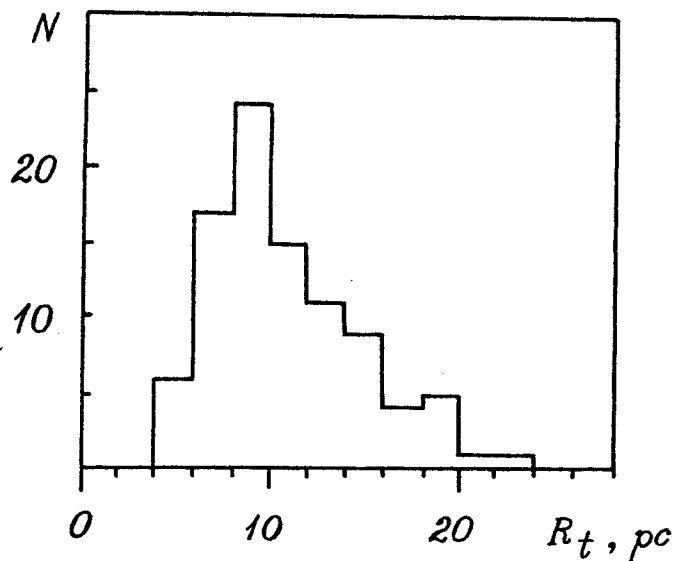
Figure 13   The distribution of the tidal radius for the sample clusters.

to different limiting magnitudes by Seleznev (1992). The increase of the maximum values of $\lg N_c$ with the increase of $M_{B,lim}$ is evident (the upper envelope has a positive slope).

Furthermore, a difference between the cluster distributions of $\lg N_c$ in different intervals of the absolute limiting magnitude can be noted (the distributions do not coincide). These distributions are shown in Figure 4.

The diagram "cluster radius (obtained from star counts) – absolute limiting magnitude" is shown in Figure 5. Solid lines show the results of star counts in three clusters up to different limiting magnitudes (as in Figure 3). The increase of R with the increase of $M_{B,lim}$ can be noted only for IC 1848. Any dependence is not evident for the whole sample.

The dependence of the structural parameters of the clusters NGC 1502, NGC 2420 and IC 1848 on the limiting magnitude of counted stars was discussed in Section 3 (see also Seleznev, 1992). Note that the dependence of the OCl structural parameters on $M_{B,lim}$ is absent on the diagrams like "parameter – absolute limiting magnitude" for the sample as a whole.

The following selection effect was found by the sample investigation: clusters with greater limiting magnitude have greater age on the average. This effect is shown in Figure 6. The "age selection" effect can be explained by the old clusters presence at large z-coordinates (where absorption is small) and by the fact that young clusters with a large number of bright stars are visible, as a rule, at large distances in the Galaxy disc. The role of the age selection effect associated with the $M_{B,lim}$ differences is discussed in Section 9.

The distributions of the structural and dynamical parameters for the sample clusters are shown in Figures 7–13 (parameters correspond to the MPD scale). These distributions are strongly affected by the dispersion of the stellar absolute magnitudes up to which star counts in the clusters were carried out.

The mean values of the structural and dynamical parameters and their dispersions are listed in Table 4 for the both catalogue parts.

Table 4   The mean structural and dynamical parameters of the OCls

Parameter	The 1st part of the catalogue (the MPD scale)	The 2nd part of the catalogue (the distance scale with Kholopov's ZAMS)
1	2	3
Cluster radius R	7.4±5.9 pc	6.6±5.4 pc
Cluster radius logarithm $\lg R$	0.75±0.33	0.70±0.33
Cluster star number N_c	210±290	210±290
Cluster star number logarithm $\lg N_c$	2.07±0.45	2.07±0.45
Concentration parameter R/r_c	5.7±3.9	5.7±3.9
Concentration parameter logarithm $\lg R/r_c$	0.68±0.25	0.68±0.25
Cluster core radius r_c	1.6±1.6 pc	1.4±1.3 pc
Mean cluster radius $\langle R \rangle$	2.5±2.0 pc	2.2±1.8 pc
Harmonic mean cluster radius $\langle R^{-1} \rangle^{-1}$	1.75±1.4 pc	1.5±1.2 pc
Mean square of the cluster radius $\langle R^2 \rangle$	13.±25. pc^2	10.±21. pc^2
Logarithm of the radius mean square $\lg \langle R^2 \rangle$	0.70±0.62	0.59±0.62
Mean mass of cluster star $\langle m \rangle$	3.4±1.6 $M_\odot$	3.1±1.5 $M_\odot$
Cluster mass (lower estimate) M_c	610±690 $M_\odot$	570±640$M_\odot$
Cluster mass logarithm $\lg M_c$	2.56±0.45	2.53±0.45
Cluster tidal radius in the Galaxy force field R_t	10.7±3.8 pc	10.3±3.6 pc
Cluster relaxation time τ, Myrs	13.±22.	11.±19.
Cluster relaxation time logarithm $\lg \tau$	6.73±0.56	6.68±0.54
$\lg \langle \delta a \rangle_{th}$	−0.93±0.34	−0.98±0.35
$\lg \langle \delta a \rangle_{eq}$	−3.2±1.2	−3.4±1.2
$\lg \left[\frac{\langle \delta a \rangle_{th} + \langle \delta a \rangle_{eq}}{\delta a_{max}} \right]$	−0.68±0.44	−0.73±0.41
Cluster disruption time logarithm $\lg t_{d1}$	9.35±0.74	9.52±0.62
Cluster disruption time logarithm $\lg t_{d2}$	9.39±0.49	9.49±0.40

The distributions of the sample cluster parameters R, N_c, R/r_c, r_c, $\langle R^2 \rangle$, M_c, and τ are very asymmetric. These distributions have extended wings. Then the dispersion of these parameters is large and often exceed their mean values. The characteristics of the distribution of the cluster parameter logarithms are listed

in Table 4 in such cases. The distribution of the parameter logarithms is more symmetric, and the logarithm dispersion is smaller than their mean values. Then parameters corresponding to the mean values of their logarithms are closer to the most probable values of these parameters.

9   THE AGE DEPENDENCE OF OCL STRUCTURAL AND DYNAMICAL PARAMETERS

The diagram "$r_c/R - \lg t$" is shown in Figure 14 (r_c/R is the reciprocal of the cluster concentration parameter, see Section 3). It can be seen from this diagram that the objects with a weak concentration to the centre are absent among old clusters. This can be caused by the disruption of OCls with small concentration parameters in the Galaxy force field and by the cluster halo-core structure development either by stellar encounters or by the interaction of stars with the changing average force field in nonstationary star clusters.
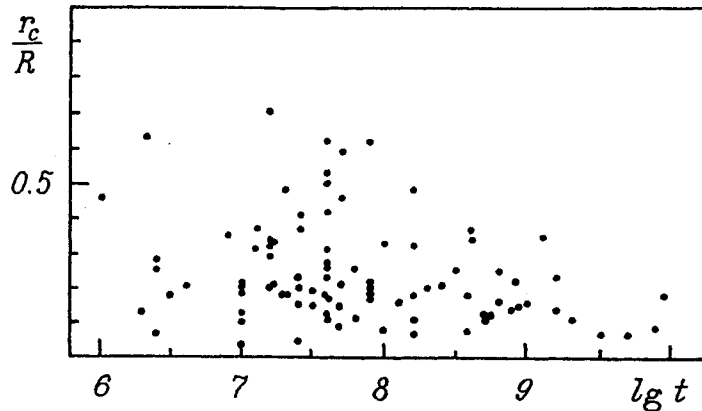
Figure 14   The dependence of the degree of star concentration to the cluster center on the cluster age.

Note that the cluster age selection effect (see Section 8) and the change of the cluster structural characteristics with the limiting magnitude can lead only to weakening this dependence for our sample. Old clusters indeed have greater values of $M_{B,\text{lim}}$ on the average and the r_c/R values increase, on the average, with $M_{B,\text{lim}}$ (Seleznev, 1992).

The distribution of the clusters on the "$R/R_t - \lg t$" diagram is shown in Figure 15 (R is the limiting cluster radius obtained from star counts and R_t is the cluster tidal radius in the Galaxy force field). The points which represent the clusters fill the region between the two dashed lines. The absence of points above the upper line is due to the fast disruption of OCls in this region by the action
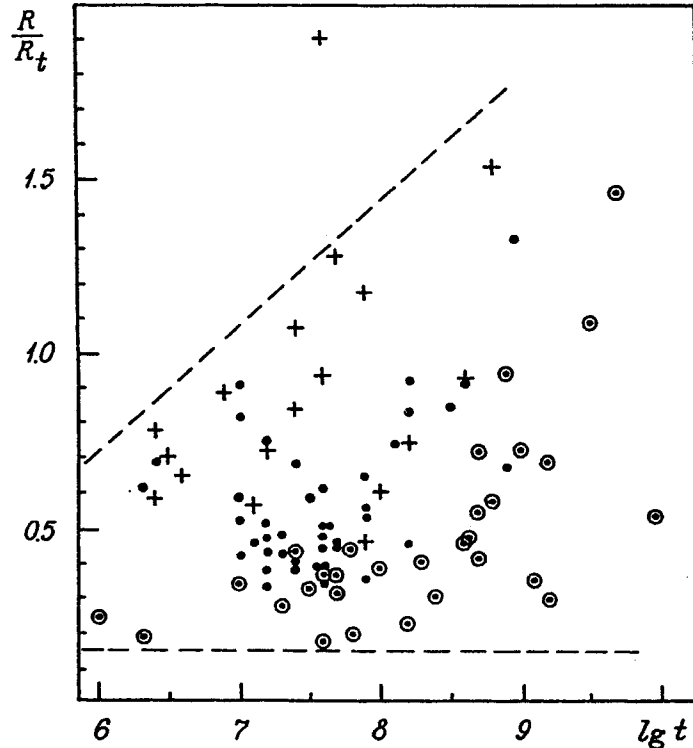
Figure 15   The run of the relative cluster radius R/R_t, in units of the cluster tidal radius, with $\lg t$. Different symbols correspond to clusters with different lifetimes T: •, $\lg T < 9.0$; +, $\lg T \in [9.0, 9.5]$; ⊙, $\lg T \geq 9.5$.

of passing-by gas and dust clouds of different masses. Different symbols denote clusters with different lifetimes,

$$T = t + \min(t_{d1}, t_{d2}). \tag{34}$$

The points near the upper and lower dashed lines correspond to clusters with the minimum and maximum lifetime T, respectively.

The diagram structure was discussed by Danilov and Seleznev (1988a). The absence in our sample of dense OCls , which correspond to the region below the lower line on the plane $(R/R_t, \lg t)$ with $\lg t \leqslant 7 \div 8$, is easily explained by the following. OCls are formed in the GMC cores (see Efremov, 1989). The R/R_t value of an OCl should be of the order of $0.05 \div 0.1$ to form a gravitationally bound cluster (Danilov, 1987a) when the GMC is intensively disrupted due to the radiation of the newborn bright cluster stars. The GMC mass loss from the OCl vicinity leads to a fast growth of the cluster size up to $R/R_t \approx 0.5$ (in the nonstationary conditions during the crossing time $t_{cr} \leqslant 10^7$ years) and to the following OCl stabilization

at $R/R_t \approx 0.28 \div 0.3$ during the time of $10^7 - 10^8$ years (Danilov, 1987a). The upper density limit of the observed clusters with the age of $t > 10^8$ years should be determined by the disruptive action of irregular forces in such OCls (see Figure 5 in Wielen, 1971b). Thus the OCls absence under the lower dashed line can be explained either by a fast broadening of a young OCl during the parent cloud destruction or by the old dense OCl disruption due to the escape of stars under stellar encounters.

The points which represent clusters fill nearly uniformly the region between the two dashed lines. This can be explained for young clusters ($t \leqslant 10^7$ years) by the difference of the initial conditions of cluster formation. For the OCls with $\lg t \sim 7.5 \div 9.5$, the scatter of the points along the R/R_t axis can be explained by two reasons:

1. Some of the OCls considered are projected onto the nonuniform stellar background. Due to the large-scale background fluctuations, it is difficult to trace the cluster halo at large distances from the OCl centre (see Danilov, Matkin and Pylskaya, 1985).

2. The OCl nonstationarity and repeated "stabilizing" escape of a portion of the cluster stars from the outer cluster regions into the Galaxy field can be one of the reasons of the scatter of the points along the R/R_t axis in Figure 15. A similar situation was considered in numerical experiments of Danilov (1985, see models 4 and 5). In that work, the dynamics of an OCl consisting of 50 stars of equal mass and moving along circular or "box" orbits in the Galaxy force field with the Galaxy potential taken according to Kutuzov and Osipkov (1981) and with the parameters listed in Section 5 is simulated. Such an escape can be probably caused by both the OCl passing over the pericentre of the galactic orbit (Danilov, 1985) and an encounter with GMC. The outer cluster regions are broadened in the nonstationary conditions, the stars with the greatest (positive) energies are lost. The total OCl energy becomes smaller and the cluster contracts under the critical surface with the subsequent relaxation and new halo-core structure formation.

It can be seen from Figure 15 that with the increase of the cluster age (on the average) they fill the volume under the tidal surface to a greater extent. Almost all young OCls are known to be located in regions of active star formation in the Galaxy, i.e., in massive, extended GSCs. Old OCls avoid the complexes (Efremov, 1989). The joint action of the force fields of the GSC and the Galaxy onto young OCls can lead to the observed decrease of the cluster tidal radius by $1.5 \div 2.5$ times (Danilov, 1990, 1991) and provide the observed dependence of the maximum R/R_t values on cluster age.

A great extent of the coronas of the old OCls NGC 188, M 67 and NGC 752 and a more compact structure of young clusters were known earlier (see, e.g., Figure 127 and Table 8.1 in Kholopov, 1981).

Note that young clusters have, on the average, shorter lifetimes (see Wielen, 1971a, b). This is hardly consistent with the fact that their stars are deeper under the tidal surface because then the cluster disruption time is longer. The tidal action of the gas-star complex onto young OCls equalizes the R/R_t values for clusters of different ages and eliminates the discrepancy between the OCl lifetimes and disruption times.

The distribution of the clusters on the diagram "$R/R_t - |z|$" can be explained in the same way. It can be seen from Figure 16 that the clusters situated deep under the tidal surface of the Galaxy gravitational field are absent at large z-coordinates. The GSC tidal field affects the clusters near the Galaxy plane, thereby equalizing the R/R_t values for clusters at different z.
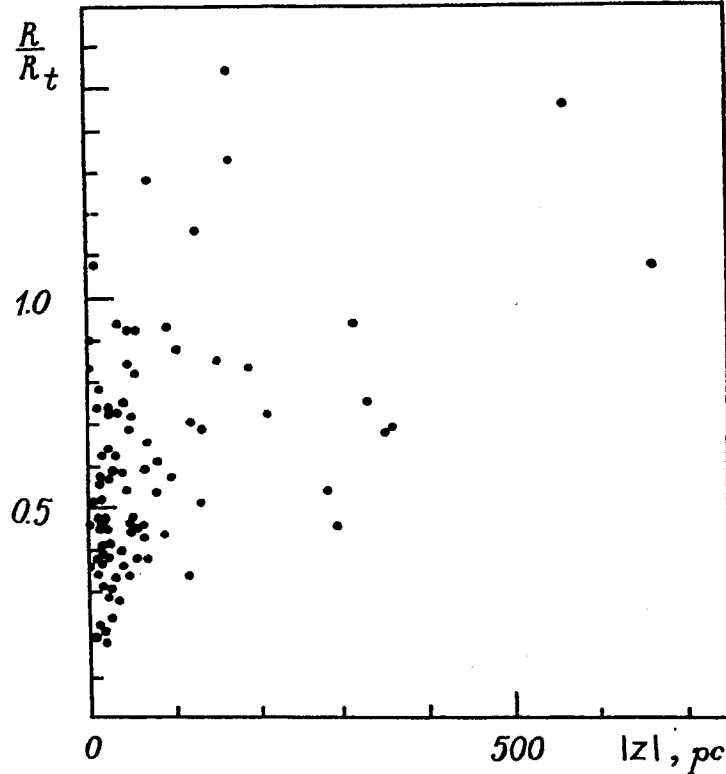
Figure 16   The run of R/R_t with $|z|$.

Let us discuss the possible influence of selection onto the diagram "$R/R_t - \lg t$". As noted above, the increase of the cluster radius with the $M_{B,\lim}$ increase was found only for IC 1848 when the star counts in three clusters were carried out up to different limiting magnitudes. However, this cluster radius and star number have increased by 1.25 and more than 10 times, respectively, with the $M_{B,\lim}$ change by 3^m (see Figures 3, 5). Thus R/R_t does not increase with $M_{B,\lim}$ for the clusters investigated ($R_t \propto M_c^{1/3}$). Because of that the dependence of maximum R/R_t values on $\lg t$ is not caused by the age selection (see Section 8).

The appearance of the diagram in Figure 15 is determined by the presence of some very extended old and middle-aged clusters. Thus, if we select a narrow $M_{B,\lim}$ interval where a sufficient number of clusters with different ages are present, then

3-2-400
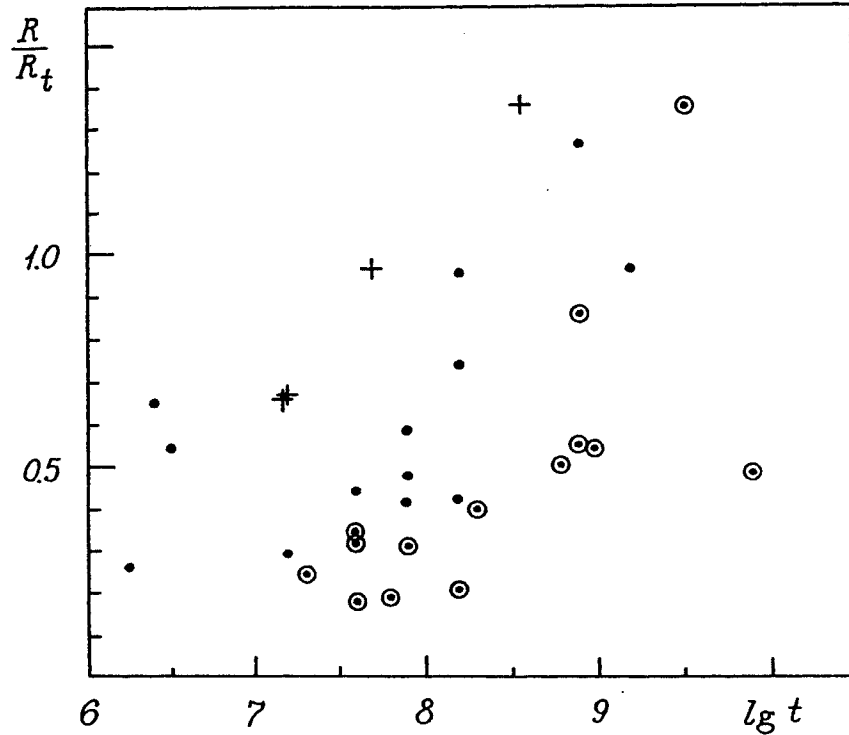
Figure 17   The run of R/R_t with $\lg t$ for the clusters with $M_{B,\lim} \in [3^m, 4^m5]$ (the distance scale according to Kholopov's ZAMS).

the dependence of R/R_t on $\lg t$ will be preserved. This is shown in Figure 17. These arguments confirm the reality of the dependence of maximum R/R_t values on $\lg t$.

The OCl characteristics, that correspond to the MPD scale, were used in Figures 15 and 16.

10   THE DYNAMICAL STATE OF THE SAMPLE CLUSTERS

The distributions of $\lg\langle\delta\alpha\rangle_{th}$ and $\lg\langle\delta\alpha\rangle_{eq}$ are shown in Figure 18 and Figure 19, respectively, for the sample clusters. We recall that $\langle\delta\alpha\rangle_{th}$ is the amplitude of the virial coefficient oscillations due to thermal fluctuations (the GSC tidal action onto the cluster was neglected when calculating this quantity) and $\langle\delta\alpha\rangle_{eq}$ is the amplitude of the α oscillations due to encounters with GMCs. Taking into account the GSC tidal field action onto the sample clusters leads to a sharp increase of $\lg\langle\delta\alpha\rangle_{th}$.

It is seen from the comparison of the $\lg\langle\delta\alpha\rangle_{th}$ and $\lg\langle\delta\alpha\rangle_{eq}$ values that encounters of OCls and GMCs on the average provide only a small additional increase of the
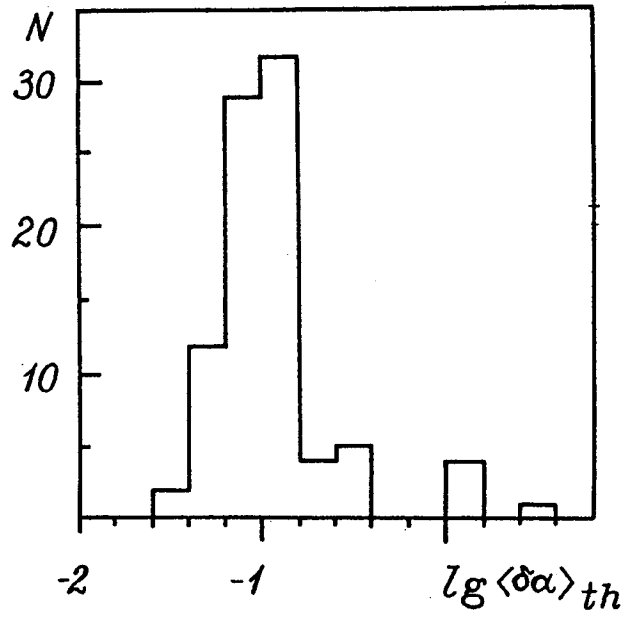
Figure 18   The distribution of lg⟨δα⟩$_{th}$ for the sample clusters.
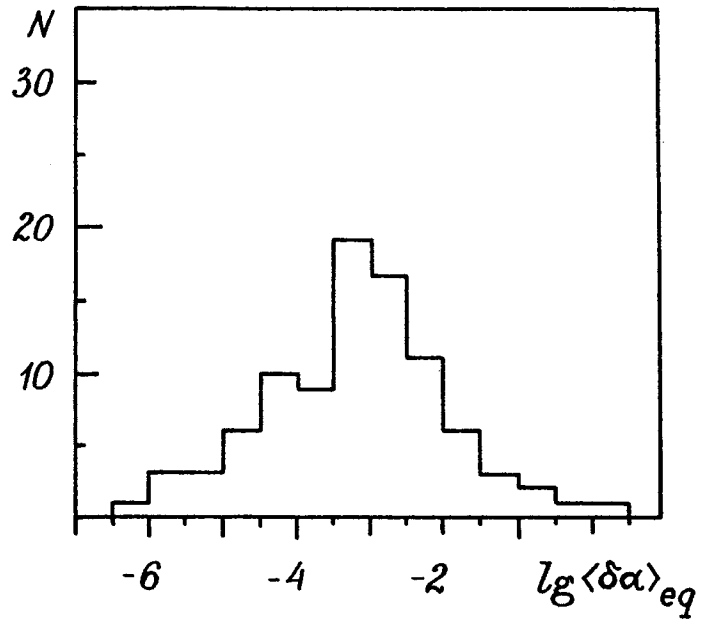
Figure 19   The distribution of lg⟨δα⟩$_{eq}$ for the sample clusters.

cluster nonstationarity degree as compared with irregular forces within the clusters.
However, the encounters of OCls and GMCs in the presence of the force fields
of GSC and the Galaxy determine the cluster disruption time and the period of
the increase of the cluster energy, size and oscillation amplitude up to the critical
values (see Section 6). Thus, encounters of OCls and GMCs determine finally (by
means of stellar encounters in the clusters in the presence of external regular force
fields) the OCl nonstationarity degree and the amplitude of the OCl virial coefficient
oscillations: $\delta\alpha = \langle\delta\alpha\rangle_{th} + \langle\delta\alpha\rangle_{eq}$.
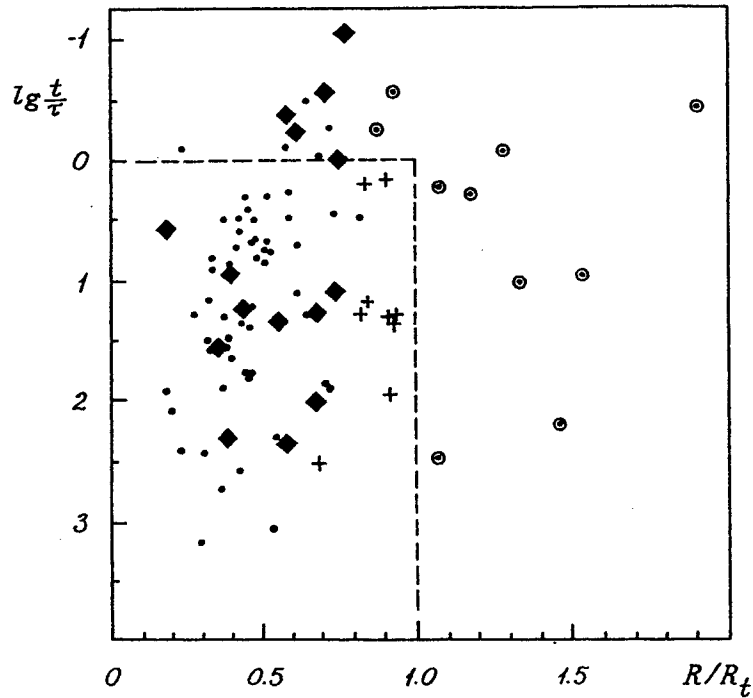
Figure 20 The diagram $(\lg t/\tau, R/R_t)$. Different symbols label clusters with $\delta\alpha/\delta\alpha_{max} = \eta$ in different intervals: •, $\eta < 0.2$; ◆, $\eta \in [0.2, 0.3]$; +, $\eta \in [0.3, 1]$; ⊙, $\eta \geq 1$.

The cluster distribution on the plot of $\lg (t/\tau)$ against R/R_t is shown in Figure 20
(τ is the collision relaxation time of OCl). The clusters shown in this diagram
beyond the region outlined by the dashed line, either have not reached a steady
state due to their small age ($t < \tau$) or deviate strongly from the steady state due
to a great extent of their coronal regions.

Different symbols in Figure 20 correspond to clusters with different nonstationarity degrees in the units of $\delta\alpha_{max}$ (it is the amplitude of virial coefficient oscillations
that correspond to the OCl disruption by an encounter with a GMC, see Section 6).

The clusters NGC 103, NGC 188, NGC 581, NGC 1027, NGC 1893, NGC 2324,
NGC 2420, NGC 2437, NGC 6664 and NGC 7789 significantly deviate from the

regular field stationarity. These clusters have $\eta = \delta\alpha/\delta\alpha_{\max} > 1$. All these clusters have extended haloes whose sizes are comparable with those of the tidal stability regions in the Galaxy force field or exceed them.

The clusters NGC 1857, NGC 2186, NGC 2194, NGC 2236, NGC 2506, NGC 6819, NGC 6823, NGC 6866 and NGC 7790 also have extended haloes ($R \gtrsim 0.8 R_t$), consequently they have large nonstationarity degree ($\eta \geq 0.3$).

Our sample contains also young clusters which, probably, have not reached the steady state due to their small age: NGC 457, NGC 663, NGC 1502, NGC 2126, NGC 2244, NGC 6830, NGC 7128, IC 1805, IC 1848 and Stock 8. Totally, there are 32% of clusters in our sample that significantly deviate from the regular field stationarity due to one of the above reasons. This is an underestimation because the GSC force field was not taken into account for the calculation of the OCl tidal radius and the nonstationarity degree in the case of young clusters.

We note that the values of $\langle R \rangle / R_t$ and results of numerical experiments of Danilov (1985) were used for the estimation of the cluster dynamical state by Danilov and Seleznev (1988).

The OCl characteristics that correspond to the MPD scale were used in Figures 18–20.

11   PARAMETERS OF CLUSTERS HALO-CORE STRUCTURE

The above estimates of the OCl destruction rate indicate that the OCl lifetime in the solar vicinity is determined by external causes with respect to the cluster (that is, encounters of the OCl and GMCs in the total gravitational field of the Galaxy and the gas-star complex, see Section 6). The external causes also affect to a certain extent the cluster evolution rate (accelerating it). The efficiency of the irregular force action in clusters increases in the presence of external tidal fields (see, e.g., Danilov, 1976). The encounters of the OCl and GMCs lead to the increase of the amplitude of the cluster regular field oscillations, which in turn also speeds up the OCl evolution (see Section 6).

In accordance with Danilov (1988a, b; 1989), the development of the halo-core structure in models of isolated clusters is determined by relaxation processes due to stellar encounters inside the OCl or due to interactions of the stars with the changing regular field of the cluster (in nonstationary systems with a large star number, $N_c > 250$).

As mentioned above, the observational data on the OCl structure can be useful in resolving the following question. Is the OCl structure (density profiles) determined by the internal relaxation processes in the cluster or by external causes associated with the action of the GMCs, GSC and Galaxy force fields onto the cluster?

The data on the sizes and populations (star numbers) of the cluster haloes and cores can be considered as the most reliable when the OCl density profiles are analyzed.

Dimensionless parameters of the OCl haloes and cores, $\xi = R_1/R$ and $\mu = N_1/N_2$, for the sample clusters are shown in Figures 21 and 22 (see Section 3).

3-4-400

We recall that R_1 is the cluster core radius (in accordance with the definition of Kholopov, 1981), and N_1 and N_2 are the star numbers in the cluster core and halo, respectively.

It is easy to see that the sample clusters group near some line $\xi = \xi(\mu)$ on the plane (ξ, μ). Circles in Figure 22 mark the values of (ξ', μ') for the cluster transition region (see Section 3).
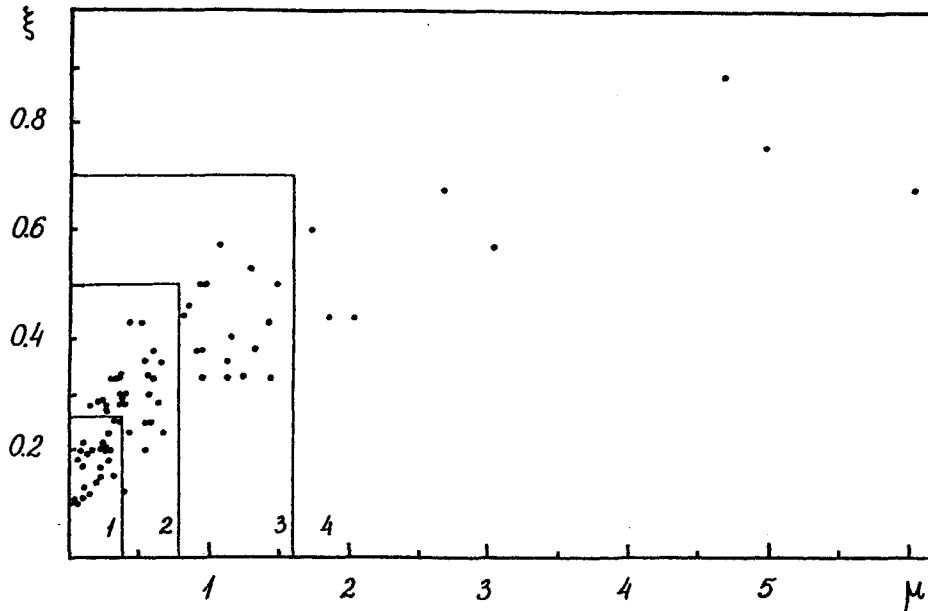
Figure 21   The (ξ, μ) diagram for the clusters with $R \leq 0.8R_t$ (in accordance with the MPD scale).

The diagram (ξ, μ) in Figure 21 is divided by straight lines into the regions that are marked with numbers 1–4. The mean logarithm of the OCl ages and their dispersion for these regions are equal to:

$$\langle \lg t \rangle_1 = 7.64 \pm 0.65,$$

$$\langle \lg t \rangle_2 = 7.76 \pm 0.84,$$

$$\cdot \langle \lg t \rangle_3 = 7.76 \pm 0.76,$$

$$\langle \lg t \rangle_4 = 7.31 \pm 0.89.$$

Thus, the mean cluster ages are not significantly different from each other along the $\xi = \xi(\mu)$ sequence on the (ξ, μ) diagram, though the clusters belonging to region 4 are younger on the average than the clusters from the other regions.

Evolution tracks for quasistationary and nonstationary isolated cluster models are shown in Figure 22 with smooth and broken solid lines, respectively, in accordance with Danilov's (1988a, b; 1989) calculations. The dynamical evolution of
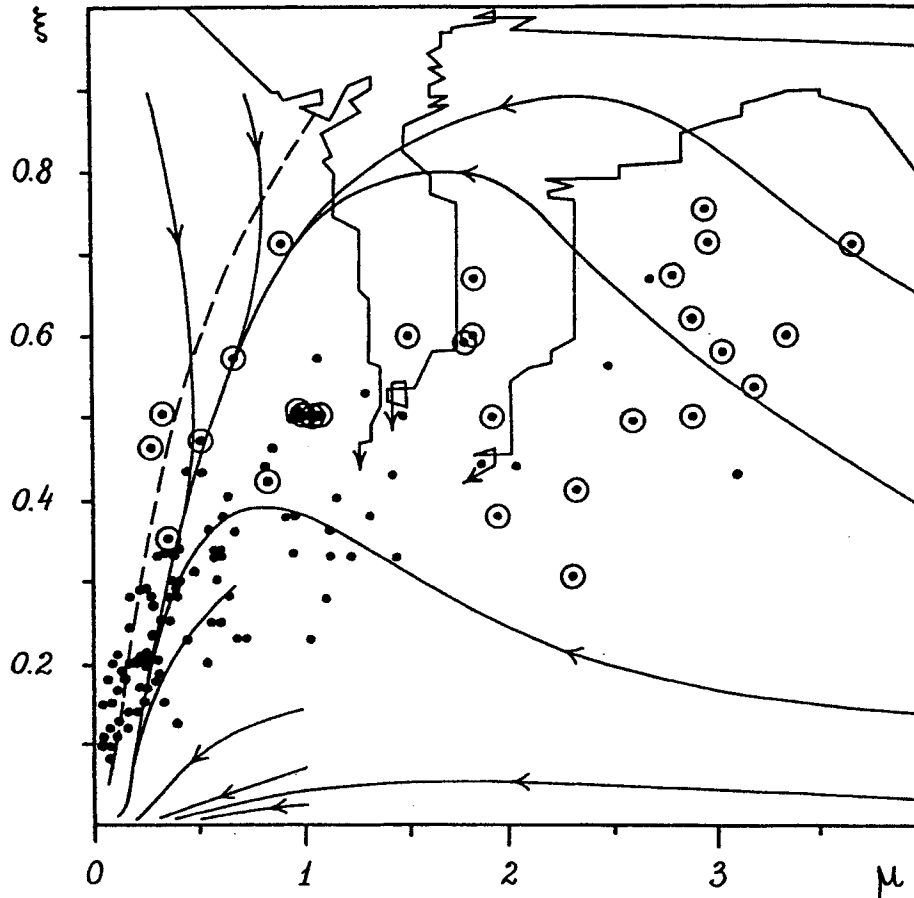
Figure 22   The (ξ, μ) diagram. Solid smooth and broken lines present evolution tracks of quasistationary and nonstationary isolated cluster models, respectively.

these models proceeds, under the action of stellar encounters, along the tracks in the directions shown by arrows. The dashed line in the (ξ, μ) diagram (see Figure 22) corresponds to the equilibrium in the process of exchange of stars between the core and the halo of quasistationary OCl models. The nonstationarity reduces the slope of the dashed line for $\xi \geq 0.4$, which brings it closer to the cluster sequence at the (ξ, μ) diagram. The period during which a cluster is at a considerable distance from the dashed line in the (ξ, μ) diagram is less than the time of the OCl evolution along the dashed line (Danilov, 1988a, b) by more than an order of magnitude.

Thus, a fast cluster dynamical evolution in the direction of this sequence at large separation from the dashed line on the plane (ξ, μ) can be one of the causes of the OCl clustering along this sequence. The cluster formation near this sequence can be another cause of the OCl clustering there, because clusters of different ages
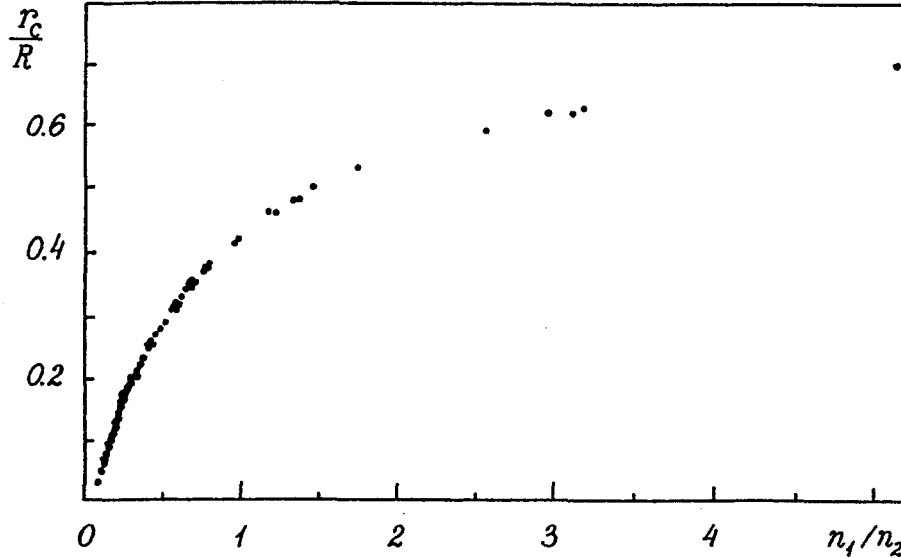
Figure 23   The diagram $(r_c/R,\ n_1/n_2)$ for the King model of the surface density distribution in the sample clusters (see Sections 3 and 7).

(including $t \sim 10^6$ years) are situated along this sequence in the (ξ, μ) diagram. The absence of clusters in the right lower corner of the (ξ, μ) diagrams in Figures 21 and 22 may be a consequence of the difficulty of revealing very extended rarefied haloes near dense cluster cores against the background of the field star density fluctuations.

The ξ and μ values are shown in Figure 21 for the clusters with the halo radius $R \leq 0.8R_t$ where R_t is the cluster tidal radius in the Galaxy force field. Note that the use of the condition $R \leq 0.8R_t$ reduces the scatter of the points around the general sequence in Figure 21. Then the causes of the star cluster grouping near this sequence are confirmed to be not connected with the presence of the external galactic field. The (ξ', μ') values corresponding to the transition regions in the cluster density profiles are not shown in Figure 21.

The dependence $\xi = \xi(\mu)$ in Figure 21 can be fitted by $\xi = 0.39\mu^{0.35}$, or

$$\frac{R}{R_1} = \frac{1}{0.39} \left[\frac{N - N_1}{N_1} \right]^{0.35}, \tag{35}$$

where N is the cluster star number. If $N_1' \ll N$ and weak dependence of N_1 on N is assumed, then

$$\frac{R}{R_1} \propto N^{0.35}. \tag{36}$$

A similar dependence for star clusters was found by Kholopov (1981).

The dependence $\xi = \xi(\mu)$ agrees well with that obtained for the King model parameters for the sample clusters (the 3rd and 4th columns of Table A.3). This dependence is shown in Figure 23.

The agreement of the observational estimates of ξ and μ with the results of isolated cluster dynamics simulation indicates that the formation and development of the halo and core in the OCls are controlled largely by internal relaxation processes, i.e., by irregular forces within the cluster. The influence of external force fields on the cluster halo-core structure is less important.

12 THE OCL SIZES NEAR GAS-STAR COMPLEXES

The distribution of OB-associations and OCls of different ages in the Galaxy plane within 3 kpc from the Sun was analyzed by Efremov and Sitnik (1988). It was shown that the OB-associations and open star clusters containing stars of O-B2 spectral classes are concentrated near some gas-star complexes. These GSCs contain GMCs of the masses $\geq 10^5 M_\odot$. Some of these complexes are associated with giant clouds of neutral hydrogen (HI superclouds). A hierarchical structure is observed in the complexes: several neighbouring complexes form a supercomplex of the sizes of about 1.5 kpc. These complexes and the associated massive objects are listed by Efremov and Sitnik (1988). The Galaxy plane projected distribution of the complexes is shown in Figure 24.

The force field of such gas-star complexes can play an important role in the dynamics of young OCls which are probable complex members. The OCl tidal size in the combined field of Galaxy and GSC was considered by Danilov (1990, 1991) and Danilov and Beshenov (1992). The clusters were investigated there that move jointly with the complex and that move apart from the complex. In accordance with these works, the cluster tidal radii in the combined field of a stationary GSC and the Galaxy decrease with the moving away from the complex centre inside the complex and increase outside it up to the values typical of the OCls in the Galaxy field.

The dependence of young OCl sizes on the distances to the gas-star complex centres is investigated in this work. The data of star counts in 85 OCls from our sample were used. These are the clusters that have their distances from the Sun listed in Becker and Fenkart (1971) and Fenkart and Binggeli (1979). The distance scale of Becker and Fenkart was used because Efremov and Sitnik's (1988) work was based on this scale. The points in Figure 24 show the clusters of the sample. The points marked by circles correspond to the clusters with $\lg t > 8.5$.

In order to diminish the scatter of the OCl sizes, the reduced clusters radii were used in this work:

$$R' = R \left[\frac{\langle M \rangle}{M} \right]^{1/3}, \tag{37}$$

where R is the limiting OCl radius obtained from star counts, M is the lower estimate of the OCl mass and $\langle M \rangle = 380 M_\odot$ (this value corresponds to the most probable value of the logarithm of the cluster mass lower estimate in our data). The cluster linear radii and masses correspond to the distance scale of Becker and Fenkart. The use of R' values reduces the radius of every sample cluster to the
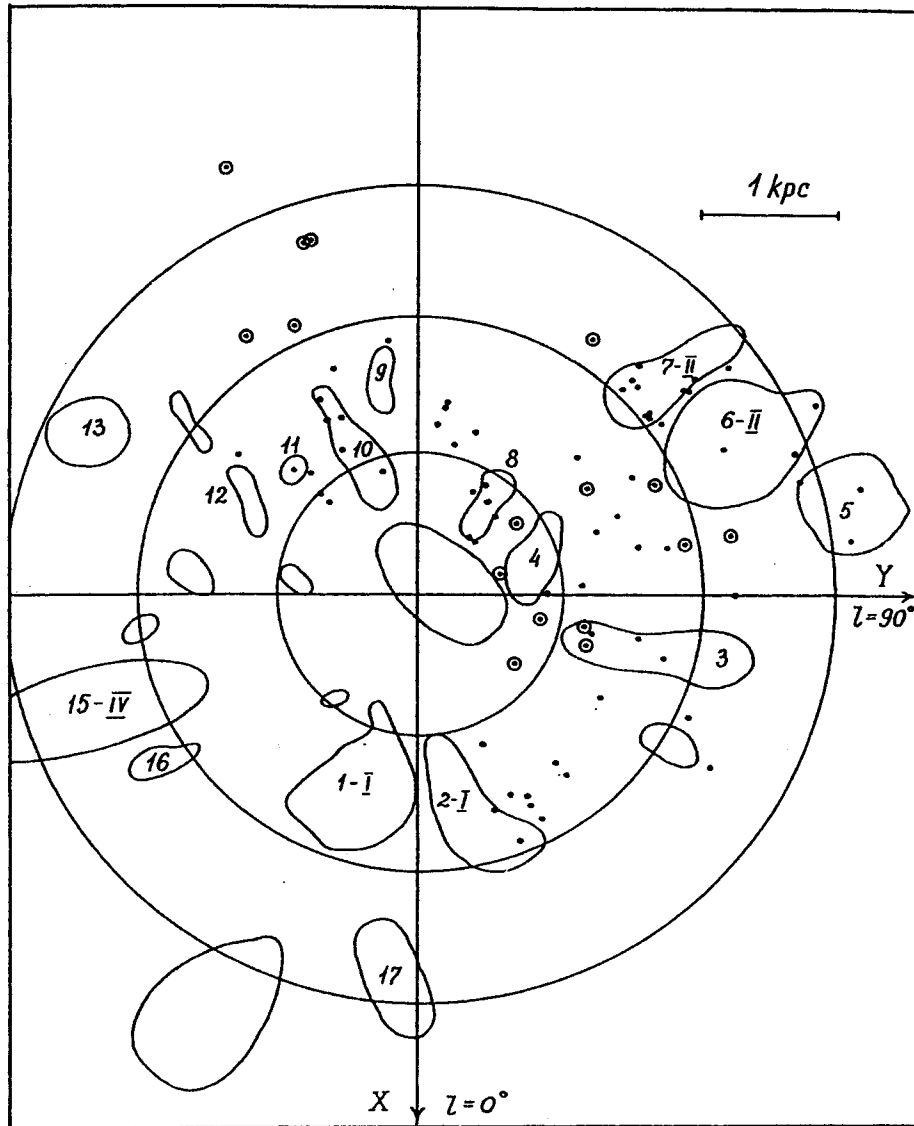
Figure 24   The distribution of the gas-star complexes according to Efremov and Sitnik (1988) and the sample clusters (points) in the projection on the Galaxy plane. Circles show the clusters with $\lg t > 8.5$.

radius of an OCl of the mass 380 $M_\odot$ and the density equal to the density of the given cluster. This reduction is just expedient also because the OCl tidal radius $R_t \propto M^{1/3}$ (see King, 1962; Danilov, 1990) corresponds to some critical value ρ_{cr} of the mean density ρ of the cluster with the given mass. Thus, R' is inversely proportional to the OCl density to the power 1/3.

R' for the clusters in the vicinities of the GSC No. 3 and GSC No. 9 and also of the supercomplexes I and II are shown in Figure 25 as a function of the distance Δr from the centres of these stellar groups. The coordinates of the GSC centres are taken from Efremov and Sitnik (1988). The GSC No. 6 centre coordinates and the coordinates of the median point between the GSC No. 1 and GSC No. 2 centres are taken as coordinates of the supercomplexes II and I centres, respectively. The OCls from the vicinity of the 9th and 10th GSCs are considered with respect to the GSC No. 9 centre because the mass of H_2 gas in the GSC No. 9 is greater than that in the GSC No. 10 by more than an order of magnitude (Efremov and Sitnik, 1988).

In order to obtain more definite results, one should use as many clusters as possible. The data on 65 OCls with $\lg t \leq 8.5$ from the vicinities of some GSCs (3, · 8, 9, 10, 11) and supercomplexes (I and II) are collected in a synthetic diagram (see Figure 26). The reduced OCl radius R' in parsecs is plotted along the ordinate. The OCl distances r from the centres of the corresponding gas-star complexes are plotted along the abscissa in the units of the GSC "radius". Half of the maximum GSC size in the projection on the Galaxy plane is taken as the GSC "radius" (in accordance with Efremov and Sitnik's (1988) data in general, see Figure 24). The GSC No. 11 radius was taken 25% larger than that of Efremov and Sitnik (1988), in accordance with the $(R', \Delta r)$ diagram. About 10 OCls correspond to each point in Figure 26. The vertical and horizontal error bars indicate the dispersion values.

Several reasons may lead to a great scatter of R' at the synthetic diagram:

1. The OCls have different densities, $\rho \geq \rho_{cr}$ in general. Then it is expedient to consider the upper envelope line for the points at the synthetic diagram.

2. Complexes of different nature, mass and structure are combined in the synthetic diagram because of the smallness of the sample.

3. The clusters under the action of neighbouring complexes fall into the sample at $r > 1$.

The upper envelope line for the majority of the OCl positions in the synthetic diagram, that is drawn through the upper ends of the vertical "one-sigma" error bars in Figure 26, approximately indicates the position of the upper boundary of the stability region for OCls in the GSC and Galaxy force field as in Figure 15. That is the probability for an OCl to be over this line is less than the probability for the OCl to be under this line.

The maximum OCl size decreases in the average with r inside a GSC ($r \leq 1$). This agrees with the results of Danilov (1990, 1991) and Danilov and Beshenov (1992) and is a consequence of the complex force field action onto the cluster. It is also one of the arguments in favour of the fact that GSCs and supercomplexes are the higher density regions in the Galaxy. The maximum OCl size increases in the average with r outside a GSC ($r > 1$). This is connected with the complex force
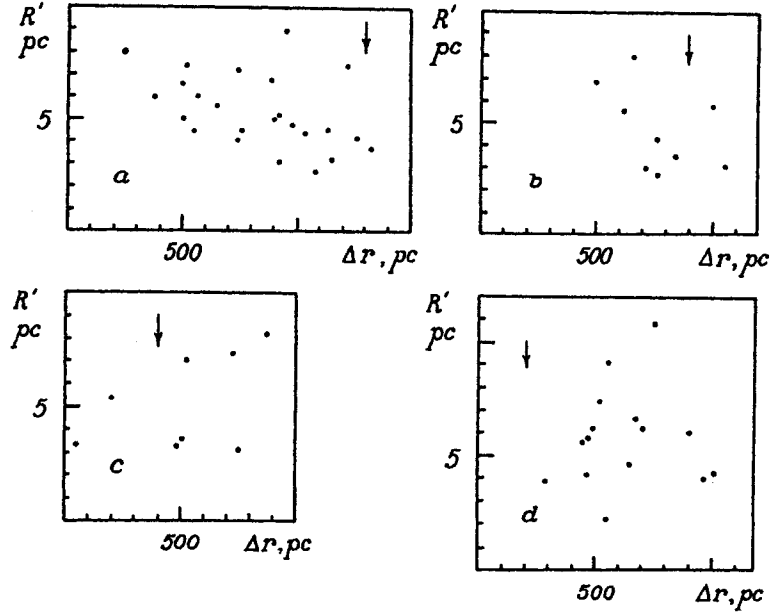
Figure 25   The OCl dimensions in the vicinities of: (a) the supercomplex II, (b) the supercomplex I, (c) the GSC No. 3 and (d) the GSC No. 9. Arrows indicate the GSC and supercomplex boundaries according to Efremov and Sitnik (1988).
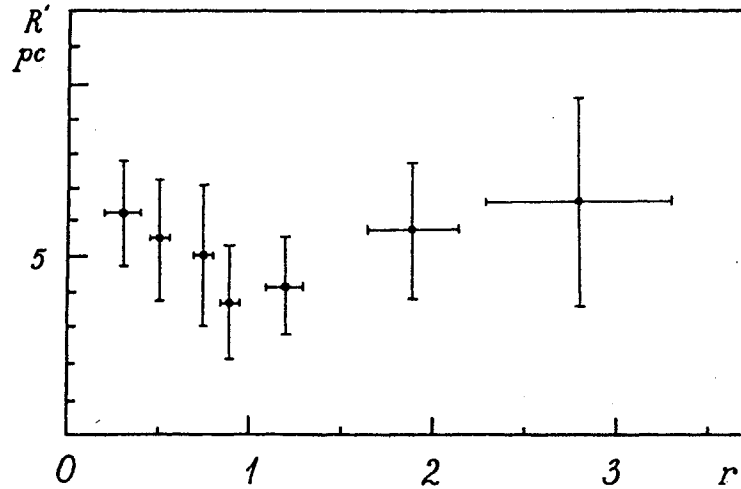
Figure 26   The synthetic diagram for 65 OCls with $\lg t \leq 8.5$ in the vicinities of some GSCs (3, 8, 9, 10, 11) and supercomplexes (I and II).

field weakening and with the clusters, included into the sample, that pass off and pass by a GSC along the orbit in the Galaxy field.

13 SUMMARY AND CONCLUSIONS

The above analysis of the open star cluster structure and dynamics allows us to draw some conclusions about the evolution of these objects, about the limitations imposed by external force fields onto the size, mean density, structure and lifetime of the clusters. The necessity of the construction of regular field nonstationary star clusters models is shown in this work when the action of external force fields of the Galaxy, gas-star complexes and giant molecular clouds onto the clusters is taken into account.

Conclusions on the action of the GSC force field onto OCls obtained in this work can be used when formulating new theoretical problems of the OCl model stability in the nonstationary GSC and Galaxy force field, as well as in connection with observational problems of the star cluster characteristics in active star formation regions in our and neighbouring galaxies.

The realization of the proposed observation program and the use of the new methods for the OCl observational data analysis and processing have allowed to obtain a number of results on the structure and nonstationarity degree of the OCls in the solar vicinity, have led to the discovery of new effective mechanisms in the open cluster dynamical evolution.

1. A catalogue of structural and dynamical characteristics of 103 OCls was obtained in this work. The catalogue includes: cluster star number up to the limiting value $B_{lim} \simeq 16^m$, the angular and linear OCl radii, the King model parameters for the star number surface density of the clusters and dimensionless parameters of the cluster cores and haloes; the lower estimates of the cluster mass, of their tidal radii in the Galaxy force field and relaxation times; the disruption time and the nonstationarity parameter for the OCls.

2. The sequence was found in the space of the OCl halo-core structure gross-parameters (the ratio of the cluster core radius to the cluster radius and the ratio of the core star population to the halo population). The clusters concentrate near this sequence. A comparison with the results of numerical experiments showed that this sequence is a result of the rate balance of the stellar transitions between the core and the halo that occurs due to the cluster relaxation.

3. The concentration degree of stars to the cluster centre is confirmed to depend on the cluster age. That is the objects with a weak concentration of stars to the cluster centre are absent among old clusters.

4. Estimates of the OCl disruption time due to GMC encounters are revised taking into account modern data on the GMC masses and concentration in the solar vicinity, and with allowance for the action, onto the cluster, of the regular tidal field of the GSC that moves jointly with the cluster. The main contribution into the OCl disruption comes from GMCs, in comparison with all the types of gas-dust clouds. The cluster "heating" under the action of encounters with GSCs or

neutral hydrogen superclouds is negligible. The GSC tidal field reduces the cluster disruption time by about 3 times and allows to reconcile the cluster disruption time and the mean cluster lifetime.

5. The OCl nonstationarity degree has been estimated. The mean values of the amplitude $(\delta\alpha)_{th}$ of the virial coefficient thermal fluctuations (due to stellar encounters) are about 0.10–0.12. They correspond to the amplitude of the OCl radius oscillations $\sim$10–12%. Encounters of the clusters and GMCs provide, in average, only a small increase of the amplitude of the OCl virial coefficient oscillations in comparison with the thermal amplitude $(\delta\alpha)_{th}$ in the clusters. However, encounters of OCls and GMCs determine the cluster disruption time and, consequently, the periods of the cluster energy, size and thermal oscillations amplitude increase up to the critical values. That is they determine also the cluster nonstationarity degree by means of stellar encounters in the clusters.

6. The dependence of the maximum OCl relative radius (in the units of the cluster tidal radius in the Galaxy field) on cluster age is found on the catalogue data. The dependence of the maximum size for young OCls on the distance from the centre of their closest GSC is also found. These dependences are both explained by the action of the complex force fields onto the young OCls. They are in agreement with the available theoretical estimates of the OCl tidal size and can be considered as arguments in favour of the fact that GSCs are the higher density regions in the Galaxy.

References

Agekyan, T. A., Vorontsov-Velyaminov, B. A. and Gorbatskij, V. G. *et al.* (1962) *Kurs Astrofiziki i Zvezdnoj Astronomii*, Vol. 2 (Gos. Izd. Fiz.-Mat. Liter., Moscow).

Arp, H. C. and Hartwick, F. D. A. (1971) *Ap. J.* **167**, 499.

Artyukhina, N. M. and Kholopov, P. N. (1961) *Astron. Zh.* **38**, 1039.

Auner, G. (1974) *A&AS* **13**, 143.

Balasz, B. (1961) *Astron. Abhand. der Hamb. Sternwarte in Bergedorf.* **5**, 317.

Barbon, R. and Hassan, S. M. (1973) *A&AS* **10**, 1.

Bard, Y. (1979) *Nelinejnoye Otsenivaniye Parametrov* (Statistika, Moscow).

Barkhatova, K. A. (1956) *Astron. Zh.* **33**, 556.

Barkhatova, K. A. (1958) *Atlas Diagramm Tsvet-Svetimost' Rasseyannykh Zvezdnykh Skoplenij* (Izd. Akad. Nauk SSSR, Moscow).

Barkhatova, K. A. (1961) *Atlas Diagramm Tsvet-Svetimost' Rasseyannykh Zvezdnykh Skoplenij: Dopolneniye Pervoye* (Izd. Akad. Nauk SSSR, Moscow).

Barkhatova, K. A. and Zhelvanova, E. I. (1963) In *Sbornik Rabot po Astronomii: Vypusk 1*, edited by K.A.Barkhatova (Izd. Ural. Univ., Sverdlovsk), p. 33.

Barkhatova, K. A., Zakharova, P. E. and Shashkina, L. P. (1978) *Astron. Zh.* **55**, 56.

Barkhatova, K. A., Zakharova, P. E., Shashkina, L. P. and Orekhova, L. K. (1985) *Astron. Zh.* **62**, 854.

Barkhatova, K. A. and Pylskaya, O. P. (1980) In *Zvezdnyye Agregaty*, edited by K.A.Barkhatova (Izd. Ural. Univ., Sverdlovsk), p. 8.

Becker, W. and Fenkart, R. (1971) *A&AS* **4**, 241.

Bergh, S. van den and Sher, D. (1960) *Publ. D. Dunlap Observ. Univ. Toronto* **2**, 203.

Bouvier, P. (1971) *A&A* **14**, 341.

Bouvier, P. and Janin, G. (1970) *A&A* **9**, 461.

Cannon, R. D. and Lloyd, C. (1969) *MNRAS* **144**, 449.

Chandrasekhar, S. (1948) *Printsipy Zvezdnoj Dinamiki* (Gos. Izd. Inostr. Liter., Moscow).

Chernoff, D. F., Kochanek, C. S. and Shapiro, S. L. (1986) *Ap. J.* **309**, 183.

Chumak, O. V. (1969) *Trudy Astrofiz. Inst. Kazakh. SSR*, Vol. 12, part 2, 75.

Claria, J. J. (1972) *AJ* **77**, 868.

Dame, T. M., Ungerechts, H. and Cohen, R. S. *et al.* (1987) *Ap. J.* **322**, 706.

Danilov, V. M. (1976) *Astrofizika* **12**, 139.

Danilov, V. M. (1985) *Astron Zh.* **62**, 704.

Danilov, V. M. (1987a) *Astron Zh.* **64**, 656.

Danilov, V. M. (1987b) *Astron Tsirk.*, No. 1492, 1.

Danilov, V. M. (1987c) *Astron Tsirk.*, No. 1522, 2.

Danilov, V. M. (1988a) *Astron Zh.* **65**, 712.

Danilov, V. M. (1988b) *Astron Tsirk.*, No. 1528, 9.

Danilov, V. M. (1989) *Astron Tsirk.*, No. 1536, 15.

Danilov, V. M. (1990) *Astron Zh.* **67**, 245.

Danilov, V. M. (1991) *Astron Zh.* **68**, 487.

Danilov, V. M. and Beshenov, G. V. (1987) *Astron Tsirk.*, No. 1520, 5.

Danilov, V. M. and Beshenov, G. V. (1988) In *Astronomo-geodezicheskiye Issledovaniya: Dinamicheskiye i Fizicheskiye Kharakteristiki Nebesnykh Tel*, edited by A. E. Vasilevskij (Izd. Ural. Univ., Sverdlovsk), p. 8.

Danilov, V. M. and Beshenov, G. V. (1992) *Astron. Zh.* **69**, 238.

Danilov, V. M., Matkin, N. V. and Pylskaya, O. P. (1985) *Astron. Zh.*, **62**, 1065.

Danilov, V. M. and Seleznev, A. F. (1988a) *Kinematika Fiz. Nebesn. Tel.* **4**, 51.

Danilov, V. M. and Seleznev, A. F. (1988b) *Astron. Tsirk.*, No. 1534, 9.

Danilov, V. M. and Seleznev, A. F. (1989) In *Astronomo-geodezicheskiye Issledovaniya: Strukturnyye Osobennosti Podsistem Galaktiki*, edited by A.E.Vasilevskij (Izd. Ural. Univ., Sverdlovsk), p. 26.

Danilov, V. M. and Seleznev, A. F. (1991) *Bull. Inf. Cent. Donnees Stellaires* **38**, 109.

Danilov, V. M., Seleznev, A. F. and Beshenov, G. V. (1989) In *Astronomo-geodezicheskiye Issledovaniya: Strukturnyye Osobennosti Podsistem Galaktiki*, edited by A.E.Vasilevskij (Izd. Ural. Univ., Sverdlovsk), p. 8.

Danilov, V. M., Seleznev, A. F., Gurto, E. Y. and Lapina, E. A. (1987) *Kinematika Fiz. Nebesn. Tel* **3**, 77.

Devadas, R. P., Ramamani, N. and Alladin, S. M. (1987) *J. Astrophys. and Astron.*, Vol. 8, No. 1, 17–31.

Efremov, Y. N. (1989) *Ochagi Zvezdoobrazovaniya v Galaktikakh* (Nauka, Moscow).

Efremov, Y. N. and Sitnik, T. G. (1988) *Pis'ma Astron. Zh.* **14**, 817.

Elmegreen, B. J. (1987) *Ap. J.* **312**, 626.

Fenkart, R. and Binggeli, B. (1979) *A&AS* **35**, 271.

Forbes, D. and Du Puy, D. L. (1978) *AJ* **83**, 266.

Fujishima, Y., Fujimoto, M. and Tosa, M. (1985) *Publ. Astron. Soc. Japan* **37**, 415.

Grubissich, C. (1973) *A&AS* **11**, 287.

Hagen, G. (1970) *An Atlas of Open Cluster Colour-magnitude Diagrams*, Publ. D. Dunlap Observ. Univ. Toronto, Vol. 4, 1.

Hassan, S. M. (1973) *A&AS* **9**, 261.

Hassan, S. M. and Barbon, R. (1973) *Mem. Soc. Astron. Ital.* **44**, 39.

Hoag, A. A., Johnson, H. L. and Iriarte, B. *et al.* (1961) *Publ. U.S. Naval. Obs.*, Vol. 17, part 7, 343.

Janes, K. and Adler, D. (1982) *ApJS* **49**, 425.

Jun-Liang, Zhao and Yan-Ping, He (1988) *Chin. Astron. and Astrophys.* **12**, 273.

Kholopov, P. N. (1968) *Astron. Zh.* **45**, 1235.

Kholopov, P. N. (1979) *Soobshch. Shternberg Astron. Inst.*, No. 205, 3.

Kholopov, P. N. (1981) *Zvezdnyye Skopleniya* (Nauka, Moscow).

King, I. R. (1962) *AJ* **67**, 471.

Kutuzov, S. A. and Osipkov, L. P. (1981) In *Dvizheniya Iskusstvennykh i Estestvennykh Nebesnykh Tel*, edited by K. A. Barkhatova (Izd. Ural. Univ., Sverdlovsk), p. 46.

Lindoff, U. (1969) *Ark. Astron.* **5**, 221.

Lynga, G. (1987) *Publ. Astron. Inst. Czechosl. Acad. Sci.*, No. 69, Vol. 4, 121.

Malysheva, L. K. (1990) *Astron. Zh.* **67**, 241.

Martynov, D. Y. (1977) *Kurs Prakticheskoj Astrofiziki* (Nauka, Moscow).

Mathieu, R. D. (1984) *ApJ* **284**, 643.

Mermilliod, J.-C. (1976) *A&AS* **24**, 159.

McClure, R. D., Twarog, B. A. and Forrester, W. T. (1981) *ApJ* **243**, 841.

Moffat, A. F. J. and Vogt, N. (1973) *A&AS* **11**, 3.

Moffat, A. F. J. and Vogt, N. (1985) *A&AS* **20**, 85.

Ogorodnikov, K. F. (1958) *Dinamika Zvezdnykh Sistem* (Gos. Izd. Fiz.-Mat. Liter., Moscow).

Paczynski, B. (1970) *Acta Astron.* **20**, 47.

Piskunov, A. E. (1977a) *Katalog Mass i Vozrastov Zvezd v 68 Rasseyannykh Skopleniyakh* (Izd. Akad. Nauk SSSR, Moscow).

Piskunov, A. E. (1977b) *Nauchn. Inform. Astron. Soveta Akad. Nauk SSSR*, is. 37, 31.

Rastorguev, A. S. (1983) In *Zvezdnyye Skopleniya i Problemy Zvezdnoj Evolutsii* (Izd. Ural. Univ., Sverdlovsk), p. 53.

Reddish, V. C. (1954) *MNRAS* **114**, 583.

Sanders, D. B., Scoville, N. Z. and Solomon, P. M. (1985) *ApJ* **289**, 373.

Sarma, M. B. K. and Walker, M. F. (1962) *ApJ* **135**, 11.

Seleznev, A. F. (1988) In *Astronomo-geodezicheskiye Issledovaniya: Dinamicheskiye i Fizicheskiye Kharakteristiki Nebesnykh Tel*, edited by A.E.Vasilevskij (Izd. Ural. Univ., Sverdlovsk), p. 126.

Seleznev, A. F. (1992) *Astron. and Astrophys. Trans.* (in press).

Sharov, A. S. (1964) *Astron. Zh.* **41**, 387.

Solomon, P. M., Rivolo, A. R., Barrett, J. and Yahil, A. (1987) *Ap.J.* **319**, 730.

Spitzer, L., Jr. (1958) *Ap.J.* **127**, 17.

Steinlin, U. W. (1968) *Zs. fur Astrophys.* **69**, 276.

Surdin, V. G. (1986) *Astron. Tsirk.*, No. 1434, 1.

Svolopoulos, S. N. (1965) *Zs. fur Astrophys.* **61**, 105.

Terlevich, E. (1987) *MNRAS* **224**, 193.

Theuns, T. (1992a) *A&A* **259**, 493.

Theuns, T. (1992b) *A&A* **259**, 502.

Wallenquist, A. (1975) *Uppsala Astron. Observ. Ann.*, Band 5, No. 8, 3.

Wielen, R. (1971a) *A&A* **13**, 309.

Wielen, R. (1971b) *ApSS* **13**, 300.

Wielen, R. (1977) *A&A* **60**, 263.

Wielen, R. (1985) In *Dynamics of Star Clusters*, IAU Symposium, No. 113, edited by J. Goodman and P. Hut (Reidel, Dordrecht), p. 449.

Wielen, R. (1987) *Publ. Astron. Inst. Czechosl. Acad. Sci.*, No. 69, Vol. 4, 157.

Wielen, R. (1988) In *Globular Cluster Systems in Galaxies*, IAU Symposium, No. 126, edited by J. E. Grindlay and A. G. D. Philip (Kluwer, Dordrecht), p. 393.

Wielen, R. and Fuchs, B. (1988) In *The Outer Galaxy*, Proceedings of a Symposium held in honor of Frank J. Kerr, edited by L. Blitz and F. J. Lockman (Springer-Verlag, Berlin) p. 100.

Yilmaz, F. (1970) *A&A* **8**, 213.

Appendix The catalogue of structural and dynamical characteristics of 103 OCLs

1 MPD scale

Table A.1.1   Structural and dynamical parameters of the OCls

NN	Name	r pc	$E(B-V)$	N_c	R arcmin	R pc	r_c pc
1	2	3	4	5	6	7	8
1	NGC 103	3000	0.46	398±9	37.4±0.8	32.6±0.7	7.6±1.3
2	NGC 129	1550	0.57	>278	>13.9	>6.3	3.9±0.7
3	NGC 188	1450	0.05	492±9	43.7±4.4	18.4±1.8	1.4±0.1
4	NGC 381	2000	–	>157	>12.4	>7.2	1.4±0.3
5	NGC 436	2060	0.16	90±0.4	7.7±1.2	4.6±0.7	1.4±0.2
6	NGC 457	2720	0.48	274±7	12.2±1.4	9.6±1.1	3.1±0.4
7	NGC 559	1350	0.45	265±11	20.1±1.4	7.9±0.5	1.3±0.2
8	NGC 581	2570	0.39	>439	>30.9	>23.1	4.9±0.7
9	NGC 637	2100	0.40	>34	>4.6	>2.8	0.52±0.05
10	NGC 654	1900	0.93	>85	>9.4	>5.2	0.82±0.06
11	NGC 659	2210	0.58	>75	>6.6	>4.3	2.1±0.6
12	NGC 663	2070	0.83	>239	>17.7	>10.6	2.2±0.2
13	NGC 744	1200	0.41	25±0.4	5.5±0.3	1.9±0.3	0.50±0.19
14	NGC 957	2050	0.80	96±2	8.8±0.8	5.3±0.5	1.8±0.3
15	NGC 1027	960	0.40	>1147	>67.2	>18.8	11.8±2.2
16	NGC 1245	2340	0.27	96±7	9.3±3.4	6.3±2.3	1.4±0.3
17	NGC 1444	890	0.70	>20	>4.4	>1.1	0.37±0.31
18	NGC 1502	940	0.77	99±4	24.8±2.5	6.8±0.7	0.51±0.08
19	NGC 1528	700	0.29	>1267	>67.2	>13.7	2.2±0.2
20	NGC 1582	1300	–	>137	>24.3	>9.2	–
21	NGC 1664	930	0.20	>1925	>67.2	>18.2	–
22	NGC 1778	1410	0.34	193±1	21.9±1.9	9.0±0.8	1.7±0.8
23	NGC 1857	1760	0.40	210±10	21.6±2.6	11.1±1.3	0.79±0.16
24	NGC 1893	3720	0.44	>65	>9.9	>10.8	3.8±0.8
25	NGC 1907	1430	0.42	174±8	10.8±0.9	4.5±0.4	0.90±0.32
26	NGC 1912	1090	0.27	476±10	21.6±0.6	6.9±0.2	2.9±0.4
27	NGC 1960	1280	0.24	244±6	20.1±0.6	7.5±0.2	1.4±0.1
28	NGC 2126	1430	0.80	191±4	23.2±2.2	9.6±0.9	2.8±0.4
29	NGC 2129	1790	0.67	41±2	5.5±0.7	2.9±0.4	0.98±0.17
30	NGC 2169	1080	0.14	50±7	15.5±5.4	4.8±1.7	0.28±0.12
31	NGC 2186	1830	0.31	149±0.2	18.6±2.5	9.9±1.3	1.2±0.5
32	NGC 2194	1470	0.51	89±3	17.0±1.9	7.3±0.8	0.60±0.27
33	NGC 2236	3400	0.45	152±2	14.4±1.5	14.2±1.5	2.6±0.4
34	NGC 2244	1700	0.46	>199	>20.2	>10.0	1.8±0.7
35	NGC 2251	1550	0.20	57±3	9.3±1.1	4.2±0.5	0.91±0.49
36	NGC 2254	2200	0.40	>43	>6.6	>4.2	0.68±0.17
37	NGC 2269	1440	0.44	27±1	2.8±0.2	1.2±0.1	0.30±0.21
38	NGC 2309	3900	–	>63	>6.6	>7.5	0.94±0.19
39	NGC 2323	970	0.24	209±6	20.1±1.8	5.7±0.5	1.0±0.2
40	NGC 2324	2730	0.11	>302	>26.9	>21.3	5.3±1.6
41	NGC 2335	1210	0.40	101±3	11.6±0.8	4.1±0.3	2.0±0.5
42	NGC 2343	860	0.20	23±1	7.7±0.9	1.9±0.2	0.16±0.06

Table A.1.1   Continued

1	2	3	4	5	6	7	8
43	NGC 2353	1060	0.12	85±2	12.2±1.3	3.7±0.4	1.4±0.4
44	NGC 2355	–	–	142±5	13.3±0.9	–	–
45	NGC 2395	1200	0.72	25±1	7.7±0.8	2.7±0.3	1.6±1.7
46	NGC 2420	1960	0.00	222	20.1	11.5	0.84±0.04
47	NGC 2423	860	0.13	138±6	15.5±1.4	3.9±0.3	1.4±0.2
48	NGC 2437	1670	0.14	370±9	33.6±3.4	16.3±1.6	3.3±0.3
49	NGC 2506	2040	0.05	48±2	7.2±1.0	4.3±0.6	1.0±0.2
50	NGC 6604ˣ	1640	0.96	21±0.5	12.2±0.4	5.8±0.2	–
51	NGC 6649	1630	1.22	49±0.1	5.0±0.5	2.4±0.2	1.1±0.1
52	NGC 6664	1390	0.60	158±3	24.8±1.8	10.0±0.8	2.4±0.4
53	NGC 6694	1500	0.58	106±0.7	12.2±0.8	5.3±0.3	0.96±0.19
54	NGC 6704	1810	0.71	44±2	5.0±0.5	2.6±0.3	0.41±0.12
55	NGC 6705	1780	0.42	805±35	15.5±1.7	8.0±0.9	1.4±0.08
56	NGC 6755	1390	0.93	391±14	21.6±2.2	8.8±0.9	1.0±0.3
57	NGC 6756	1650	1.44	56±0.8	6.6±0.5	3.2±0.2	0.29±0.05
58	NGC 6802	950	0.81	102±2	7.7±0.5	2.1±0.1	0.30±0.04
59	NGC 6811	990	0.14	199±6	21.9±1.4	6.3±0.4	0.84±0.28
60	NGC 6819	2100	0.28	1000±11	24.8±2.6	15.1±1.6	2.2±0.2
61	NGC 6823	2290	0.82	165±11	15.5±2.6	10.3±1.8	1.1±0.2
62	NGC 6830	1320	0.53	>535	>26.3	>10.1	3.3±0.4
63	NGC 6834	2250	0.66	96±3	5.4±0.5	3.5±0.3	1.3±0.4
64	NGC 6838	4110	0.31	446±10	20.1±1.8	24.0±2.2	2.2±0.4
65	NGC 6866	1200	0.14	281±7	26.3±2.2	9.2±0.8	2.4±0.2
66	NGC 6910	1650	1.05	138±5	15.5±1.6	7.4±0.8	1.4±0.2
67	NGC 6913	1410	0.83	60±2	8.8±0.6	3.6±0.2	0.77±0.11
68	NGC 6939	1320	0.50	274±4	15.5±1.2	5.9±0.5	1.1±0.08
69	NGC 7031	940	0.93	94±1	17.7±1.1	4.8±0.3	0.57±0.12
70	NGC 7062	1840	0.25	112±4	9.9±1.0	5.3±0.5	1.8±0.2
71	NGC 7086	1300	0.70	83±1	7.7±0.8	2.9±0.3	0.67±0.21
72	NGC 7128	2680	0.92	43±1	2.8±0.3	2.2±0.2	0.99±0.17
73	NGC 7142	–	–	265±14	21.6±1.8	–	–
74	NGC 7226	2320	0.60	49±0.8	4.4±0.2	3.0±0.1	0.41±0.15
75	NGC 7235	3250	0.95	247±8	16.6±0.9	15.7±0.8	0.53±0.29
76	NGC 7245	1740	0.60	134±3	8.8±0.9	4.5±0.4	1.6±0.7
77	NGC 7261	810	0.58	>18	>3.3	>0.8	0.39±0.23
78	NGC 7380	2100	0.50	86±2	6.2±0.5	3.8±0.3	2.6±0.6
79	NGC 7419	4700	1.50	48±0.9	4.4±0.2	6.0±0.3	1.3±0.2
80	NGC 7510	2580	0.89	>57	>7.2	>5.4	0.70±0.16
81	NGC 7654	1670	0.60	368±6	15.5±1.2	7.5±0.6	2.0±0.2
82	NGC 7788	2400	0.28	209±28	13.3±2.2	9.2±1.5	1.8±0.4
83	NGC 7789	1890	0.26	>1028	>47.0	>25.8	3.9±0.2
84	NGC 7790	3100	0.52	>195	>13.1	>11.8	2.4±0.3
85	IC 1369	1500	0.52	65±2	5.4±0.5	2.4±0.2	0.84±0.27
86	IC 1442	1810	0.53	37±2	5.5±0.6	2.9±0.3	0.35±0.14
87	IC 1805	2020	0.76	76±7	10.8±0.9	6.4±0.5	1.8±1.1
88	IC 1848	2150	0.61	386±4	23.2±1.4	14.5±0.9	3.7±0.5
89	IC 2157	1960	0.60	70±2	8.5±0.9	4.8±0.5	0.97±0.13
90	IC 4996	1610	0.64	71±3	6.2±0.6	2.9±0.3	0.58±0.14
91	Berk 3	1900	0.50	>100	>10.0	>5.6	1.2±0.2
92	Berk 8	1490	–	>29	>2.8	>1.2	–
93	Berk 94	1610	0.59	>32	>4.6	>2.2	0.47±0.87
94	Harv 21	3500	0.69	65±2	5.4±0.8	5.5±0.8	1.0±0.3

Table A.1.1   Continued

1	2	3	4	5	6	7	8
95	King 4	2190	0.86	48±3	3.9±0.5	2.5±0.3	0.46±0.21
96	King 16	2300	–	42±4	5.5±2.6	3.7±1.7	0.63±0.15
97	King 19	1300	0.82	59±2	7.7±0.6	2.9±0.2	0.38±0.06
98	Stock 7	560	0.64	13±1	5.0±0.8	0.8±0.1	0.51±0.26
99	Stock 8	2260	0.54	66±2	10.0±0.7	6.6±0.4	0.86±0.30
100	Tomb 5	1800	0.35	186±1	15.5±0.9	8.1±0.5	3.1±0.4
101	Tr 1	2400	0.58	37±0.8	4.6±0.6	3.2±0.4	1.4±0.2
102	Tr 2	610	0.32	138±6	17.0±1.2	3.0±0.2	0.47±0.19
103	Tr 35	2010	1.19	43±1	5.0±0.3	2.9±0.2	1.6±0.5

Table A.1.1   Continued

NN	Name	k pc^{-2}	$\frac{R}{r_c}$	$\langle R \rangle$ pc	$\langle R^2 \rangle$ pc^2	$\langle R^{-1} \rangle^{-1}$ pc	$\langle m \rangle$ $M_\odot$	κ
1	2	9	10	11	12	13	14	15
1	NGC 103	2.8±0.2	4.3	11.9	178.4	8.45	3.4	1.05
2	NGC 129	40.3±8.8	1.6	3.05	10.8	2.43	3.0	1.08
3	NGC 188	24.8±3.5	13.0	4.45	30.3	2.58	1.44	1.04
4	NGC 381	11.8±1.0	5.0	2.49	7.96	1.72	–	–
5	NGC 436	23.7±0.5	3.2	1.86	4.21	1.38	2.5	1.07
6	NGC 457	13.9±0.4	3.1	3.89	18.4	2.87	4.6	1.15
7	NGC 559	27.9±2.7	6.2	2.46	8.25	1.73	1.7	1.09
8	NGC 581	2.3±0.1	4.8	8.14	84.5	5.67	3.7	1.11
9	NGC 637	30.9±1.3	5.4	0.95	1.18	0.65	3.4	1.09
10	NGC 654	29.0±2.1	6.3	1.61	3.53	1.13	5.1	1.08
11	NGC 659	20.6±4.8	2.1	1.95	4.45	1.52	3.7	1.06
12	NGC 663	14.4±0.7	4.8	3.72	17.7	2.59	5.6	1.16
13	NGC 744	37.6±5.4	3.8	0.73	0.66	0.53	2.4	1.08
14	NGC 957	15.2±0.9	2.8	2.20	5.81	1.64	5.4	1.15
15	NGC 1027	13.1±3.2	1.6	9.15	96.6	7.30	2.5	1.11
16	NGC 1245	10.5±1.1	4.4	2.28	6.55	1.61	2.2	1.07
17	NGC 1444	34.2±18.	3.1	0.46	0.26	0.34	2.1	1.02
18	NGC 1502	42.5±8.9	13.3	1.62	4.03	0.93	3.4	1.16
19	NGC 1528	27.8±2.1	6.2	4.24	24.6	2.98	1.8	1.08
20	NGC 1582	–	–	–	–	–	–	–
21	NGC 1664	–	–	–	–	–	1.9	1.08
22	NGC 1778	8.2±2.2	5.3	3.04	12.0	2.08	2.7	1.10
23	NGC 1857	23.0±4.9	14.0	2.66	10.8	1.45	2.3	1.03
24	NGC 1893	2.8±0.2	2.8	4.50	24.4	3.38	5.0	1.12
25	NGC 1907	25.8±4.6	5.0	1.56	3.12	1.08	2.4	1.04
26	NGC 1912	28.3±2.1	2.4	3.02	10.8	2.32	2.5	1.13
27	NGC 1960	25.3±1.2	5.2	2.56	8.43	1.75	2.6	1.16
28	NGC 2126	10.9±0.5	3.4	3.80	17.7	2.79	3.4	1.06
29	NGC 2129	18.1±0.8	2.9	1.19	1.70	0.89	4.2	1.12
30	NGC 2169	19.9±10.	17.3	1.08	1.86	0.56	2.4	1.17
31	NGC 2186	8.7±3.7	8.6	2.82	11.1	1.75	3.2	1.14
32	NGC 2194	21.3±11.	12.1	1.89	5.01	1.04	1.7	1.00

Table A.1.1 Continued

1	2	9	10	11	12	13	14	15
33	NGC 2236	4.6±0.4	5.4	4.78	29.6	3.25	4.6	1.06
34	NGC 2244	5.1±1.3	5.4	3.34	14.5	2.27	4.1	1.29
35	NGC 2251	13.4±3.3	4.6	1.49	2.82	1.04	2.2	1.05
36	NGC 2254	18.6±3.4	6.2	1.32	2.38	0.93	2.4	1.02
37	NGC 2269	82.2±17.	3.8	0.44	0.24	0.32	2.3	1.05
38	NGC 2309	9.9±1.8	8.0	2.20	6.68	1.39	–	–
39	NGC 2323	32.0±3.7	5.4	1.91	4.73	1.30	2.3	1.12
40	NGC 2324	3.7±0.4	4.0	7.97	79.2	5.72	2.1	1.02
41	NGC 2335	21.6±4.0	2.0	1.87	4.10	1.46	2.3	1.06
42	NGC 2343	58.8±24.	12.0	0.50	0.35	0.28	1.9	1.09
43	NGC 2353	18.1±1.7	2.7	1.59	3.03	1.20	2.0	1.10
44	NGC 2355	–	4.6	–	–	–	–	–
45	NGC 2395	18.8±24.	1.7	1.30	1.96	1.03	2.8	1.06
46	NGC 2420	33.6±1.9	13.7	2.77	11.6	1.53	1.5	1.03
47	NGC 2423	33.4±2.0	2.7	1.64	3.22	1.24	1.6	1.05
48	NGC 2437	7.6±0.3	5.0	5.65	40.9	3.90	2.4	1.09
49	NGC 2506	14.9±0.9	4.2	1.57	3.08	1.12	1.5	1.02
50	NGC 6604^x	–	–	–	–	–	10.6	1.08
51	NGC 6649	56.8±4.4	2.1	1.07	1.34	0.83	5.6	1.06
52	NGC 6664	7.2±0.5	4.2	3.68	16.9	2.62	3.2	1.09
53	NGC 6694	22.4±2.6	5.5	1.78	4.10	1.20	3.3	1.10
54	NGC 6704	40.2±8.3	6.4	0.80	0.88	0.56	3.5	1.04
55	NGC 6705	61.4±2.3	5.9	2.62	8.99	1.75	2.9	1.08
56	NGC 6755	37.1±10.	8.8	2.48	8.61	1.53	4.2	1.08
57	NGC 6756	74.0±14.	10.9	0.83	1.01	0.49	7.2	1.01
58	NGC 6802	141.6±13.	7.0	0.66	0.58	0.42	1.8	1.01
59	NGC 6811	30.8±9.2	7.5	1.89	4.86	1.21	1.6	1.04
60	NGC 6819	30.0±2.5	7.0	4.65	29.2	3.02	1.98	1.07
61	NGC 6823	9.2±1.5	9.3	2.86	11.5	1.73	5.0	1.07
62	NGC 6830	16.7±0.6	3.1	4.10	20.4	3.04	2.6	1.06
63	NGC 6834	26.9±3.1	2.7	1.50	2.71	1.14	4.1	1.06
64	NGC 6838	5.8±1.2	10.8	6.32	57.8	3.70	–	–
65	NGC 6866	15.8±0.3	3.9	3.47	15.0	2.50	2.0	1.15
66	NGC 6910	14.2±1.1	5.4	2.50	8.12	1.71	6.5	1.15
67	NGC 6913	20.2±1.4	4.7	1.28	2.09	0.89	4.8	1.19
68	NGC 6939	47.2±2.2	5.4	2.00	5.20	1.36	1.98	1.03
69	NGC 7031	29.6±5.5	8.4	1.39	2.68	0.86	3.1	1.06
70	NGC 7062	16.6±0.6	3.0	2.18	5.77	1.62	2.4	1.01
71	NGC 7086	45.8±5.7	4.4	1.06	1.42	0.75	2.6	1.04
72	NGC 7128	43.7±4.8	2.2	0.97	1.11	0.75	6.2	1.05
73	NGC 7142	–	8.8	–	–	–	–	–
74	NGC 7226	36.0±12.	7.3	0.90	1.11	0.58	2.7	1.01
75	NGC 7235	12.0±9.5	29.4	2.92	15.2	1.26	9.0	1.11
76	NGC 7245	26.5±3.5	2.8	1.86	4.18	1.40	2.6	1.02
77	NGC 7261	100.3±47.	2.0	0.36	0.15	0.28	1.9	1.03
78	NGC 7380	10.8±0.9	1.4	1.89	4.07	1.52	3.9	1.13
79	NGC 7419	8.9±0.4	4.7	2.14	5.81	1.49	–	–
80	NGC 7510	16.9±2.9	7.6	1.60	3.52	1.02	6.0	1.06
81	NGC 7654	38.8±1.1	3.7	2.88	10.3	2.09	3.7	1.12
82	NGC 7788	15.0±1.7	5.0	3.20	13.2	2.21	2.8	1.06
83	NGC 7789	11.0±0.6	6.7	8.08	87.3	5.29	2.4	1.06
84	NGC 7790	9.0±0.6	5.0	4.10	21.6	2.84	4.0	1.05

Table A.1.1 Continued

1	2	9	10	11	12	13	14	15
85	IC 1369	32.5±3.5	2.8	0.99	1.18	0.74	1.9	1.04
86	IC 1442	27.2±12.	8.3	0.84	0.98	0.52	2.9	1.04
87	IC 1805	5.4±0.8	3.5	2.48	7.59	1.82	4.9	1.12
88	IC 1848	6.3±0.3	3.9	5.45	.36.9	3.92	4.8	1.18
89	IC 2157	11.8±1.0	5.0	1.68	3.62	1.16	3.9	1.09
90	IC 4996	41.2±4.6	5.0	1.00	1.29	0.69	4.0	1.15
91	Berk 3	16.4±1.6	4.8	1.95	4.85	1.36	2.9	1.05
92	Berk 8	–	–	–	–	–	–	–
93	Berk 94	9.9±7.6	4.6	0.77	0.76	0.54	4.0	1.18
94	Harv 21	12.7±2.6	5.4	1.86	4.48	1.27	5.8	1.07
95	King 4	31.5±8.9	5.4	0.83	0.89	0.57	4.2	1.03
96	King 16	16.1±2.9	5.9	1.21	1.92	0.81	–	–
97	King 19	52.6±8.2	7.7	0.87	1.03	0.55	3.2	1.04
98	Stock 7	135.8±86.	1.6	0.40	0.18	0.32	2.4	1.15
99	Stock 8	6.6±1.9	7.6	1.97	5.29	1.25	4.6	1.16
100	Tomb 5	12.2±0.6	2.6	3.46	14.3	2.63	2.5	1.05
101	Tr 1	8.9±0.7	2.4	1.42	2.40	1.09	4.1	1.08
102	Tr 2	43.8±12.	6.5	0.95	1.21	0.63	2.1	1.14
103	Tr 35	26.8±7.7	1.9	1.36	2.16	1.07	7.3	1.05

Table A.1.1 Continued

NN	Name	M_c $M_\odot$	R_t pc	τ Myrs	$\lg\tau$ years	$\lg t$	R_G pc	z pc
1	2	16	17	18	19	20	21	22
1	NGC 103	1350±370	17.0±1.4	108.2±13.6	8.0	7.6	10030	–64
2	NGC 129	>830	>13.4	>16.0	7.2	7.9	9080	–60
3	NGC 188	710±190	12.6±1.0	29.8±3.7	7.5	9.7	9000	562
4	NGC 381	–	–	–	–	–	9490	–34
5	NGC 436	220±60	9.0±0.8	5.6±0.7	6.8	7.6	9560	–132
6	NGC 457	1260±350	16.7±1.4	16.6±2.1	7.2	7.1	10050	–198
7	NGC 559	450±130	10.9±0.9	12.6±1.6	7.1	9.0	9080	26
8	NGC 581	>1620	>18.1	>58.8	7.8	7.7	9990	–70
9	NGC 637	>120	>7.3	>1.3	6.1	7.6	9650	70
10	NGC 654	>430	>11.2	>2.9	6.5	7.7	9510	–3
11	NGC 659	>280	>9.8	>5.2	6.7	7.3	9750	–50
12	NGC 663	>1340	>16.5	>12.3	7.1	6.6	9650	–25
13	NGC 744	60±20	5.6±0.5	1.1±0.1	6.0	7.6	9050	–120
14	NGC 957	520±140	12.1±1.0	5.1±0.6	6.7	7.2	9780	–87
15	NGC 1027	>2870	>20.0	>141.6	8.2	7.6	8910	33
16	NGC 1245	210±70	9.3±0.8	7.7±1.0	6.9	8.9	10210	–355
17	NGC 1444	>40	>4.9	>0.6	5.8	8.2	8970	–12
18	NGC 1502	340±100	9.8±0.8	2.8±0.3	6.4	6.4	8970	133
19	NGC 1528	>2280	>18.4	>45.1	7.6	8.1	8820	11
20	NGC 1582	–	–	–	–	7.7	9430	74
21	NGC 1664	>3660	>22.0	–	–	7.9	9090	1
22	NGC 1778	520±130	12.0±1.0	12.1±1.5	7.1	8.2	9590	–41

　　　　　　V. M. DANILOV AND A. F. SELEZNEV

Table A.1.1　Continued

1	2	16	17	18	19	20	21	22
23	NGC 1857	480±140	12.0±1.0	7.8±1.0	6.9	8.2	9930	47
24	NGC 1893	>320	>12.2	>14.4	7.2	6.9	11900	−102
25	NGC 1907	420±120	11.1±0.9	4.6±0.6	6.7	8.3	9620	15
26	NGC 1912	1190±320	15.4±1.3	19.2±2.4	7.3	7.6	9280	21
27	NGC 1960	630±170	12.7±1.1	10.2±1.3	7.0	7.5	9480	31
28	NGC 2126	650±180	12.8±1.1	16.7±2.1	7.2	7.2	9540	335
29	NGC 2129	170±50	8.5±0.7	2.0±0.2	6.3	7.2	9980	12
30	NGC 2169	120±50	7.1±0.7	1.3±0.2	6.1	7.4	9240	−47
31	NGC 2186	480±120	11.9±1.0	8.0±1.0	6.9	8.2	9890	−189
32	NGC 2194	150±40	7.9±0.7	4.5±0.6	6.6	8.6	9610	−51
33	NGC 2236	700±180	15.2±1.3	17.1±2.1	7.2	8.6	11380	−92
34	NGC 2244	>820	>14.1	11.3	7.0	6.5	9750	−51
35	NGC 2251	120±40	7.5±0.6	3.6±0.4	6.6	7.9	9640	12
36	NGC 2254	>100	>7.4	>2.8	6.4	8.8	10240	11
37	NGC 2269	60±20	5.8±0.5	0.5±0.1	5.7	7.8	9500	18
38	NGC 2309	–	–	–	–	–	11470	−145
39	NGC 2323	480±130	11.0±0.9	6.6±0.8	6.8	7.6	8950	−12
40	NGC 2324	>630	>13.8	>70.8	7.8	8.8	10580	166
41	NGC 2335	230±60	8.8±0.7	6.6±0.8	6.8	8.2	9110	−18
42	NGC 2343	40±10	4.9±0.4	0.5±0.1	5.7	8.0	8840	−9
43	NGC 2353	170±40	7.8±0.6	5.1±0.6	6.7	7.1	8980	15
44	NGC 2355	–	–	–	–	–	–	–
45	NGC 2395	70±20	6.0±0.5	2.8±0.4	6.4	7.7	9270	297
46	NGC 2420	330±80	10.6	10.6	7.0	9.5	9970	667
47	NGC 2423	220±60	8.4±0.7	6.6±0.8	6.8	8.4	8770	61
48	NGC 2437	890±240	14.0±1.2	39.6±5.0	7.6	7.9	9320	126
49	NGC 2506	70±20	6.2±0.5	4.7±0.6	6.7	9.2	9600	359
50	NGC 6604ˣ	220±60	6.9±0.6	–	–	6.4	6660	56
51	NGC 6649	270±70	7.4±0.6	1.6±0.2	6.2	7.7	6710	−14
52	NGC 6664	500±140	9.3±0.8	14.9±1.9	7.2	7.4	6950	−4
53	NGC 6694	350±90	8.2±0.7	4.2±0.5	6.6	7.9	6860	−68
54	NGC 6704	150±40	6.1±0.5	1.1±0.1	6.0	7.4	6660	−62
55	NGC 6705	2330±680	15.1±1.3	13.8±1.7	7.1	7.9	6670	−78
56	NGC 6755	1640±470	14.1±1.2	7.5±0.9	6.9	7.6	7170	−33
57	NGC 6756	400±110	8.7±0.7	0.6±0.1	5.8	7.7	7000	−40
58	NGC 6802	180±50	7.2±0.6	1.2±0.1	6.1	9.2	7700	23
59	NGC 6811	320±80	8.9±0.7	7.0±0.9	6.8	8.7	8080	213
60	NGC 6819	1980±520	16.1±1.3	40.5±5.1	7.6	8.9	7880	317
61	NGC 6823	820±260	11.4±1.0	6.5±0.8	6.8	7.0	7310	3
62	NGC 6830	>1390	>14.0	>29.2	7.5	7.2	7630	−34
63	NGC 6834	390±110	9.1±0.8	3.3±0.4	6.5	7.4	7560	54
64	NGC 6838	–	–	–	–	9.9	6870	−318
65	NGC 6866	560±150	10.8±0.9	20.6±2.6	7.3	8.5	8070	152
66	NGC 6910	900±260	12.5±1.0	5.3±0.7	6.7	7.0	8040	66
67	NGC 6913	290±80	8.6±0.7	2.0±0.2	6.3	7.0	8000	23
68	NGC 6939	540±140	11.0±0.9	8.3±1.0	6.9	9.9	8430	289
69	NGC 7031	290±80	8.8±0.7	2.5±0.3	6.4	8.7	8280	45
70	NGC 7062	270±80	8.7±0.7	7.8±1.0	6.9	8.0	8400	−79
71	NGC 7086	220±60	8.0±0.7	2.2±0.3	6.3	7.9	8400	12
72	NGC 7128	270±70	9.1±0.8	1.3±0.2	6.1	6.0	8950	28
73	NGC 7142	–	–	–	–	9.3	–	–
74	NGC 7226	130±40	7.2±0.6	1.3±0.2	6.1	8.7	8950	−16

Table A.1.1   Continued

1	2	16	17	18	19	20	21	22
75	NGC 7235	2220±630	19.2±1.6	3.3±0.4˙	6.5	7.0	9460	52
76	NGC 7245	350±90	9.7±0.8	6.2±0.8	6.8	8.6	8710	−49
77	NGC 7261	>30	>4.4	>0.5	5.7	7.6	8430	20
78	NGC 7380	340±90	9.9±0.8	5.2±0.6	6.7	7.2	9040	−24
79	NGC 7419	−	−	−	−	−	10070	102
80	NGC 7510	>340	>10.3	>2.1	6.3	7.0	9440	10
81	NGC 7654	1360±360	15.7±1.3	12.5±1.6	7.1	7.6	8980	21
82	NGC 7788	580±220	12.4±1.2	13.3±1.7	7.1	7.2	9510	−25
83	NGC 7789	>2470	>19.4	>86.1	7.9	8.9	9170	−168
84	NGC 7790	>780	>14.1	>15.9	7.2	7.4	9980	−46
85	IC 1369	120±30	6.6±0.6	2.4±0.3	6.4	9.1	8320	−2
86	IC 1442	110±30	6.6±0.6	1.1±0.1	6.0	7.8	8740	−61
87	IC 1805	370±130	10.8±1.0	5.9±0.7	6.8	6.4	9730	40
88	IC 1848	1850±480	18.7±1.6	28.5±3.6	7.4	6.4	9890	11
89	IC 2157	270±80	10.1±0.8	3.3±0.4	6.5	7.2	10150	51
90	IC 4996	280±80	8.5±0.7	1.5±0.2	6.2	7.0	7950	45
91	Berk 3	>290	>9.6	>5.2	6.7	−	9340	−21
92	Berk 8	−	−	−	−	−	9150	351
93	Berk 94	>130	>7.0	>0.9	6.0	8.4	8710	−25
94	Harv 21	380±100	11.3±1.0	3.1±0.4	6.5	7.3*	10240	−14
95	King 4	200±60	8.9±0.8	1.0±0.1	6.0	7.3	9890	−37
96	King 16	−	−	−	−	−	9620	61
97	King 19	190±50	7.9±0.7	1.2±0.1	6.1	7.6	8740	11
98	Stock 7	30±10	4.3±0.4	0.5±0.1	5.7	6.3	8600	8
99	Stock 8	300±80	10.7±0.9	3.4±0.4	6.5	6.3	10450	17
100	Tomb 5	460±120	11.6±1.0	17.7±2.2	7.2	−	9710	120
101	Tr 1	150±40	8.1±0.7	2.7±0.3	6.4	7.4	9870	−39
102	Tr 2	290±80	9.1±0.8	2.1±0.3	6.3	7.5	8660	−33
103	Tr 35	310±80	7.6±0.6	2.0±0.2	6.3	7.6	6500	8

Notes:

x – star counts in the cluster NGC 6604 up to $B_{lim} \simeq 14^m$;

* – NGC 7788, NGC 7790 and Harv 21 are supposed to form the united system in accordance with Barkhatova and Zhelvanova (1963).

Table A.1.2   The disruption times and nonstationarity parameters of OCls

NN	Name		t_{d1} years	t_{d2} years	p_o pc	$\langle\delta\alpha\rangle_{eq}$	$\langle\delta\alpha\rangle_{th}$	$\delta\alpha$	$\frac{\delta\alpha}{\delta\alpha_{max}}$	$\delta\alpha_{max}$
1	2		3	4	5	6	7	8	9	10
1	NGC	103	−	1.0E8	80	1.53	−	−	−	−
2	NGC	129	8.0E8	1.0E9	25	0.0061	0.048	0.054	0.109	0.494
3	NGC	188	5.3E9	7.4E9	15	0.0015	−	−	−	0.445
4	NGC	381	−	−	−	−	−	−	−	−
5	NGC	436	9.7E8	1.2E9	23	0.0019	0.089	0.090	0.164	0.553
6	NGC	457	8.9E8	3.2E9	23	0.0052	0.060	0.066	0.128	0.514
7	NGC	559	4.4E9	7.2E9	15	8.3E-4	0.084	0.084	0.156	0.542

V. M. DANILOV AND A. F. SELEZNEV

Table A.1.2 Continued

1	2	3	4	5	6	7	8	9	10
8	NGC 581	5.3E7	2.2E8	54	0.225	3.13	3.36	15.4	0.217
9	NGC 637	4.4E9	2.7E9	16	9.0E-5	0.126	0.126	0.183	0.688
10	NGC 654	2.9E9	2.2E9	17	3.3E-4	0.086	0.087	0.131	0.663
11	NGC 659	1.1E9	1.2E9	23	0.0015	0.087	0.088	0.161	0.549
12	NGC 663	7.4E8	1.0E9	25	0.0056	0.075	0.081	0.148	0.545
13	NGC 744	5.2E9	2.8E9	15	5.9E-5	0.140	0.140	0.206	0.676
14	NGC 957	1.4E9	1.5E9	21	0.0011	0.084	0.085	0.144	0.590
15	NGC 1027	3.6E7	1.7E8	62	0.462	0.137	0.600	5.53	0.108
16	NGC 1245	2.3E9	5.2E9	18	9.4E-4	0.119	0.120	0.234	0.511
17	NGC 1444	2.8E10	1.7E10	10	3.4E-6	0.136	0.136	0.187	0.729
18	NGC 1502	2.4E9	2.0E9	18	4.1E-4	0.133	0.134	0.198	0.676
19	NGC 1528	1.1E9	3.6E9	22	0.012	0.040	0.052	0.098	0.536
20	NGC 1582	–	–	–	–	–	–	–	–
21	NGC 1664	–	–	–	–	–	–	–	–
22	NGC 1778	7.9E8	3.0E9	24	0.0043	0.107	0.111	0.218	0.511
23	NGC 1857	1.2E9	4.0E9	20	0.0019	0.270	0.272	0.437	0.621
24	NGC 1893	7.4E7	2.7E8	49	0.049	0.359	0.408	1.39	0.293
25	NGC 1907	5.9E9	9.0E9	14	2.1E-4	0.054	0.054	0.081	0.671
26	NGC 1912	1.2E9	1.3E9	22	0.0048	0.037	0.042	0.075	0.559
27	NGC 1960	1.1E9	1.3E9	22	0.0031	0.067	0.070	0.119	0.586
28	NGC 2126	1.3E9	3.6E9	21	0.0034	0.103	0.106	0.255	0.417
29	NGC 2129	3.3E9	2.2E9	17	1.8E-4	0.113	0.113	0.173	0.655
30	NGC 2169	3.1E9	2.3E9	17	1.5E-4	0.181	0.181	0.255	0.709
31	NGC 2186	9.7E8	3.5E9	22	0.0024	0.178	0.181	0.319	0.566
32	NGC 2194	2.0E9	5.1E9	18	6.7E-4	0.398	0.398	0.666	0.598
33	NGC 2236	4.5E8	2.2E9	28	0.0099	0.359	0.369	0.865	0.426
34	NGC 2244	6.3E8	9.4E8	26	0.0061	0.109	0.115	0.214	0.537
35	NGC 2251	1.0E9	1.2E9	23	0.0012	0.118	0.119	0.204	0.584
36	NGC 2254	4.4E9	7.6E9	15	1.9E-4	0.134	0.134	0.220	0.611
37	NGC 2269	3.8E10	6.3E9	10	2.7E-6	0.120	0.120	0.158	0.759
38	NGC 2309	–	–	–	–	–	–	–	–
39	NGC 2323	2.1E9	1.8E9	19	0.0011	0.062	0.063	0.100	0.627
40	NGC 2324	2.2E6	1.2E8	120	0.149	–	–	–	0.005
41	NGC 2335	1.5E9	4.2E9	20	0.0012	0.078	0.079	0.149	0.526
42	NGC 2343	1.2E10	4.5E9	12	1.3E-5	0.154	0.154	0.204	0.755
43	NGC 2353	1.2E9	1.3E9	22	0.0013	0.089	0.090	0.163	0.552
44	NGC 2355	–	–	–	–	–	–	–	–
45	NGC 2395	3.0E9	5.8E9	17	2.4E-4	0.152	0.153	0.297	0.514
46	NGC 2420	7.9E9	1.0E10	13	3.9E-4	1.168	1.168	2.042	0.572
47	NGC 2423	3.8E9	6.8E9	16	4.6E-4	0.066	0.066	0.117	0.565
48	NGC 2437	1.1E8	3.3E8	44	0.093	1.10	1.20	4.12	0.290
49	NGC 2506	4.1E9	6.8E9	16	3.2E-4	0.167	0.168	0.338	0.496
50	NGC 6604x	–	–	–	–	–	–	–	–
51	NGC 6649	9.1E9	3.2E9	14	4.1E-5	0.097	0.097	0.151	0.639
52	NGC 6664	2.1E8	4.6E8	38	0.018	1.45	1.47	5.18	0.283
53	NGC 6694	1.8E9	1.6E9	20	7.5E-4	0.108	0.109	0.192	0.568
54	NGC 6704	9.2E9	3.7E9	13	3.4E-5	0.110	0.110	0.162	0.682
55	NGC 6705	4.0E9	2.5E9	16	0.0011	0.031	0.032	0.050	0.632
56	NGC 6755	3.3E9	2.3E9	17	7.6E-4	0.053	0.053	0.083	0.647
57	NGC 6756	2.7E10	6.4E9	10	5.9E-6	0.090	0.090	0.118	0.757
58	NGC 6802	2.2E11	5.1E10	6	1.0E-6	0.062	0.062	0.083	0.752
59	NGC 6811	4.4E9	7.5E9	15	4.6E-4	0.088	0.088	0.149	0.589

Table A.1.2   Continued

1	2	3	4	5	6	7	8	9	10
60	NGC 6819	2.5E9	5.2E9	18	0.0045	0.148	0.153	0.318	0.481
61	NGC 6823	1.0E9	1.2E9	23	0.0021	0.258	0.260	0.467	0.556
62	NGC 6830	5.1E8	7.9E8	29	0.017	0.056	0.073	0.175	0.419
63	NGC 6834	3.8E9	2.3E9	17	2.4E–4	0.073	0.073	0.119	0.612
64	NGC 6838	–	–	–	–	–	–	–	–
65	NGC 6866	7.5E8	2.7E9	25	0.0069	0.144	0.151	0.389	0.389
66	NGC 6910	1.7E9	1.6E9	20	0.0010	0.088	0.089	0.152	0.588
67	NGC 6913	4.4E9	2.8E9	16	1.3E–4	0.107	0.107	0.163	0.658
68	NGC 6939	7.6E10	3.2E10	7	3.0E–5	0.051	0.051	0.083	0.615
69	NGC 7031	1.0E10	1.2E10	12	6.8E–5	0.091	0.091	0.136	0.670
70	NGC 7062	7.0E8	9.6E8	26	0.0035	0.089	0.092	0.190	0.484
71	NGC 7086	6.3E9	3.0E9	15	9.8E–5	0.075	0.076	0.111	0.678
72	NGC 7128	1.4E10	3.9E9	13	2.1E–5	0.097	0.097	0.138	0.702
73	NGC 7142	–	–	–	–	–	–	–	–
74	NGC 7226	1.8E10	1.6E10	10	2.0E–5	0.101	0.101	0.143	0.706
75	NGC 7235	3.1E9	2.4E9	16	3.8E–4	0.126	0.127	0.172	0.737
76	NGC 7245	4.2E9	7.1E9	15	3.9E–4	0.065	0.065	0.114	0.572
77	NGC 7261	4.4E10	5.9E9	10	2.0E–6	0.142	0.142	0.192	0.741
78	NGC 7380	1.5E9	1.4E9	21	9.9E–4	0.082	0.083	0.150	0.552
79	NGC 7419	–	–	–	–	–	–	–	–
80	NGC 7510	2.5E9	2.0E9	18	2.8E–4	0.113	0.113	0.170	0.667
81	NGC 7654	1.7E9	1.6E9	20	0.0024	0.044	0.046	0.077	0.595
82	NGC 7788	5.0E8	8.2E8	28	0.0088	0.096	0.105	0.210	0.501
83	NGC 7789	4.7E8	2.0E9	29	0.040	1.433	1.473	4.871	0.302
84	NGC 7790	3.0E8	6.2E8	32	0.017	0.146	0.163	0.361	0.452
85	IC 1369	2.7E10	1.8E10	10	2.0E–5	0.085	0.085	0.133	0.640
86	IC 1442	6.0E9	3.2E9	14	5.8E–5	0.122	0.122	0.173	0.710
87	IC 1805	6.7E8	9.6E8	26	0.0029	0.116	0.118	0.227	0.521
88	IC 1848	3.0E8	6.1E8	33	0.030	0.089	0.118	0.272	0.435
89	IC 2157	1.7E9	1.6E9	20	6.5E–4	0.097	0.098	0.155	0.634
90	IC 4996	1.0E10	3.8E9	13	3.9E–5	0.088	0.088	0.126	0.704
91	Berk 3	1.1E9	1.3E9	22	0.0015	0.093	0.095	0.164	0.578
92	Berk 8	–	–	–	–	–	–	–	–
93	Berk 94	2.0E10	1.6E10	10	9.8E–6	0.132	0.132	0.186	0.713
94	Harv 21	1.8E9	1.7E9	20	5.9E–4	0.101	0.101	0.159	0.639
95	King 4	1.3E10	4.4E9	12	2.0E–5	0.092	0.092	0.124	0.740
96	King 16	–	–	–	–	–	–	–	–
97	King 19	1.0E10	4.0E9	13	3.5E–5	0.090	0.090	0.123	0.729
98	Stock 7	3.2E10	5.0E9	11	2.7E–6	0.187	0.187	0.261	0.719
99	Stock 8	1.2E9	1.4E9	22	0.0010	0.136	0.137	0.217	0.630
100	Tomb 5	2.7E8	5.7E8	34	0.019	0.088	0.107	0.269	0.399
101	Tr 1	1.6E9	1.5E9	21	5.4E–4	0.121	0.121	0.204	0.592
102	Tr 2	1.2E10	4.3E9	12	4.7E–5	0.062	0.062	0.085	0.730
103	Tr 35	4.3E9	2.3E9	17	1.2E–4	0.107	0.107	0.185	0.579

2   The distance scale corresponding to Kholopov's ZAMS

Table A.2.1   Structural and dynamical parameters of the OCls

NN	Name	r pc	E(B − V)	N_c	R arcmin	R pc	r_c pc
1	2	3	4	5	6	7	8
1	NGC 103	2800	0.46	398±9	37.4±0.8	30.4±0.7	7.1±1.2
2	NGC 129	1280	0.57	>278	>13.9	>5.2	3.2±0.6
3	NGC 188	1480	0.05	492±9	43.7±4.4	18.8±1.9	1.4±0.1
4	NGC 381	–	–	>157	>12.4	–	–
5	NGC 436	1660	0.16	90±0.4	7.7±1.2	3.7±0.6	1.2±0.2
6	NGC 457	2000	0.48	274±7	12.2±1.4	7.1±0.8	2.2±0.3
7	NGC 559	900	0.45	265±11	20.1±1.4	5.3±0.4	0.85±0.12
8	NGC 581	1680	0.39	>439	>30.9	>15.1	3.2±0.4
9	NGC 637	1740	0.40	>34	>4.6	>2.3	0.43±0.04
10	NGC 654	1740	0.93	>85	>9.4	>4.8	0.75±0.06
11	NGC 659	1000	0.58	>75	>6.6	>1.9	0.93±0.26
12	NGC 663	1540	0.83	>239	>17.7	>7.9	1.6±0.2
13	NGC 744	1100	0.41	25±0.4	5.5±0.3	1.8±0.1	0.46±0.18
14	NGC 957	1580	0.80	96±2	8.8±0.8	4.1±0.4	1.4±0.2
15	NGC 1027	720	0.40	>1147	>67.2	>14.1	8.9±1.6
16	NGC 1245	1820	0.27	96±7	9.3±3.4	4.9±1.8	1.1±0.2
17	NGC 1444	800	0.70	>20	>4.4	>1.0	0.33±0.28
18	NGC 1502	870	0.77	99±4	24.8±2.5	6.3±0.6	0.47±0.08
19	NGC 1528	720	0.29	>1267	>67.2	>14.1	2.2±0.2
20	NGC 1582	–	–	>137	>24.3	–	–
21	NGC 1664	750	0.20	>1925	>67.2	>14.6	–
22	NGC 1778	1000	0.34	193±1	21.9±1.9	6.4±0.6	1.2±0.6
23	NGC 1857	1900	0.40	210±10	21.6±2.6	12.0±1.4	0.85±0.17
24	NGC 1893	1890	0.44	>65	>9.9	>5.5	1.9±0.4
25	NGC 1907	1400	0.42	174±8	10.8±0.9	4.4±0.4	0.88±0.31
26	NGC 1912	1100	0.27	476±10	21.6±0.6	6.9±0.2	2.9±0.4
27	NGC 1960	1200	0.24	244±6	20.1±0.6	7.0±0.2	1.4±0.1
28	NGC 2126	1580	0.80	191±4	23.2±2.2	10.7±1.0	3.1±0.4
29	NGC 2129	1650	0.67	41±2	5.5±0.7	2.6±0.3	0.90±0.16
30	NGC 2169	850	0.14	50±7	15.5±5.4	3.8±1.3	0.22±0.09
31	NGC 2186	1560	0.31	149±0.2	18.6±2.5	8.4±1.1	0.98±0.42
32	NGC 2194	1970	0.51	89±3	17.0±1.9	9.8±1.1	0.81±0.36
33	NGC 2236	2020	0.45	152±2	14.4±1.5	8.4±0.9	1.6±0.3
34	NGC 2244	1160	0.46	>199	>20.2	>6.8	1.2±0.4
35	NGC 2251	1260	0.20	57±3	9.3±1.1	3.4±0.4	0.74±0.40
36	NGC 2254	1810	0.40	>43	>6.6	>3.5	0.56±0.14
37	NGC 2269	1430	0.44	27±1	2.8±0.2	1.1±0.1	0.30±0.21
38	NGC 2309	–	–	>63	>6.6	–	–
39	NGC 2323	880	0.24	209±6	20.1±1.8	5.1±0.5	0.95±0.16
40	NGC 2324	2200	0.11	>302	>26.9	>17.2	4.3±1.3
41	NGC 2335	1070	0.40	101±3	11.6±0.8	3.6±0.2	1.8±0.4
42	NGC 2343	960	0.20	23±1	7.7±0.9	2.2±0.2	0.18±0.07
43	NGC 2353	1000	0.12	85±2	12.2±1.3	3.5±0.4	1.3±0.4
44	NGC 2355			142±5	13.3±0.9	–	–

Table A.2.1   Continued

1	2	3	4	5	6	7	8
45	NGC 2395	1100	0.72	25±1	7.7±0.8	2.5±0.2	1.5±1.6
46	NGC 2420	2900	0.00	222	20.1	17.0	1.2±0.06
47	NGC 2423	1200	0.13	138±6	15.5±1.4	5.4±0.5	2.0±0.3
48	NGC 2437	1300	0.14	370±9	33.6±3.4	12.7±1.3	2.5±0.2
49	NGC 2506	3470	0.05	48±2	7.2±1.0	7.2±1.0	1.7±0.3
50	NGC 6604^x	1670	0.96	21±0.5	12.2±0.4	5.9±0.2	–
51	NGC 6649	1150	1.22	49±0.1	5.0±0.5	1.7±0.2	0.78±0.07
52	NGC 6664	1380	0.60	158±3	24.8±1.8	9.9±0.7	2.4±0.4
53	NGC 6694	1360	0.58	106±0.7	12.2±0.8	4.8±0.3	0.87±0.17
54	NGC 6704	1670	0.71	44±2	5.0±0.5	2.4±0.2	0.38±0.11
55	NGC 6705	1600	0.42	805±35	15.5±1.7	7.2±0.8	1.2±0.07
56	NGC 6755	1200	0.93	391±14	21.6±2.2	7.6±0.8	0.86±0.27
57	NGC 6756	–	1.44	56±0.8	6.6±0.5	–	–
58	NGC 6802	1000	0.81	102±2	7.7±0.5	2.2±0.1	0.32±0.05
59	NGC 6811	1090	0.14	199±6	21.9±1.1	6.9±0.5	0.92±0.31
60	NGC 6819	1900	0.28	1000±11	24.8±2.6	13.7±1.4	2.0±0.2
61	NGC 6823	1280	0.82	165±11	15.5±2.6	5.8±1.0	0.62±0.08
62	NGC 6830	1210	0.53	>535	>26.3	>9.2	3.0±0.4
63	NGC 6834	1600	0.66	96±3	5.4±0.5	2.5±0.2	0.94±0.29
64	NGC 6838	4110	0.31	446±10	20.1±1.8	24.0±2.2	2.2±0.4
65	NGC 6866	1200	0.14	281±7	26.3±2.2	9.2±0.8	24±0.2
66	NGC 6910	1600	1.05	138±5	15.5±1.6	7.2±0.8	1.3±0.2
67	NGC 6913	1400	0.83	60±2	8.8±0.6	3.6±0.2	0.76±0.11
68	NGC 6939	1150	0.50	274±4	15.5±1.2	5.2±0.4	0.96±0.07
69	NGC 7031	1200	0.93	94±1	17.7±1.1	6.2±0.4	0.73±0.15
70	NGC 7062	1050	0.25	112±4	9.9±1.0	3.0±0.3	1.0±0.1
71	NGC 7086	1050	0.70	83±1	7.7±0.8	2.4±0.2	0.54±0.17
72	NGC 7128	1900	0.92	43±1	2.8±0.3	1.5±0.2	0.70±0.12
73	NGC 7142	–	–	265±14	21.6±1.8	–	–
74	NGC 7226	1500	0.60	49±0.8	4.4±0.2	1.9±0.1	0.26±0.10
75	NGC 7235	2500	0.95	247±8	16.6±0.9	12.0±0.6	0.41±0.22
76	NGC 7245	1380	0.60	134±3	8.8±0.9	3.5±0.4	1.2±0.5
77	NGC 7261	800	0.58	>18	>3.3	>0.8	0.38±0.23
78	NGC 7380	1440	0.50	86±2	6.2±0.5	2.6±0.2	1.8±0.4
79	NGC 7419	–	1.50	48±0.9	4.4±0.2	–	–
80	NGC 7510	2000	0.89	>57	>7.2	>4.2	0.55±0.13
81	NGC 7654	1660	0.60	368±6	15.5±1.2	7.5±0.6	2.0±0.2
82	NGC 7788	2050	0.28	209±28	13.3±2.2	7.9±0.3	1.6±0.3
83	NGC 7789	1760	0.26	>1028	>47.0	>24.1	3.6±0.2
84	NGC 7790	2200	0.52	>195	>13.1	>8.4	1.7±0.2
85	IC 1369	1610	0.52	65±2	5.4±0.5	2.5±0.2	0.90±0.29
86	IC 1442	1580	0.53	37±2	5.5±0.6	2.5±0.3	0.30±0.13
87	IC 1805	1500	0.76	76±7	10.8±0.9	4.7±0.4	1.4±0.8
88	IC 1848	1700	0.61	386±4	23.2±1.4	11.5±0.7	3.9±0.4
89	IC 2157	1400	0.60	70±2	8.5±0.9	3.5±0.4	0.69±0.09
90	IC 4996	1250	0.64	71±3	6.2±0.6	2.2±0.2	0.45±0.11
91	Berk 3	–	0.50	>100	>10.0	–	–
92	Berk 8	–	–	>29	>2.8	–	–
93	Berk 94	1450	0.59	>32	>4.6	>2.0	0.42±0.78
94	Harv 21	–	0.69	65±2	5.4±0.8	–	–
95	King 4	2300	0.86	48±3	3.9±0.5	2.6±0.3	0.48±0.22
96	King 16	–	–	42±4	5.5±2.6	–	–

Table A.2.1   Continued

1	2	3	4	5	6	7	8
97	King 19	1800	0.82	59±2	7.7±0.6	4.0±0.3	0.53±0.08
98	Stock 7	820	0.64	13±1	5.0±0.8	1.2±0.2	0.75±0.38
99	Stock 8	1870	0.54	66±2	10.0±0.7	5.5±0.4	0.72±0.25
100	Tomb 5	–	0.35	186±1	15.5±0.9	–	–
101	Tr 1	2000	0.58	37±0.8	4.6±0.6	2.7±0.4	1.1±0.2
102	Tr 2	650	0.32	138±6	17.0±1.2	3.2±0.2	0.50±0.20
103	Tr 35	2450	1.19	43±1	5.0±0.3	3.5±0.2	1.9±0.6

Table A.2.1   Continued

NN	Name	k pc^{-2}	$\frac{R}{r_c}$	$\langle R \rangle$ pc	$\langle R^2 \rangle$ pc^2	$\langle R^{-1} \rangle^{-1}$ pc	$\langle m \rangle$ $M_\odot$	κ
1	2	9	10	11	12	13	14	15
1	NGC 103	3.2±0.2	4.3	11.1	155.4	7.89	3.2	1.05
2	NGC 129	59.1±13.0	1.6	2.52	7.34	2.01	2.7	1.07
3	NGC 188	23.8±3.3	. 13.0	4.54	31.5	2.63	1.4	1.04
4	NGC 381	–	5.0	–	–	–	–	–
5	NGC 436	36.6±0.7	3.2	1.50	2.73	1.11	2.2	1.06
6	NGC 457	25.6±0.7	3.1	2.86	9.93	2.11	3.7	1.14
7	NGC 559	62.8±6.1	6.2	1.64	3.66	1.15	1.3	1.09
8	NGC 581	5.4±0.3	4.8	5.32	36.1	3.71	2.8	1.09
9	NGC 637	45.0±2.0	5.4	0.79	0.81	0.54	3.0	1.08
10	NGC 654	34.5±2.6	6.3	1.47	2.96	1.03	4.7	1.08
11	NGC 659	100.7±23.2	2.1	0.88	0.91	0.69	2.3	1.04
12	NGC 663	26.1±1.2	4.8	2.77	9.81	1.92	4.8	1.15
13	NGC 744	44.8±6.4	3.8	0.67	0.56	0.48	2.3	1.08
14	NGC 957	25.6±1.6	2.8	1.69	3.45	1.27	4.6	1.14
15	NGC 1027	23.2±5.6	1.6	6.86	54.4	5.47	2.1	1.09
16	NGC 1245	17.3±1.8	4.4	1.77	3.96	1.25	2.0	1.09
17	NGC 1444	42.4±22.7	3.1	0.42	0.21	0.31	2.0	1.02
18	NGC 1502	49.6±10.4	13.3	1.50	3.45	0.86	3.3	1.16
19	NGC 1528	26.3±2.0	6.2	4.37	26.0	3.07	1.8	1.08
20	NGC 1582	–	–	–	–	–	–	–
21	NGC 1664	–	–	–	–	–	1.7	1.06
22	NGC 1778	16.4±4.4	5.3	2.16	6.03	1.48	2.2	1.09
23	NGC 1857	19.7±4.2	14.0	2.87	12.6	1.57	2.5	1.03
24	NGC 1893	10.8±0.8	2.8	2.29	6.30	1.72	3.2	1.10
25	NGC 1907	27.0±4.8	5.0	1.53	2.99	1.05	2.3	1.04
26	NGC 1912	27.8±2.0	2.4	3.05	11.0	2.34	2.5	1.13
27	NGC 1960	28.8±1.4	5.2	2.40	7.41	1.64	2.5	1.16
28	NGC 2126	8.9±0.4	3.4	4.20	21.6	3.09	3.7	1.07
29	NGC 2129	21.3±1.0	2.9	1.09	1.45	0.82	4.0	1.12
30	NGC 2169	32.2±17.4	17.3	0.85	1.16	0.44	2.1	1.16
31	NGC 2186	12.0±5.1	8.6	2.41	8.06	1.49	2.9	1.13
32	NGC 2194	11.8±6.2	12.1	2.53	8.99	1.40	2.1	1.01
33	NGC 2236	13.0±1.2	5.4	2.84	10.5	1.93	3.3	1.05
34	NGC 2244	11.0±2.8	5.4	2.28	6.77	1.55	3.4	1.26

Table A.2.1   Continued

1	2	9	10	11	12	13	14	15
35	NGC 2251	20.2±5.0	4.6	1.21	1.86	0.85	1.9	1.05
36	NGC 2254	27.5±5.0	6.2	1.09	1.61	0.76	2.2	1.02
37	NGC 2269	83.3±17.0	3.8	0.44	0.23	0.31	2.3	1.05
38	NGC 2309	–	8.0	–	–	–	–	–
39	NGC 2323	38.9±4.5	5.4	1.73	3.89	1.18	2.1	1.12
40	NGC 2324	5.6±0.6	4.0	6.43	51.5	4.61	1.8	1.01
41	NGC 2335	27.6±5.2	2.0	1.65	3.21	1.29	2.2	1.06
42	NGC 2343	47.2±19.3	12.0	0.56	0.44	0.31	2.0	1.09
43	NGC 2353	20.3±1.9	2.7	1.50	2.70	1.13	1.9	1.09
44	NGC 2355	–	4.6	–	–	–	–	–
45	NGC 2395	22.4±28.8	1.7	1.19	1.65	0.95	2.6	1.05
46	NGC 2420	15.3±0.9	13.7	4.10	25.5	2.26	2.0	1.09
47	NGC 2423	17.1±1.0	2.7	2.29	6.27	1.73	1.9	1.07
48	NGC 2437	12.5±0.6	5.0	4.40	24.8	3.04	2.2	1.08
49	NGC 2506	5.1±0.3	4.2	2.67	8.90	1.90	2.0	1.07
50	NGC 6604^x	–	–	–	–	–	10.7	1.08
51	NGC 6649	114.2±8.8	2.1	0.75	0.67	0.58	4.7	1.05
52	NGC 6664	7.3±0.5	4.2	3.65	16.7	2.60	3.1	1.09
53	NGC 6694	27.2±3.1	5.5	1.61	3.37	1.09	3.1	1.09
54	NGC 6704	47.2±9.7	6.4	0.74	0.75	0.52	3.3	1.04
55	NGC 6705	76.0±2.9	5.9	2.35	7.27	1.58	2.8	1.07
56	NGC 6755	49.7±13.4	8.8	2.14	6.42	1.32	3.9	1.07
57	NGC 6756	–	10.9	–	–	–	–	–
58	NGC 6802	127.8±11.6	7.0	0.69	0.64	0.45	1.9	1.01
59	NGC 6811	25.4±7.6	7.5	2.08	5.88	1.33	1.7	1.04
60	NGC 6819	36.7±3.0	7.0	4.21	23.9	2.73	1.86	1.05
61	NGC 6823	29.5±4.7	9.3	1.60	3.60	0.97	3.4	1.06
62	NGC 6830	19.9±0.7	3.1	3.76	17.2	2.79	2.5	1.06
63	NGC 6834	53.2±6.2	2.7	1.07	1.37	0.81	3.3	1.06
64	NGC 6838	5.8±1.2	10.8	6.32	57.8	3.70	–	–
65	NGC 6866	15.8±0.3	3.9	3.47	15.0	2.50	2.0	1.15
66	NGC 6910	15.1±1.1	5.4	2.43	7.64	1.65	6.4	1.15
67	NGC 6913	20.5±1.4	4.7	1.27	2.06	0.89	4.7	1.19
68	NGC 6939	62.2±2.9	5.4	1.74	3.95	1.19	1.8	1.02
69	NGC 7031	18.2±3.4	8.4	1.77	4.37	1.10	3.6	1.08
70	NGC 7062	50.9±1.8	3.0	1.25	1.88	0.93	1.5	1.01
71	NGC 7086	70.2±8.8	4.4	0.86	0.92	0.60	2.3	1.03
72	NGC 7128	86.9±9.6	2.2	0.69	0.56	0.53	4.6	1.05
73	NGC 7142	–	8.8	–	–	–	–	–
74	NGC 7226	86.0±27.5	7.3	0.58	0.46	0.38	–	–
75	NGC 7235	20.3±16.1	29.4	2.25	9.02	0.97	7.3	1.11
76	NGC 7245	42.2±5.6	2.8	1.48	2.63	1.11	2.2	1.02
77	NGC 7261	102.8±48.4	2.0	0.36	0.15	0.28	1.9	1.03
78	NGC 7380	22.9±1.9	1.4	1.29	1.91	1.04	3.1	1.11
79	NGC 7419	–	4.7	–	–	–	–	–
80	NGC 7510	28.1±4.8	7.6	1.24	2.11	0.79	4.8	1.06
81	NGC 7654	39.2±1.1	3.7	2.86	10.1	2.08	3.7	1.12
82	NGC 7788	20.5±2.3	5.0	2.74	9.61	1.89	2.6	1.05
83	NGC 7789	12.7±0.7	6.7	7.52	75.7	4.93	2.3	1.05
84	NGC 7790	18.0±1.2	5.0	2.91	10.9	2.01	3.2	1.04
85	IC 1369	28.2±3.0	2.8	1.06	1.36	0.80	2.1	1.01
86	IC 1442	35.7±15.5	8.3	0.73	0.74	0.46	2.5	1.04

Table A.2.1   Continued

1	2	9	10	11	12	13	14	15
87	IC 1805	9.9±1.5	3.5	1.84	4.18	1.35	4.0	1.12
88	IC 1848	10.1±0.5	3.9	4.31	23.1	3.10	4.2	1.17
89	IC 2157	23.2±2.0	5.0	1.20	1.84	0.83	3.1	1.08
90	IC 4996	68.3±7.6	5.0	0.78	0.78	0.54	3.4	1.14
91	Berk 3	–	4.8	–	–	–	–	–
92	Berk 8	–	–	–	–	–	–	–
93	Berk 94	12.2±9.4	4.6	0.70	0.62	0.49	3.8	1.18
94	Harv 21	–	5.4	–	–	–	–	–
95	King 4	28.5±8.0	5.4	0.87	0.99	0.59	4.4	1.03
96	King 16	–	5.9	–	–	–	–	–
97	King 19	27.4±4.3	7.7	1.20	1.98	0.76	4.0	1.05
98	Stock 7	63.3±40.3	1.6	0.58	0.39	0.46	3.0	1.17
99	Stock 8	9.6±2.8	7.6	1.63	3.62	1.04	3.8	1.15
100	Tomb 5	–	2.6	–	–	–	–	–
101	Tr 1	12.8±1.0	2.4	1.18	1.66	0.91	3.6	1.07
102	Tr 2	38.6±10.5	6.5	1.02	1.38	0.67	2.1	1.14
103	Tr 35	18.1±5.2	1.9	1.66	3.22	1.31	8.8	1.05

Table A.2.1   Continued

NN	Name	M_c $M_\odot$	R_t pc	τ Myrs	$\lg\tau$ years	$\lg t$	R_G pc	z pc
1	2	16	17	18	19	20	21	22
1	NGC 103	1270±350	16.5±1.4	100.6±12.6	8.0	7.6	9890	–59
2	NGC 129	>750	>12.8	>12.7	7.1	7.9	8910	–48
3	NGC 188	690±180	12.5±1.0	31.2±3.9	7.5	9.7	9010	573
4	NGC 381	–	–	–	–	–	–	–
5	NGC 436	200±50	8.4±0.7	4.3±0.5	6.6	7.6	9270	–105
6	NGC 457	1010±280	14.9±1.2	11.6±1.4	7.1	7.1	9520	–143
7	NGC 559	340±100	9.7±0.8	7.8±1.0	6.9	9.0	8770	20
8	NGC 581	>1230	>15.6	>35.7	7.6	7.7	9330	–43
9	NGC 637	>100	>6.8	>1.1	6.0	7.6	9380	60
10	NGC 654	>400	>10.8	>2.6	6.4	7.7	9400	–2
11	NGC 659	>170	>7.8	>2.0	6.3	7.3	8870	–18
12	NGC 663	>1150	>15.1	>8.6	6.9	6.6	9260	–17
13	NGC 744	60±20	5.4±0.4	1.0±0.1	6.0	7.6	8970	–110
14	NGC 957	440±120	11.2±0.9	3.7±0.5	6.6	7.2	9400	–65
15	NGC 1027	>2410	>18.5	>100.4	8.0	7.6	8730	26
16	NGC 1245	190±60	8.7±0.8	5.5±0.7	6.7	8.9	9750	–274
17	NGC 1444	>40	>4.8	>0.6	5.8	8.2	8890	–10
18	NGC 1502	330±90	9.7±0.8	2.5±0.3	6.4	6.4	8910	123
19	NGC 1528	>2280	>18.4	>47.0	7.7	8.1	8840	11
20	NGC 1582	–	–	–	–	7.7	–	–
21	NGC 1664	>3270	>20.9	–	–	7.9	8920	3
22	NGC 1778	420±110	10.8±0.9	8.0±1.0	6.9	8.2	9180	–26
23	NGC 1857	520±160	12.5±1.0	8.4±1.1	6.9	8.2	10070	50
24	NGC 1893	>210	>9.2	>6.5	6.8	6.9	10080	–48

Table A.2.1 Continued

1	2	16	17	18	19	20	21	22
25	NGC 1907	400±120	11.0±0.9	4.6±0.6	6.7	8.3	9590	15
26	NGC 1912	1190±320	15.4±1.3	19.5±2.4	7.3	7.6	9290	21
27	NGC 1960	610±170	12.4±1.0	9.4±1.2	7.0	7.5	9400	30
28	NGC 2126	710±190	13.4±1.1	18.6±2.3	7.3	7.2	9680	369
29	NGC 2129	160±50	8.3±0.7	1.8±0.2	6.3	7.2	9840	12
30	NGC 2169	100±40	6.7±0.6	1.0±0.1	6.0	7.4	9020	-35
31	NGC 2186	430±110	11.3±0.9	6.6±0.8	6.8	8.2	9640	-160
32	NGC 2194	190±50	8.9±0.7	6.3±0.8	6.8	8.6	10100	-72
33	NGC 2236	500±130	12.3±1.0	9.2±1.2	7.0	8.6	10070	-51
34	NGC 2244	>680	>12.7	>7.0	6.8	6.5	9250	-32
35	NGC 2251	110±30	7.0±0.6	2.9±0.4	6.5	7.9	9370	11
36	NGC 2254	>90	>6.9	>2.2	6.3	8.8	9880	11
37	NGC 2269	60±20	5.8±0.5	0.5±0.1	5.7	7.8	9490	18
38	NGC 2309	–	–	–	–	–	–	–
39	NGC 2323	440±120	10.6±0.9	6.0±0.7	6.8	7.6	8880	-11
40	NGC 2324	>540	>12.6	>55.3	7.7	8.8	10100	135
41	NGC 2335	220±60	8.6±0.7	5.6±0.7	6.8	8.2	8000	-15
42	NGC 2343	50±10	5.0±0.4	0.6±0.1	5.8	8.0	8910	-11
43	NGC 2353	160±40	7.7±0.6	4.8±0.6	6.7	7.1	8940	15
44	NGC 2355	–	–	–	–	–	–	–
45	NGC 2395	60±20	5.8±0.5	2.6±0.3	6.4	7.7	9180	273
46	NGC 2420	440±110	12.5	16.5	7.2	9.5	10830	983
47	NGC 2423	260±80	9.1±0.8	10.0±1.2	7.0	8.6	9010	82
48	NGC 2437	810±220	13.3±1.1	28.4±3.6	7.4	7.9	9060	100
49	NGC 2506	100±30	7.4±0.6	9.1±1.1	7.0	9.2	10700	605
50	NGC 6604ˣ	220±60	6.9±0.6	–	–	6.4	6640	57
51	NGC 6649	230±60	7.3±0.6	1.0±0.1	6.0	7.7	7140	-7
52	NGC 6664	490±130	9.2±0.8	15.0±1.9	7.2	7.4	6960	-4
53	NGC 6694	330±80	8.1±0.7	3.7±0.5	6.6	7.9	6980	-61
54	NGC 6704	140±40	6.0±0.5	1.0±0.1	6.0	7.4	6780	-56
55	NGC 6705	2250±660	15.1±1.3	12.0±1.5	7.1	7.9	6820	-69
56	NGC 6755	1520±440	13.9±1.2	6.2±0.8	6.8	7.6	7300	-27
57	NGC 6756	–	–	–	–	7.7	–	–
58	NGC 6802	190±50	7.3±0.6	1.2±0.2	6.1	9.2	7680	24
59	NGC 6811	340±80	9.1±0.8	7.8±1.0	6.9	8.7	8100	165
60	NGC 6819	1860±480	15.8±1.3	36.0±4.5	7.6	8.9	7890	288
61	NGC 6823	560±180	10.3±0.9	3.3±0.4	6.5	7.0	7630	5
62	NGC 6830	>1340	>13.8	>26.2	7.4	7.2	7670	-30
63	NGC 6834	320±90	8.6±0.7	2.2±0.3	6.3	7.4	7680	41
64	NGC 6838	–	–	–	–	9.9	6870	-318
65	NGC 6866	560±150	10.8±0.9	20.6±2.6	7.3	8.5	8070	152
66	NGC 6910	880±250	12.5±1.0	5.1±0.6	6.7	7.0	8040	65
67	NGC 6913	280±80	8.5±0.7	2.0±0.2	6.3	7.0	8000	23
68	NGC 6939	490±130	10.6±0.9	7.0±0.9	6.8	9.9	8390	253
69	NGC 7031	340±90	9.3±0.8	3.4±0.4	6.5	8.7	8310	55
70	NGC 7062	170±50	7.3±0.6	4.2±0.5	6.6	8.0	8270	-41
71	NGC 7086	190±50	7.7±0.6	1.7±0.2	6.2	7.9	8350	12
72	NGC 7128	200±50	8.0±0.7	0.9±0.1	6.0	6.0	8650	22
73	NGC 7142	–	–	–	–	9.3	–	–
74	NGC 7226	–	–	–	–	8.7	8620	-7
75	NGC 7235	1800±510	17.4±1.4	2.5±0.3	6.4	7.0	9080	42
76	NGC 7245	290±80	9.1±0.8	4.8±0.6	6.7	8.6	8580	-37

5-3-400

Table A.2.1　Continued

1	2	16	17	18	19	20	21	22
77	NGC 7261	>30	>4.4	>0.5	5.7	7.6	8430	20
78	NGC 7380	270±70	8.9±0.7	3.3±0.4	6.5	7.2	8730	−14
79	NGC 7419	–	–	–	–	–	–	–
80	NGC 7510	>270	>9.3	>1.6	6.2	7.0	9110	10
81	NGC 7654	1360±360	15.6±1.3	12.4±1.5	7.1	7.6	8970	21
82	NGC 7788	540±210	11.8±1.1	10.9±1.4	7.0	7.2	9300	−20
83	NGC 7789	>2360	>19.0	>79.0	7.9	8.9	9090	−156
84	NGC 7790	>620	>12.5	>10.6	7.0	7.4	9390	−30
85	IC 1369	140±40	6.9±0.6	2.6±0.3	6.4	9.1	8340	−3
86	IC 1442	90±30	6.2±0.5	0.9±0.1	6.0	7.8	8650	−52
87	IC 1805	300±100	9.8±0.9	4.2±0.5	6.6	6.4	9320	32
88	IC 1848	1620±420	17.4±1.4	21.4±2.7	7.3	6.4	9520	11
89	IC 2157	220±60	8.9±0.8	2.2±0.3	6.3	7.2	9590	38
90	IC 4996	240±70	8.0±0.7	1.1±0.1	6.0	7.0	7980	36
91	Berk 3	–	–	–	–	–	–	–
92	Berk 8	–	–	–	–	–	–	–
93	Berk 94	>120	>6.8	>0.8	5.9	8.4	8640	−21
94	Harv 21	–	–	–	–	7.3*	–	–
95	King 4	210±70	9.1±0.8	1.1±0.1	6.0	7.3	9980	−40
96	King 16	–	–	–	–	–	–	–
97	King 19	240±70	8.7±0.7	1.7±0.2	6.2	7.6	8990	13
98	Stock 7	40±10	4.7±0.4	0.9±0.1	6.0	6.3	8800	8
99	Stock 8	250±70	9.7±0.8	2.8±0.4	6.4	6.3	10060	16
100	Tomb 5	–	–	–	–	–	–	–
101	Tr 1	130±40	7.6±0.6	2.2±0.3	6.3	7.4	9570	−31
102	Tr 2	290±80	9.1±0.8	2.3±0.3	6.4	7.5	8690	−36
103	Tr 35	380±100	7.8±0.6	2.4±0.3	6.4	7.6	6150	8

Notes:

^{x} – star counts in the cluster NGC 6604 up to $B_{lim} \simeq 14^m$;

* – NGC 7788, NGC 7790 and Harv 21 are supposed to form a united system in accordance with Barkhatova and Zhelvanova (1963).

Table A.2.2　The disruption times and nonstationarity parameters of OCls

NN	Name	t_{d1} years	t_{d2} years	p_o pc	$\langle\delta\alpha\rangle_{eq}$	$\langle\delta\alpha\rangle_{th}$	$\delta\alpha$	$\dfrac{\delta\alpha}{\delta\alpha_{max}}$	$\delta\alpha_{max}$
1	2	3	4	5	6	7	8	9	10
1	NGC 103				1.230				
2	NGC 129	1.4E9	1.4E9	22	0.0027	0.044	0.047	0.086	0.545
3	NGC 188	4.8E9	7.0E9	15	0.0017	–	–	–	0.433
4	NGC 381	–	–	–	–	–	–	–	–
5	NGC 436	1.8E9	1.6E9	20	7.6E-4	0.080	0.081	0.135	0.598
6	NGC 457	1.1E9	3.7E9	21	0.0029	0.052	0.054	0.094	0.578
7	NGC 559	1.2E10	1.2E10	12	1.9E-4	0.056	0.056	0.089	0.626
8	NGC 581	2.0E8	4.8E8	37	0.051	0.377	0.429	1.142	0.376
9	NGC 637	6.9E9	3.3E9	14	4.6E-5	0.120	0.120	0.169	0.708

Table A.2.2 Continued

1	2	3	4	5	6	7	8	9	10
10	NGC 654	3.6E9	2.4E9	16	2.4E–4	0.084	0.084	0.125	0.675
11	NGC 659	1.1E10	3.5E9	14	3.9E–5	0.072	0.072	0.105	0.689
12	NGC 663	1.6E9	1.6E9	20	0.0018	0.060	0.061	0.101	0.608
13	NGC 744	7.0E9	3.2E9	14	3.9E–5	0.139	0.139	0.202	0.688
14	NGC 957	2.9E9	2.0E9	18	3.8E–4	0.077	0.077	0.122	0.637
15	NGC 1027	1.4E8	3.7E8	42	0.165	0.044	0.210	0.825	0.254
16	NGC 1245	4.4E9	7.5E9	15	3.5E–4	0.095	0.096	0.167	0.573
17	NGC 1444	4.2E10	2.0E10	9	2.1E–6	0.135	0.135	0.183	0.739
18	NGC 1502	2.9E9	2.2E9	17	3.0E–4	0.119	0.119	0.173	0.689
19	NGC 1528	9.8E8	3.4E9	22	0.014	0.044	0.057	0.109	0.525
20	NGC 1582	–	–	–	–	–	–	–	–
21	NGC 1664	–	–	–	–	–	–	–	–
22	NGC 1778	1.8E9	4.9E9	18	0.0012	0.071	0.072	0.123	0.587
23	NGC 1857	1.1E9	3.7E9	21	0.0023	0.444	0.446	0.730	0.611
24	NGC 1893	4.7E8	7.9E8	29	0.0044	0.124	0.128	0.266	0.482
25	NGC 1907	6.0E9	9.1E9	14	2.0E–4	0.054	0.054	0.080	0.674
26	NGC 1912	1.2E9	1.3E9	22	0.0050	0.037	0.042	0.076	0.556
27	NGC 1960	1.3E9	1.4E9	21	0.0024	0.064	0.066	0.111	0.597
28	NGC 2126	1.2E9	3.4E9	22	0.0040	0.125	0.129	0.330	0.391
29	NGC 2129	4.1E9	2.4E9	16	1.2E–4	0.111	0.111	0.166	0.668
30	NGC 2169	5.2E9	3.1E9	14	6.6E–5	0.142	0.142	0.192	0.737
31	NGC 2186	1.4E9	4.3E9	20	0.0014	0.123	0.124	0.208	0.598
32	NGC 2194	1.0E9	3.5E9	22	0.0018	1.825	1.826	3.353	0.545
33	NGC 2236	1.7E9	4.5E9	19	0.0016	0.094	0.096	0.176	0.545
34	NGC 2244	1.7E9	1.6E9	20	0.0014	0.073	0.074	0.120	0.619
35	NGC 2251	1.8E9	1.7E9	20	5.2E–4	0.105	0.106	0.171	0.620
36	NGC 2254	1.2E9	1.0E10	13	8.7E–5	0.122	0.122	0.189	0.644
37	NGC 2269	4.6E10	6.5E9	10	2.1E–6	0.119	0.119	0.156	0.763
38	NGC 2309	–	–	–	–	–	–	–	–
39	NGC 2323	2.6E9	2.0E9	18	7.6E–4	0.058	0.059	0.092	0.641
40	NGC 2324	7.5E7	7.2E8	48	0.071	–	–	–	0.107
41	NGC 2335	2.2E9	5.0E9	18	6.6E–4	0.073	0.074	0.132	0.560
42	NGC 2343	1.0E10	4.2E9	12	1.8E–5	0.163	0.163	0.219	0.745
43	NGC 2353	1.4E9	1.4E9	22	0.0011	0.086	0.087	0.153	0.567
44	NGC 2355	–	–	–	–	–	–	–	–
45	NGC 2395	2.7E9	5.6E9	17	2.5E–4	0.148	0.148	0.279	0.531
46	NGC 2420	4.6E9	8.9E9	17	9.9E–4	2.354	2.355	4.754	0.495
47	NGC 2423	1.5E9	4.1E9	20	0.0018	0.082	0.084	0.176	0.476
48	NGC 2437	2.4E8	5.3E8	35	0.035	0.315	0.350	0.886	0.395
49	NGC 2506	1.3E9	4.0E9	24	0.0016	1.264	1.266	3.767	0.336
50	NGC 6604ˣ	–	–	–	–	–	–	–	–
51	NGC 6649	3.2E10	5.3E9	11	5.8E–6	0.090	0.090	0.127	0.708
52	NGC 6664	2.1E8	4.6E8	38	0.018	1.452	1.470	5.222	0.282
53	NGC 6694	2.4E9	1.9E9	18	5.1E–4	0.096	0.096	0.162	0.592
54	NGC 6704	1.1E10	4.0E9	13	2.4E–5	0.107	0.107	0.155	0.693
55	NGC 6705	5.6E9	2.9E9	15	6.5E–4	0.028	0.029	0.044	0.655
56	NGC 6755	4.8E9	2.8E9	15	4.2E–4	0.045	0.046	0.067	0.676
57	NGC 6756	–	–	–	–	–	–	–	–
58	NGC 6802	1.9E11	4.8E10	6	1.2E–6	0.063	0.63	0.084	0.746
59	NGC 6811	3.5E9	6.8E9	16	6.5E–4	0.103	0.104	0.182	0.568
60	NGC 6819	3.2E9	6.1E9	16	0.0032	0.078	0.081	0.158	0.512
61	NGC 6823	4.3E9	2.7E9	16	2.6E–4	0.071	0.071	0.105	0.677

Table A.2.2   Continued

1	2	3	4	5	6	7	8	9	10
62	NGC 6830	6.6E8	9.1E8	27	0.012	0.048	0.061	0.135	0.450
63	NGC 6834	1.1E10	3.6E9	13	4.6E–5	0.067	0.067	0.100	0.677
64	NGC 6838	–	–	–	–	–	–	–	–
65	NGC 6866	7.5E8	2.7E9	25	0.0069	0.144	0.151	0.389	0.389
66	NGC 6910	1.8E9	1.7E9	20	9.3E–4	0.086	0.087	0.145	0.598
67	NGC 6913	4.3E9	2.6E9	16	1.4E–4	0.108	0.108	0.165	0.655
68	NGC 6939	1.1E11	3.8E10	7	1.8E–5	0.047	0.047	0.074	0.639
69	NGC 7031	5.8E9	8.8E9	14	1.7E–4	0.118	0.119	0.189	0.627
70	NGC 7062	2.7E9	2.0E9	18	4.5E–4	0.066	0.066	0.109	0.607
71	NGC 7086	1.2E10	4.0E9	13	3.7E–5	0.072	0.072	0.101	0.711
72	NGC 7128	4.2E10	5.7E9	11	3.8E–6	0.094	0.094	0.128	0.736
73	NGC 7142	–	–	–	–	–	–	–	–
74	NGC 7226	–	–	–	–	–	–	–	–
75	NGC 7235	5.5E9	3.2E9	14	1.6E–4	0.080	0.080	0.106	0.758
76	NGC 7245	7.4E9	9.6E9	13	1.6E–4	0.059	0.059	0.096	0.619
77	NGC 7261	4.4E10	5.9E9	10	2.0E–6	0.142	0.142	0.192	0.741
78	NGC 7380	4.7E9	2.4E9	16	1.7E–4	0.074	0.075	0.118	0.630
79	NGC 7419	–	–	–	–	–	–	–	–
80	NGC 7510	4.4E9	2.7E9	15	1.2E–4	0.102	0.102	0.147	0.697
81	NGC 7654	1.7E9	1.6E9	20	0.0023	0.044	0.046	0.078	0.595
82	NGC 7788	7.5E8	1.0E9	25	0.0048	0.078	0.082	0.153	0.539
83	NGC 7789	5.9E8	2.3E9	27	0.031	0.854	0.885	2.681	0.330
84	NGC 7790	7.1E8	1.0E9	25	0.0050	0.080	0.085	0.158	0.537
85	IC 1369	2.5E10	1.8E10	10	2.3E–5	0.082	0.082	0.131	0.632
86	IC 1442	7.6E9	3.5E9	14	3.6E–5	0.118	0.118	0.164	0.719
87	IC 1805	1.4E9	1.4E9	21	9.8E–4	0.096	0.097	0.166	0.586
88	IC 1848	5.6E8	8.7E8	27	0.012	0.062	0.075	0.149	0.501
89	IC 2157	4.0E9	2.5E9	16	1.7E–4	0.088	0.088	0.130	0.679
90	IC 4996	2.3E10	5.3E9	11	1.1E–5	0.083	0.083	0.114	0.733
91	Berk 3	–	–	–	–	–	–	–	–
92	Berk 8	–	–	–	–	–	–	–	–
93	Berk 94	2.6E10	1.8E10	10	6.3E–6	0.130	0.130	0.180	0.724
94	Harv 21	–	–	–	–	–	–	–	–
95	King 4	1.2E10	4.2E9	12	2.5E–5	0.092	0.092	0.125	0.739
96	King 16	–	–	–	–	–	–	–	–
97	King 19	4.4E9	2.7E9	16	1.3E–4	0.100	0.100	0.145	0.692
98	Stock 7	9.0E9	3.1E9	14	2.2E–5	0.197	0.197	0.295	0.669
99	Stock 8	1.7E9	1.7E9	20	5.5E–4	0.122	0.123	0.189	0.650
100	Tomb 5	–	–	–	–	–	–	–	–
101	Tr 1	2.5E9	1.9E9	18	2.6E–4	0.115	0.115	0.185	0.624
102	Tr 2	9.6E9	3,9E9	13	6.8E–5	0.063	0.064	0.088	0.720
103	Tr 35	2.6E9	1.8E9	19	2.4E–4	0.115	0.115	0.221	0.522

3 Dimensionless parameters of the OCl haloes and cores

Table A.3   Dimensionless parameters of the OCl haloes and cores

NN	Name	$\frac{r_c}{R}$	$\frac{n_1}{n_2}$	$\xi = \frac{R_1}{R}$	$\mu = \frac{N_1}{N_2}$	$\xi' = \frac{R_1'}{R}$	$\mu' = \frac{N_1'}{N_2'}$
1	2	3	4	5	6	7	8
1	NGC 103	0.23	0.38	0.17	0.24	–	–
2	NGC 129	0.62	2.95	0.11	0.05	0.67	1.83
3	NGC 188	0.07	0.14	0.23	1.04	–	–
4	NGC 381	0.20	0.31	0.19	0.13	0.50	1.04
5	NGC 436	0.31	0.55	0.20	0.24	0.50	2.61
6	NGC 457	0.31	0.58	0.36	0.66	–	–
7	NGC 559	0.16	0.24	0.23	0.44	–	–
8	NGC 581	0.21	0.33	0.10	0.08	–	–
9	NGC 637	0.18	0.29	0.33	0.94	0.67	2.79
10	NGC 654	0.15	0.24	0.23	0.68	–	–
11	NGC 659	0.48	1.33	0.33	0.30	–	–
12	NGC 663	0.20	0.32	0.44	1.86	–	–
13	NGC 744	0.26	0.43	0.40	1.15	–	–
14	NGC 957	0.34	0.68	0.50	1.47	–	–
15	NGC 1027	0.62	3.10	0.15	0.08	–	–
16	NGC 1245	0.22	0.36	0.33	0.60	0.42	0.83
17	NGC 1444	0.32	0.60	0.75	4.97	–	–
18	NGC 1502	0.07	0.13	0.12	0.40	0.31	2.31
19	NGC 1528	0.16	0.24	0.10	0.06	0.35	0.36
20	NGC 1582	–	–	0.20	0.19	–	–
21	NGC 1664	–	–	0.15	0.04	–	–
22	NGC 1778	0.18	0.29	0.11	0.11	–	–
23	NGC 1857	0.07	0.13	0.28	1.09	–	–
24	NGC 1893	0.35	0.70	0.33	0.60	–	–
25	NGC 1907	0.20	0.31	0.29	0.24	0.71	3.66
26	NGC 1912	0.42	0.97	0.21	0.10	0.57	0.66
27	NGC 1960	0.19	0.30	0.23	0.28	0.54	3.19
28	NGC 2126	0.29	0.51	0.20	0.27	0.60	3.34
29	NGC 2129	0.34	0.64	0.50	0.97	–	–
30	NGC 2169	0.05	0.12	0.28	0.17	–	–
31	NGC 2186	0.11	0.19	0.17	0.24	–	–
32	NGC 2194	0.08	0.15	0.43	3.10	–	–
33	NGC 2236	0.18	0.29	0.08	0.08	0.38	1.95
34	NGC 2244	0.18	0.29	0.17	0.10	0.50	0.31
35	NGC 2251	0.21	0.34	0.50	0.94	–	–
36	NGC 2254	0.16	0.24	0.33	1.22	–	–
37	NGC 2269	0.26	0.43	0.20	0.26	0.60	1.82
38	NGC 2309	0.12	0.20	0.25	0.60	0.50	2.89
39	NGC 2323	0.18	0.29	0.46	0.85	–	–
40	NGC 2324	0.25	0.41	0.12	0.22	0.62	4.56
41	NGC 2335	0.48	1.35	0.53	1.29	–	–
42	NGC 2343	0.08	0.15	0.20	0.55	–	–
43	NGC 2353	0.37	0.76	0.27	0.27	–	–
44	NGC 2355	0.21	0.34	0.17	0.24	0.58	3.04
45	NGC 2395	0.59	2.56	0.57	3.04	–	–

Table A.3   Continued

1	2	3	4	5	6	7	8
46	NGC 2420	0.07	0.13	0.23	0.74	–	–
47	NGC 2423	0.37	0.75	0.20	0.09	0.60	1.51
48	NGC 2437	0.20	0.31	0.40	0.64	–	–
49	NGC 2506	0.23	0.39	0.38	0.93	–	–
50	NGC 6604^x	–	–	0.18	0.14	–	–
51	NGC 6649	0.46	1.22	0.67	6.03	–	–
52	NGC 6664	0.23	0.38	0.56	2.48	–	–
53	NGC 6694	0.18	0.28	0.18	0.28	0.54	7.16
54	NGC 6704	0.15	0.23	0.33	0.58	–	–
55	NGC 6705	0.17	0.26	0.30	0.40	0.50	0.99
56	NGC 6755	0.11	0.19	0.36	1.11	–	–
57	NGC 6756	0.09	0.16	0.33	1.45	–	–
58	NGC 6802	0.14	0.22	0.28	0.37	–	–
59	NGC 6811	0.13	0.21	0.44	2.05	–	–
60	NGC 6819	0.14	0.23	0.31	0.47	–	–
61	NGC 6823	0.10	0.18	0.14	0.17	0.50	0.96
62	NGC 6830	0.32	0.59	0.29	0.22	0.71	0.90
63	NGC 6834	0.37	0.75	0.43	0.43	–	–
64	NGC 6838	0.09	0.16	0.28	0.27	–	–
65	NGC 6866	0.25	0.43	0.12	0.08	0.59	1.78
66	NGC 6910	0.18	0.29	0.21	0.25	–	–
67	NGC 6913	0.21	0.34	0.38	0.61	–	–
68	NGC 6939	0.18	0.29	0.28	0.64	–	–
69	NGC 7031	0.11	0.19	0.25	0.36	–	–
70	NGC 7062	0.33	0.62	0.33	0.36	–	–
71	NGC 7086	0.22	0.37	0.29	0.39	0.71	2.95
72	NGC 7128	0.46	1.17	0.60	1.72	–	–
73	NGC 7142	0.11	0.19	0.28	0.41	–	–
74	NGC 7226	0.13	0.22	0.25	0.56	–	–
75	NGC 7235	0.03	0.09	0.20	0.23	–	–
76	NGC 7245	0.34	0.68	0.12	0.15	0.75	2.94
77	NGC 7261	0.50	1.45	0.33	0.36	–	–
78	NGC 7380	0.70	5.11	0.88	4.69	–	–
79	NGC 7419	0.21	0.34	0.38	1.32	–	–
80	NGC 7510	0.13	0.21	0.15	0.33	–	–
81	NGC 7654	0.27	0.45	0.30	0.40	0.60	4.88
82	NGC 7788	0.20	0.31	0.33	1.12	–	–
83	NGC 7789	0.15	0.23	0.28	0.63	–	–
84	NGC 7790	0.20	0.31	0.18	0.29	0.41	2.33
85	IC 1369	0.35	0.70	0.57	1.06	–	–
86	IC 1442	0.12	0.19	0.20	0.30	–	–
87	IC 1805	0.28	0.49	0.43	0.50	–	–
88	IC 1848	0.25	0.42	0.13	0.12	0.47	0.51
89	IC 2157	0.20	0.31	0.36	0.54	–	–
90	IC 4996	0.20	0.31	0.25	0.32	0.62	2.88
91	Berk 3	0.20	0.33	0.15	0.25	–	–
92	Berk 8	–	–	0.80	8.34	–	–
93	Berk 94	0.21	0.34	0.33	0.34	–	–
94	Harv 21	0.18	0.29	0.43	1.42	–	–
95	King 4	0.18	0.29	0.14	0.20	–	–
96	King 16	0.17	0.26	0.20	0.18	0.50	1.93
97	King 19	0.13	0.21	0.30	0.58	–	–

Table A.3   Continued

1	2	3	4	5	6	7	8
98	Stock 7	0.63	3.17	0.56	7.41	–	–
99	Stock 8	0.13	0.21	0.38	0.95	–	–
100	Tomb 5	0.38	0.78	0.10	0.04	0.50	1.07
101	Tr 1	0.41	0.94	0.67	2.67	–	–
102	Tr 2	0.15	0.24	0.18	0.06	0.46	0.26
103	Tr 35	0.53	1.74	0.44	0.81	–	–